Earth-Science Reviews 160 (2016) 350–385

Contents lists available at ScienceDirect

Earth-Science Reviews

journal homepage: www.elsevier.com/locate/earscirev

Invited review

Plio-Pleistocene exhumation of the eastern Himalayan syntaxis and its domal 'pop-up'

Laura Bracciali [a,b,*], Randall R. Parrish [c], Yani Najman [b], Andrew Smye [d], Andrew Carter [e], Jan R. Wijbrans [f]

[a] NERC Isotope Geosciences Laboratory, British Geological Survey, Keyworth, Nottingham, United Kingdom
[b] Lancaster Environment Centre, Lancaster University, Lancaster, United Kingdom
[c] British Geological Survey, Keyworth, Nottingham and Department of Earth and Environmental Sciences, University of Portsmouth, Portsmouth, United Kingdom
[d] Department of Geosciences, The Pennsylvania State University, University Park, USA
[e] Department of Earth and Planetary Sciences, Birkbeck College, University of London, London, United Kingdom
[f] Petrology Department, Vrije Universiteit, Amsterdam, Netherlands

ARTICLE INFO

Article history:
Received 19 December 2015
Received in revised form 24 July 2016
Accepted 25 July 2016
Available online 27 July 2016

Keywords:
Eastern Himalayan syntaxis
Namche Barwa
Surma Basin
Yarlung Tsangpo–Brahmaputra
U–Pb rutile dating
Thermal modelling

ABSTRACT

The eastern termination of the Himalayan orogen forms a structural syntaxis that is characterised by young (from 10 to <1 Ma) mineral growth and cooling ages that document Late Miocene to Pleistocene structural, metamorphic, igneous and exhumation events. This region is a steep antiformal and in part domal structure that folds the suture zone between the Indian and Asian plates. It is dissected by the Yarlung Tsangpo, one of the major rivers of the eastern Himalayan–Tibet region, which becomes the Brahmaputra River in the Indian foreland basin before emptying into the Bay of Bengal. Exceptionally high relief and one of the deepest gorges on Earth have developed where the river's tortuous route crosses the Namche Barwa–Gyala Peri massif (>7 km in elevation) in the core of the syntaxis. Very high erosion rates documented in sediment downstream of the gorge at the foot of the Himalaya contribute ~50% of total detritus to the sediment load of the Brahmaputra.

The initiation of very high rates of exhumation has been attributed either to the extreme erosive power of a river flowing across a deforming indentor corner and the associated positive feedback, or to the geometry of the Indian plate indentor, with the corner being thrust beneath the Asian plate resulting in buckling which accommodates shortening; both processes may be important.

The northern third of the syntaxis corresponds to a steep domal 'pop-up' structure bounded by the India–Asia suture on three sides and a thrust zone to the south. Within the dome, Greater Himalaya rocks equilibrated at ~800 °C and 25–30 km depth during the Miocene, with these conditions potentially persisting into the latest Miocene and possibly the Pliocene, with modest decompression prior to ~4 Ma. This domal 'pop-up' corresponds to the area of youngest bedrock ages on a wide variety of thermochronometers and geochronometers.

In this paper we review the extensive scientific literature that has focused on the eastern syntaxis and provide new chronological data on its bedrock and erosion products to constrain the age of inception of the very rapid uplift and erosion. We then discuss its cause, with the ultimate aim to reconstruct the exhumation history of the syntaxis and discuss the tectonic context for its genesis. We use zircon and rutile U–Pb, white mica Ar–Ar and zircon fission track dating methods to extract age data from bedrock, Brahmaputra modern sediments (including an extensive compilation of modern detrital chronometry from the eastern Himalaya) and Neogene palaeo-Brahmaputra deposits of the Surma Basin (Bangladesh). Numerical modelling of heat flow and erosion is also used to model the path of rocks from peak metamorphic conditions of ~800 °C to <250 °C. Our new data include U–Pb bedrock rutile ages as young as 1.4 Ma from the Namche Barwa massif and 0.4 Ma from the river downstream of the syntaxis.

Combined with existing data, our new data and heat flow modelling show that: i) the detrital age signature of the modern syntaxis is unique within the eastern Himalayan region; ii) the rocks within the domal pop-up were >575 ± 75 °C only 1–2 Myr ago; iii) the Neogene Surma Basin does not record evidence of the rise and erosion of the domal pop-up until latest Pliocene–Pleistocene time; iv) Pleistocene exhumation of the north-easternmost part of the syntaxis took place at rates of at least 4 km/Myr, with bedrock erosion of 12–21 km during the last 3 Ma; v) the inception of rapid syntaxial exhumation may have started as early as 7 Ma or as late as 3 Ma; and vi) the Yarlung Tsangpo is antecedent and subsequently distorted by the developing antiform. Together our data and modelling demonstrate that the domal pop-up with its exceptional erosion and topographic relief is

* Corresponding author at: NERC Isotope Geosciences Laboratory, British Geological Survey, Keyworth, Nottingham, United Kingdom.
E-mail address: laurabrac74@gmail.com (L. Bracciali).

http://dx.doi.org/10.1016/j.earscirev.2016.07.010

likely a Pleistocene feature that overprinted earlier structural and metamorphic events typical of Himalayan evolution.

Contents

1. Introduction

Due to its ongoing deformation and scale, the Himalayan orogen (Fig. 1) is one of the best natural laboratories to investigate causes and consequences of continental scale crustal deformation and its surface expression and processes, including the complex links between continental tectonics, surface processes and climate feedbacks (e.g. Searle et al., 1987; Molnar and England, 1990; Raymo and Ruddiman, 1992; Prell and Kutzbach, 1992; Krishnaswami et al., 1992; Willett et al., 1993; Houseman and England, 1993; Molnar et al., 1993; Royden et al., 1997; Beaumont et al., 2001; Tapponnier et al., 2001; Zeitler et al., 2001a; Koons et al., 2002; Burbank et al., 2003, 2013; Thiede et al., 2005; Harris, 2006; Owen, 2008; Whipple, 2009; Ouimet et al., 2010; Iaffaldano et al., 2011; Copley et al., 2011).

The easternmost Himalaya is characterised by an arcuate geology with the suture zone between the Asian and Indian plates trending ~E–W in southeast Tibet, then bending about 180° in a mostly continuous fashion around the Namche Barwa–Gyala Peri massif before turning to a southeast and then southerly trend in western Myanmar (Fig. 2A).

This location corresponds to the north-eastern edge of the Indian plate indentor. There is widespread deformation and seismicity of rocks within this zone but the essential feature of the syntaxis is that the underlying Indian plate rocks have deformed into a sharp and northeast-terminating complex antiformal uplift that has lifted and bent the Asian plate above it (Burg et al., 1997) and caused the suture pattern to resemble a sharp bend in map view (Fig. 2C; Ding et al., 2001; Quanru et al., 2006; Kidd et al., 2006; Booth et al., 2009; Liu et al., 2011; Xu et al., 2012). Within the Indian plate of the syntaxis are high grade metamorphic rocks, locally at granulite facies (Liu and Zhong, 1997; Burg et al., 1998; Ding et al., 2001; Zhang et al., 2012a; Guilmette et al., 2011) and with very young cooling ages (Section 2.4).

Many studies have addressed the relationship between Cenozoic tectonic and erosion processes in the eastern Tibet–Himalayan region and the coeval development of topography and the regional drainage network (Gansser, 1966; Seeber and Gornitz, 1983; Harrison et al., 1992; Brookfield, 1998; Hallet and Molnar, 2001; Zeitler et al., 2001b; Clark et al., 2004; Seward and Burg, 2008; Robl et al., 2008; Cina et al., 2009; Ouimet et al., 2010; Chirouze et al., 2013; Lang and Huntington, 2014; Zeitler et al., 2014; Bracciali et al., 2015). Clark et al. (2004) showed that a number of river courses have been modified by progressive deformation of this region and the eastward extrusion of the eastern Asian plate.

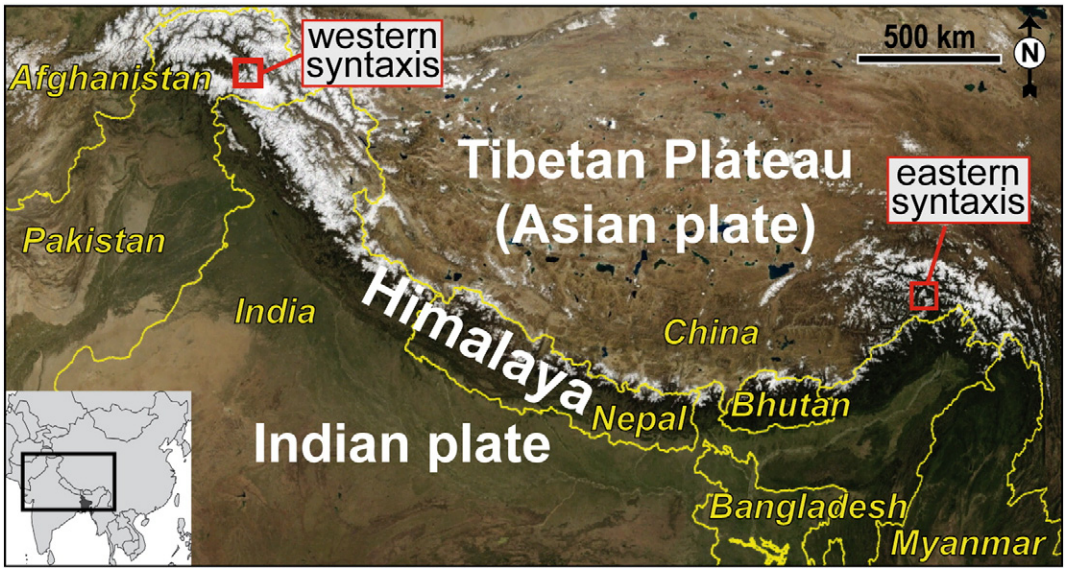

Fig. 1. General view of the Himalaya and its syntaxial terminations. The Himalayan orogen is the result of the collision between the Asian and Indian plates. National boundaries and main geological elements are superimposed on a NASA (www.nasa.gov) Landsat 7 image. Inset shows the location of the figure within eastern Asia.

The main river in the eastern Himalaya is the Brahmaputra, with a catchment area of 580,000 km^2 and an average erosional flux of ~1×10^9 t/yr (Galy and France-Lanord, 2001). The river originates in southern Tibet as the Yarlung Tsangpo and is called the Siang as it flows into the Indian plain. With the Ganges, which it joins before emptying into the Bay of Bengal (Fig. 2), the Brahmaputra is the main carrier of the erosion products of the central–eastern Himalaya (Galy et al., 2010). Current erosion rates averaged over the area of the entire Brahmaputra catchment are estimated to be ~2.9 mm/yr (Galy and France-Lanord, 2001).

The Yarlung Tsangpo after flowing eastward along the India–Asia suture with a low gradient cuts a peculiar and tortuous course across the eastern Himalayan syntaxis (Fig. 2). Here it carves a canyon that has up to 5.6 km of local relief (Korup et al., 2010) with glaciers terminating as low as ~3000 m elevation beneath the Namche Barwa (7782 m) and Gyala Peri (7294 m) massifs (Fig. 3). As a result, although the eastern Himalaya has peak elevations lower than the central Himalaya, it boasts amongst the highest topographic relief on Earth. As the river exits the plateau through this gorge with the Namche Barwa and Gyala Peri peaks on either side, it bends its course by nearly 180° (Fig. 2; the "Big Bend" of Zeitler et al., 2014 and references therein), locally crossing the structural grain of the orogen but largely following the curved syntaxial geology. This peculiar drainage pattern has been interpreted as resulting from one or more river capture events including the capture of the Yarlung Tsangpo drainage by the Brahmaputra (e.g. Seeber and Gornitz, 1983; Brookfield, 1998; Clark et al., 2004; Stüwe et al., 2008; Bracciali et al., 2015). The distortion by the developing syntaxis of an antecedent (with respect to the uplift of the syntaxis; Seward and Burg, 2008; Lang and Huntington, 2014) Yarlung Tsangpo–Brahmaputra in the last 4 Ma has also been suggested (Seward and Burg, 2008).

A further striking feature of the syntaxial region occurs along the "Big Bend", where an impressive knickzone has developed, with a drop in downstream river level of ~2 km along a reach of only ~200 km (Zeitler et al., 2001b), resulting in one of the deepest gorges in the world. Modern erosion rates suggested to be as high as 10 mm/yr or more (Burbank et al., 1996; Singh, 2006; Stewart et al., 2008; Enkelmann et al., 2011) testify to the most rapid erosional exhumation recorded anywhere (Finlayson et al., 2002; Seward and Burg, 2008).

The syntaxial area, despite comprising only ~2% of the vast drainage basin of the Yarlung Tsangpo covering southern Tibet and the eastern Himalaya (Stewart et al., 2008), alone supplies an estimated ~50% of the bulk sediment flux of the Brahmaputra (Singh and France-Lanord, 2002; Garzanti et al., 2004; Stewart et al., 2008; Lang et al., 2013; up to 70% according to Enkelmann et al., 2011). High exhumation rates for the eastern syntaxis are supported by exceptionally young bedrock and detrital mineral cooling ages of different isotopic systems (e.g. Burg et al., 1997; Seward and Burg, 2008; Finnegan et al., 2008; Stewart et al., 2008; Booth et al., 2009; Enkelmann et al., 2011. See Section 2 for a comprehensive description of these data).

The striking geological and geomorphological features of the eastern syntaxis and the mechanisms and processes leading to its development have generated wide interest and debate amongst the Earth science community that has produced a large number of studies and publications. These include and combine: mapping and structural analysis (Quanru et al., 2006; Kidd et al., 2006; Liu et al., 2011; Xu et al., 2012), igneous and metamorphic petrology (Liu and Zhong, 1997; Burg et al., 1998; Ding and Zhong, 1999; Ding et al., 2001; Guilmette et al., 2011; Zhang et al., 2010a, 2012a; Zeng et al., 2012; Palin et al., 2014), seismology (Sol et al., 2007), bedrock and detrital geo- and thermo-chronology (Burg et al., 1997; Booth et al., 2004, 2009; Seward and Burg, 2008; Finnegan et al., 2008; Xu et al., 2010; Enkelmann et al., 2011; Xu et al., 2013; Lang and Huntington, 2014; Lang et al., 2016), geomorphology (Korup and Montgomery, 2008; Korup et al., 2010; Larsen and Montgomery, 2012; Lang et al., 2013; Wang et al., 2014) and numerical modelling of surface and lithospheric processes (Burg and Podladchikov, 1999, 2000; Burg and Schmalholz, 2008; Robl et al., 2008; Stüwe et al., 2008).

Despite intensive study, profound questions remain concerning the timing and cause of the exceptionally rapid exhumation in the syntaxis. Many explanations have been advocated, such as structural buckling (Burg et al., 1997) due to contraction in the corner of the acute indentor of the orogen or fluvial erosion-driven tectonic uplift and incision (the "tectonic aneurysm" model of Zeitler et al., 2001a; see also Koons et al., 2002; 2013). The latter model suggests that focused, very rapid erosion has partially removed cold, strong upper crust, facilitating a doming of upper crust because of local flow of weaker lower crust with ductile behaviour in the region of maximum erosion (hence the "aneurysm", in the sense of "a self-sustained failure of a normally strong boundary", Zeitler et al., 2001b). This is suggested to generate a self-sustaining feedback arrangement between erosion, deformation and rock uplift. In this interpretation, metamorphism, partial melting and focused deformation (related to the evolving indentor corner) began at ~10 Ma (the time when the southeastern Tibetan Plateau was uplifted, Zeitler et al., 2014) and likely remained active due to feedback between these

processes and erosion (Zeitler et al., 2014). The initial deformation along the Namche Barwa antiform and the coincidence of extreme stream power associated with the significant "Big Bend" knickzone along the Yarlung Tsangpo (a long-lived, 5 to 10 Myr, feature in Zeitler and coauthors' interpretation; see also Koons et al., 2013) led to the focused rock uplift at Namche Barwa.

In its early formulation (Zeitler et al., 2001a), the model suggested the capture of an ancestral Yarlung Tsangpo by the palaeo-Brahmaputra in the latest Miocene as the trigger for the tectonic aneurysm (Zeitler et al., 2001b), with rapid exhumation of the syntaxis closely following and caused by increased river power via the capture, thought to have occurred several millions year ago (Brookfield, 1998). Zeitler et al. (2014), although suggesting that the coupling between deep river incision and advection of rocks at the Namche Barwa antiform would have been enhanced by possible capture of the Yarlung Tsangpo by the Brahmaputra, recognise that their data cannot provide any direct insight into whether the rapidly incising river valley required by the model was the result of a river capture event or achieved via an antecedent Yarlung Tsangpo flowing astride a deforming region of the crust. Although an attractive concept, a river capture mechanism as the trigger of the tectonic aneurysm appears untenable due to capture being ~18 Ma (Bracciali et al., 2015; Robinson et al., 2014), i.e. at least 10 Ma older than the supposed tectonic–erosion coupling (responsible for sustaining the rapid exhumation of the syntaxis) established following the capture event.

In an alternative analysis, Bendick and Ehlers (2014) performed 3D thermo-mechanical modelling of collision and deformation of geometrically-stiffened syntaxial indentors in subducting slabs. Their numerical predictions agreed with observed spatial variations in zircon fission track (FT) cooling ages <4 Ma and the variations in metamorphic grade exposed at the surface. The authors thus suggested that the extreme localised deformation and exhumation at the syntaxis may have been initiated by subduction geometry rather than an erosion–tectonic feedback mechanism and that a positive feedback between erosion, thermal structure and deformation only established afterwards.

The recent discovery by Wang et al. (2014) of an incised and sediment-filled Yarlung Tsangpo canyon upstream of the gorge (the infilling of which began at least 2.5 Ma) suggests that the incision and steepening of the gorge was the result of the uplift not its cause.

The studies by both Bendick and Ehlers (2014) and Wang et al. (2014, 2015) consider that it is unlikely that feedbacks between erosion and tectonics are the *primary* cause for the exceptionally rapid exhumation that is observed at the eastern syntaxis.

Past exhumation rates for the eastern syntaxis have been variably suggested to be: 10 mm/yr between 3.5 and 3 Ma and 3–5 mm/yr since 2.2 Ma (Burg et al., 1997), subsequently revised to a maximum of 2 mm/yr for the last 2.5 Myr (Seward and Burg, 2008); 4–8 mm/yr over the past 0.6 Myr (Stewart et al., 2008); 5–10 mm/yr for up to 10 Ma within the Namche Barwa massif (Zeitler et al., 2014, based on the petrologic and geochronological constraints of Booth et al., 2009), the latter being excessive with its implied removal of >50 km of rock when P–T equilibration suggests no more than 35–40 km of maximum burial. Enkelmann et al. (2011) identified spatial variations in denudation rates, being generally >2 mm/yr over the past 1 Myr in the south/

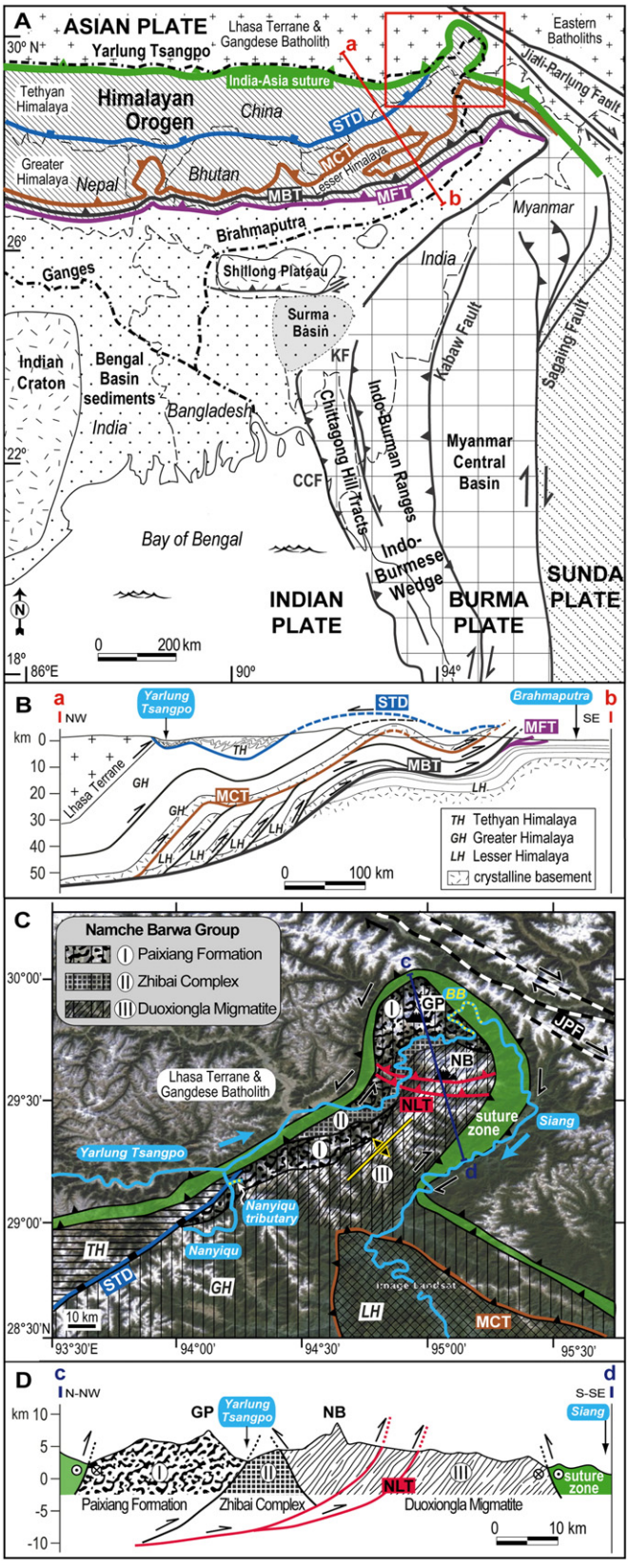

Fig. 2. Schematic geological maps and cross sections of the study area. A: Geological map of the Indo-Burman region in Eastern Asia showing the Asia, India, Burma and Sunda Plates and their main tectonic boundaries. The India–Asia suture separates the Lhasa Terrane intruded by the Gangdese Batholith from the Indian Plate to the south. This includes the Himalayan Orogen (of which the central-eastern part is shown), the Indian Craton and the Bengal Basin sediments. The location of the Surma Basin, national country boundaries and the Yarlung Tsangpo–Brahmaputra and Ganges River drainages is also shown. The Yarlung Tsangpo flows eastwards along the suture and after crossing the eastern Himalayan syntaxis sharply bends south as the Siang and then Brahmaputra River in the Assam plains. The red boxed area is shown in more detail in panel C. B: Schematic cross section of the eastern Himalaya along line a–b shown in panel A. C: Main features of the syntaxial area superimposed on a Google Earth Landsat Image. D: Schematic cross section of the northern part of the eastern syntaxis along line c–d shown in panel C. STD: South Tibetan Detachment Fault; MCT: Main Central Thrust; MBT: Main Boundary Thrust; MFT: Main Frontal Thrust; TH, GH and LH: Tethyan, Greater and Lesser Himalaya; NLT: Nam–La Thrust; JPF: Jiali–Parlung Fault; BB: "Big Bend" of Zeitler et al. (2014); GP and NB: Gyala Peri and Namche Barwa massifs.
Maps and cross sections redrawn after Najman et al. (2012), Maurin and Rangin (2009), Zeitler et al. (2014), Yin et al. (2010a), Xu et al. (2012), Ding et al. (2001).

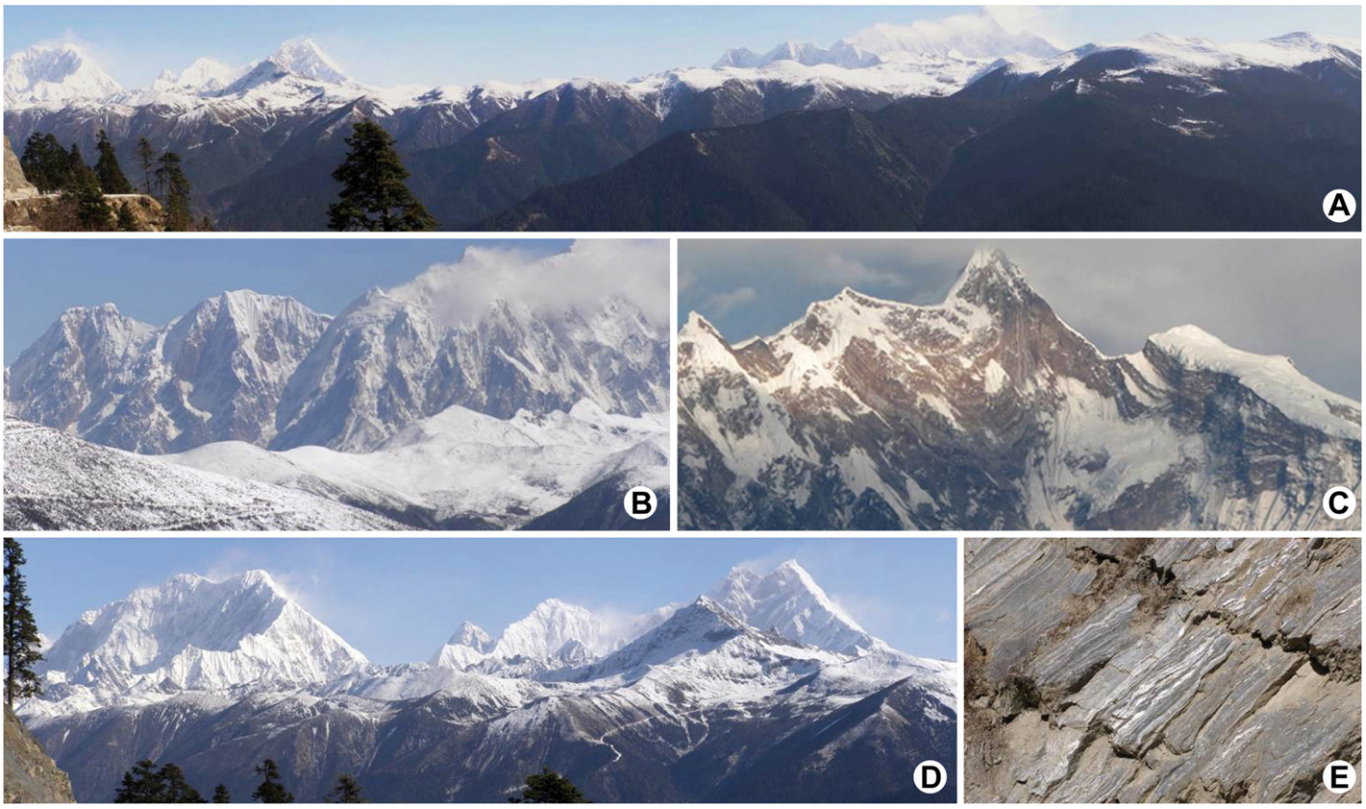

Fig. 3. Photographs of the eastern syntaxial area. A: Panoramic view of the eastern syntaxis from the Gyala Peri massif (left) to the Namche Barwa massif (right) looking east-southeast; B: close-up view of the left-hand part of the Namche Barwa massif showing strong layering in gneiss dipping to the left (north-eastern dip); C: view of Namche Barwa showing prominent synclinal fold on face with other less obvious upright folds to its left and right (courtesy summitpost.org); D: the Gyala Peri massif seen from the west consisting of Tiba Kangri on the left and Gyala Peri on the right; E: mylonitic migmatitic para- and ortho-gneiss of shear zone on the west side of the Namche Barwa massif (width of image ~3 m). Photos taken by R Parrish.

central part of the antiform (8 mm/yr at the Namche Barwa–Gyala Peri massif) but lower in the northern and western areas of the antiform (respectively 1 and 0.6 mm/yr). Based on a detrital thermo- and geo-chronological study of foreland Himalayan deposits, Lang et al. (2016) suggested an increase of rock exhumation rates within the eastern syntaxis by a factor of 5–10 between 7 and 5 Ma and sustained extremely rapid exhumation rates (>5–10 km/Myr) since ~5 Ma. Lang et al. (2016) did, however, note that onset of rapid exhumation may have begun earlier, as their lower boundary is not well constrained.

As can be inferred from the variation of ages from different thermochronometers as a function of changes in position in time and space, and the difficulties in estimating long-term denudation rates, in the syntaxial region there may be considerable spatial and temporal erosion rate variability.

A key remaining question concerns the time when exceptional exhumation of the syntaxial region began. On the basis of bedrock geo- and thermo-chronological studies, suggestions of a Late Miocene–Pliocene age have been put forward (Seward and Burg, 2008; Booth et al., 2009; Zhang et al., 2012a; Xu et al., 2012; Zeitler et al., 2014; Palin et al., 2014).

In this study we complement this kind of approach by testing the erosional response to the uplift. We focus our detrital study on the sedimentary archive of the palaeo-Brahmaputra: the Surma Basin in Bangladesh, a northern domain of the Bengal Basin. The Surma Basin preserves key information on the erosion of the eastern Himalaya including the first arrival of Himalayan-derived detritus at the Eocene–Oligocene boundary (Najman et al., 2008) and the further addition of Transhimalayan input via the capture of the Yarlung Tsangpo since the Early Miocene (Bracciali et al., 2015). Deposition of palaeo-Brahmaputra river deposits in this basin continued until the latest Neogene, when the Brahmaputra, due to the topographic growth of the Shillong Plateau and the coeval westward encroachment of the adjacent basin-bounding Indo-Burman Ranges (IBR) was diverted west of the plateau (Najman et al., 2016). In the Pleistocene, the locus of Brahmaputra deposition shifted west to the current Bengal Fan thus interrupting the direct source-to-sink connection between the syntaxis and the Surma Basin (Najman et al., 2016).

The ability of a bulk detrital sample to be representative of its hinterland source(s) depends on various factors (Johnsson and Basu, 1993; Morton and Hallsworth, 1999; Weltje and von Eynatten, 2004; Garzanti et al., 2009; Andò et al., 2012; von Eynatten and Dunkl, 2012; Bracciali et al., 2007, 2014; Malusà et al., 2015): i) the relative size of the sources within the drainage basin; ii) the variable erosion rates within the drainage basin, in turn affected by tectonic and climatic processes; iii) the fertility of each source (ability to generate sufficient grains of a specific mineral phase of a certain age or composition so to allow the identification of that source in the detritus, cf. Moecher and Samson, 2006); and iv) the mechanical and chemical behaviour of the detrital components of the sample when subject to erosion, transport, depositional and post-depositional processes. Key to a successful provenance study is thus the choice of appropriate provenance proxies, i.e. properties of the hinterland source that vary according to the nature of the source, that can survive surface and burial processes and that we can measure. In this study we apply a multi-chronometer approach (U–Pb dating of zircon and rutile, Ar–Ar dating of white mica and zircon fission track, ZFT, dating) in order to track crystallization and cooling events that occurred in the hinterland sources (with ZFT dating and zircon U–Pb dating applied to different mineral grains). By using different mineral phases (zircon, rutile and white mica) we enhance our possibilities to identify rock sources of variable composition. Importantly, large part of our study relies on zircon and rutile that are ultra-stable heavy minerals (Morton and Hallsworth, 1999, and references therein).

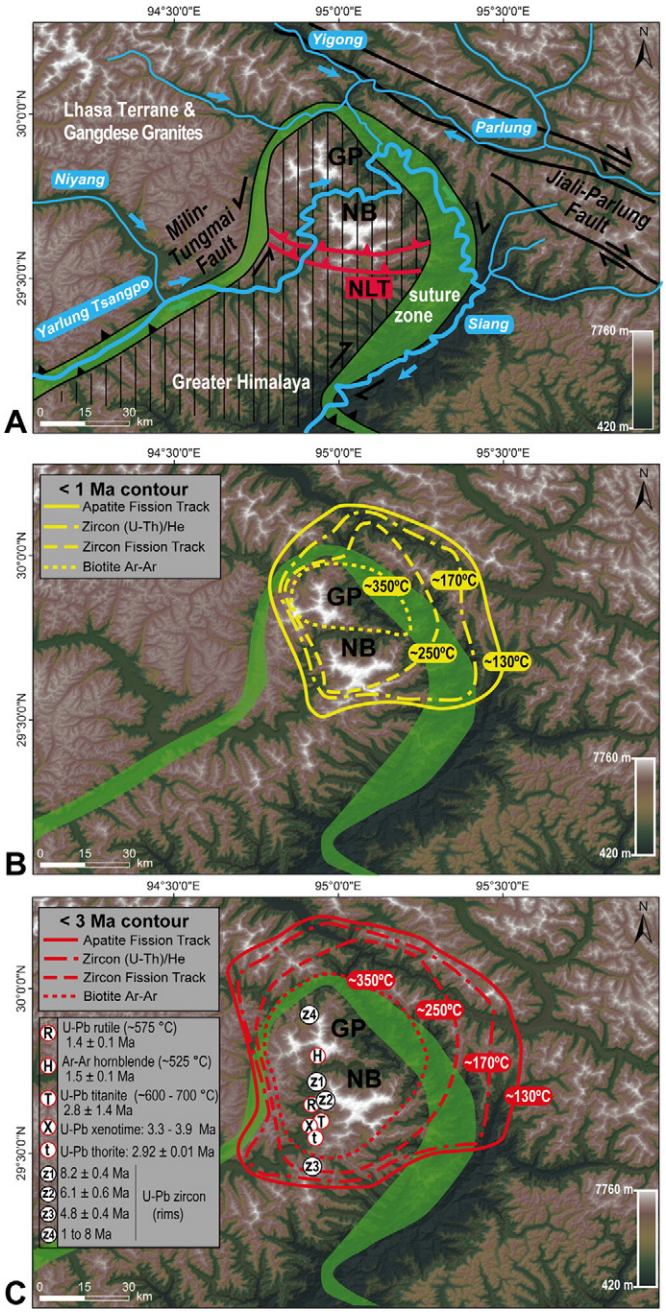

Fig. 4. Thermal state of the eastern Himalayan syntaxis in the last few Ma superimposed on a SRTM (Shuttle Radar Topography Mission) DEM V4 image at 90 m resolution (released by NASA, generated through interferometric processing of C-band (5.6 cm wavelength) radar imagery acquired in February 2000 and made available by srtm.csi.cgiar.org). Grid coordinates referenced to the WGS84 datum. A: Main tectonic elements and main drainages of the syntaxial region (cf. Fig. 2C); NB: Namche Barwa massif; GP: Gyala Peri massif; NLT: Nam–La Thrust. Light blue arrows indicate river flow direction. B: Contour lines of bedrock palaeo-T at <1 Ma. C: Contour lines of bedrock palaeo-T at <3 Ma. Contour lines have been drawn based on spatial distribution of published cooling mineral age data (AFT, (U–Th)/He Zircon, ZFT and Ar–Ar biotite (Supplemental Fig. A4; data from: Burg et al., 1998; Seward and Burg, 2008; Stewart et al., 2008; Enkelmann et al., 2011; Zeitler et al., 2014). Additional U–Pb and Ar–Ar bedrock age data (and the closing T of the corresponding isotopic system, see main text for details) are also plotted; data from: R: this study (Supplemental Table A3); H: Liu et al. (2006); T: Booth et al. (2009); X, t: Burg et al. (1997); z1: Zhang et al. (2012a); z2: our unpublished data; z3: Xu et al. (2012); z4: detrital zircons from glacial float, Zeitler et al. (2014).

Potential limitations in particular of ZFT and white mica Ar–Ar chronometers in defining the true constituent age components of the source(s) will be addressed in Sections 4.1 and 4.2 when discussing the results of this and other published studies. By using isotopic systems (U–Pb, Ar–Ar and FT dating and other published low temperature ages) sensitive to different temperatures (from >700 °C down to ~<150 °C) we are able to track crystallization and cooling events for the first ~20 km of the upper crust.

We first apply our dating tools to modern river sands from the Brahmaputra drainage to show how the unique thermochronological fingerprint of the fast-exhuming eastern syntaxis can be tracked downstream of the syntaxis in the Brahmaputra sediments of the Assam plains. In doing so, we integrate our data with a compilation of published modern detrital chronology from the eastern Himalayan region (Section 5). We also provide new U–Pb rutile bedrock data to better constrain the higher-T portion of the cooling path of the syntaxial rocks, and we document ~1 Ma rutile cooling ages, the youngest ever dated.

Input from a rapidly exhuming and eroding syntaxis would be identified in the palaeo-Brahmaputra sedimentary record by the appearance of mineral grains with very short lag times (the difference between the mineral cooling age and the host sediment depositional age). Such an appearance, followed by increasing abundance in the sedimentary record, would constrain the minimum age of accelerated erosion in the eastern syntaxis. We express caution here since a confounding factor in uniquely solving this question is the difficulty of recognising an early incipient erosional signal, discussed further in Section 6.

We also use new and existing data on bedrock and detrital cooling ages and rates with a simple numerical model of heat flow and erosion to constrain the range of possible exhumation scenarios that are consistent with the data.

With the tectonic aneurism model challenged by recent studies (Bendick and Ehlers, 2014; Wang et al., 2014, 2015) we then speculate on the mechanism of rapid uplift within the eastern Himalaya and the geological structure of the syntaxis produced by this late Neogene event.

2. Geological framework and previous chronological constraints

2.1. General geological framework

The western and eastern syntaxial orogenic bends of the Himalaya (Fig. 1), respectively named Nanga Parbat and Namche Barwa after the highest peaks within them, manifest the progressive indentation of Indian lithosphere into Asia (Wadia, 1931) as a consequence of continued convergence and continental collision since ~50 Ma (Garzanti et al., 1987; de Sigoyer et al., 2000; Najman et al., 2010; Meng et al., 2012).

The Yarlung Tsangpo Suture Zone separates the Indian plate from the Asian Plate (Fig. 2A). North and south of the suture, respectively lie the Lhasa Terrane (intruded by the Jurassic–Paleogene Transhimalayan Andean-type continental arc; Chu et al., 2006) and the Tethyan Himalaya (TH, Paleozoic–Eocene sedimentary succession deposited on the northern passive margin of India). The South Tibetan Detachment zone (STD) separates the TH from the Greater Himalaya (GH, mostly Neoproterozoic metasedimentary rocks at amphibolite facies). The Main Central Thrust (MCT) separates the latter from the Lesser Himalaya (LH, mostly Precambrian to Paleozoic unmetamorphosed or low-grade Indian crust material (see Hodges, 2000 and Yin et al., 2010a for a review of Himalayan geology). The Main Boundary Thrust (MBT) separates the LH from the foreland basin. A cross section showing the stacking of these unit south-west of the syntaxis is shown in Fig. 2B.

The eastern syntaxial termination of the Himalayan orogen has two components. The larger is expressed by the topographic depression in Assam along the floodplain of the Brahmaputra River with the main NE-trending Himalaya to the north, the broad arc of topography and geological trends to its east, and the southwest- to south-trending IBR to its south (Fig. 2A). This larger arc defines broadly the shape of the

north-eastern Indian craton as it collided and subducted beneath eastern Asia.

Within this larger arc lies a much tighter and smaller arc defined by the trend of the suture zone as it bounds on three sides the Indian plate rocks with the Namche Barwa and Gyala Peri massifs in its core (Figs. 2C and D). This smaller syntaxis is the subject of this study as it is the area where very high exhumation rates are taking place.

2.2. Structure and geology of the eastern Himalayan syntaxis

The structure of the eastern syntaxis is an elongate (~40 km by ~120 km) steep-sided anticline plunging steeply dominantly to the northeast and less steeply to the southwest, as described by Burg et al. (1997; 1998).

Whilst relatively poorly mapped and understood in detail, the structure of the northern part of the syntaxis has been addressed by many authors and is characterised by major folds, one or more major thrust faults, thick mylonite zones around the syntaxis and adjacent to the suture zone boundary, and both thrust and strike-slip bounding faults/shear zones. To the northeast of the arcuate syntaxial suture zone trace is the dextral Jiali–Parlung fault zone (Fig. 2) for which Lee et al. (2003) constrained the timing of the main stage of right-lateral motion between 18 and 12 Ma.

From periphery to core, three main lithotectonic units comprise the syntaxial area (Fig. 2C): the Asian plate Gangdese unit (belonging to the Lhasa Terrane of the Asian plate and the associated Transhimalayan Arc), the Yarlung Tsangpo suture zone and the GH unit of the Indian plate (Namche Barwa Group) in the core of the antiform (Burg et al., 1997; Liu and Zhong, 1997; Ding et al., 2001; Quanru et al., 2006).

These units are separated by strike-slip faults and shear zones including extensive and thick mylonites that define an inverted U-shaped pattern in map view. Various authors have inferred that the sense of shear on the northeast-trending bounding shear zones is left-lateral on the west and right-lateral on the east (Burg et al., 1998; Ding et al., 2001; Booth et al., 2009; Zeitler et al., 2014; Palin et al., 2014). The boundary zone between GH and the suture zone rocks comprises substantial quartzo-feldspathic mylonites (Fig. 3E) of probable GH affinity and for the most part at amphibolite facies metamorphic grade (though retrogressed).

The Yarlung Tsangpo Suture Zone in the syntaxial area (Fig. 2C) is a 2–10 km wide continuous shear zone, wider in the east than in the west, consisting of rocks highly deformed and metamorphosed under greenschist-facies conditions that include ultramafic rocks, meta-gabbro, meta-basalt and meta-quartzites (possibly meta-cherts). According to Quanru et al. (2006) these represent a dismembered ophiolitic suite. Booth et al. (2009) recognised remnants of the suture zone in amphibolitic mylonites containing blue-green amphiboles but also observed staurolite–kyanite-bearing metasediments that they interpreted to be part of the TH.

The Gangdese unit in the syntaxial area includes the middle- to high-grade metamorphic Nyingchi Group and Bomi Groups of the Lhasa Terrane, intruded by Gangdese and other granites. These were mainly emplaced in the Late Cretaceous–Paleocene (Burg et al., 1998; Booth et al., 2004; Zhang et al., 2010b; Guo et al., 2011, 2012). Post-collisional 25–30 Ma granites intruding the Lhasa Terrane along the western and eastern margin of the syntaxis (Booth et al., 2004; Zhang et al., 2010b; Guo et al., 2011; Pan et al., 2012) have been interpreted as adakitic melts derived from partial melting of thickened lower crust of the Lhasa Terrane (Zhang et al., 2010b; Pan et al., 2012), in analogy with other adakites from southern Tibet (Chung et al., 2003, 2009). Some are muscovite-bearing and resemble the GH leucogranites in terms of lithology (Zhang et al., 2010b).

The Namche Barwa Group (Quanru et al., 2006), structurally the lowest of the three units, is part of the Indian plate and is mostly equivalent to the GH of the main Himalaya (though some older basement gneisses are likely extensive). The Namche Barwa Group (Fig. 2C) includes felsic para- and orthogneiss containing sporadic lenses of high-P granulite and minor amphibolite and clinopyroxenite (Zhibai Complex), migmatitic gneiss and amphibolite (Duoxiongla migmatite) and felsic gneiss with subordinate marble (Paixiang Formation). The affinity of the high-P rocks with the GH unit is suggested by Paleoproterozic protoliths, as constrained by U–Pb zircon dating and Nd isotopic data (Xu et al., 2010; Liu et al., 2011; Zhang et al., 2012a; Guo et al., 2016).

The main structural features and tectonic boundaries between the different lithotectonic units are variably mapped on the existing geological maps of the syntaxial area, especially in its inaccessible, highest elevation core (e.g. Ding et al., 2001; Quanru et al., 2006; Kidd et al., 2006; Booth et al., 2009; Liu et al., 2011; Xu et al., 2012). In all maps, a few km south of the Namche Barwa peak a main thrust fault system is identified, mapped as a mainly ~E–W trending, N-dipping fault named Nam–La Thrust (Liu and Zhong, 1997; Ding et al., 2001; Quanru et al., 2006; Kidd et al., 2006; Booth et al., 2009; Zeitler et al., 2014; Fig. 2C). The Nam–La (or Namula) thrust system is regarded as a very important tectonic boundary within the syntaxis by Liu and Zhong (1997). Citing the early mapping by Chinese geologists, Liu and Zhong map the thrust as a E–W trending continuous structure cropping out for ca. 20 km south of the Namche Barwa peak and describe it as "a set of moderately north-dipping structures that displaced the granulite facies rocks southwards over the amphibolite facies thrust rocks". As such the thrust belongs to an early phase of deformation within the syntaxis and is associated with east-striking folds. According to Ding et al. (2001), the thrust acts as the southern boundary of a pop-up structure with the Namche Barwa massif at its core (Fig. 2D), in analogy with a similar structural model suggested for the western Himalayan syntaxis (Schneider et al., 1999). Craw et al. (2005) and Kidd et al. (2006) recognise and map the Nam–La Thrust as an arcuate thrust zone, E-trending south of the Namche Barwa massif and passing into the shear and fault zone along the suture bounding the syntaxis to the west (Fig. 2C). Zeitler et al. (2014) suggest that the Nam–La Thrust remains an active structure likely accumulating strain, although it is virtually aseismic (at least during a 16-month observation period; Sol et al., 2007). In Liu et al. (2011), Xu et al. (2012) and a recent compilation by Palin et al. (2014) based mainly on various Chinese research contributions, the Nam–La thrust (also named Upper or DF2 Thrust) is somewhat different in terms of its trace and complexity and is mapped as the tectonic boundary between the higher grade rocks to the north and the lower grade migmatites to the south. As such it continues within the southern syntaxis as an ~SW trending structure.

Despite these differences, a similar fundamental structure results from both interpretations, with a south- to southeast-vergent thrust emplacing folded deeper rocks with an overall domal geometry upon panel(s) of rock that dip more broadly and which can be traced with continuity to the southwest into the main part of the Himalaya. Clearly much more structural and lithological mapping is needed to refine this pattern further.

2.3. Metamorphic evolution of the eastern Himalayan syntaxis

The peak metamorphic conditions in the core of the antiform have been variably estimated at 17–18 kbar and ~890 °C (Liu and Zhong, 1997), 8–10 kbar and 720–760 °C (Burg et al., 1998); 14–18 kbar and 750–850 °C (Ding et al., 2001); 11–14 kbar and 800–950 °C (Booth et al., 2009), 14 kbar and 825 °C (Guilmette et al., 2011). The age of peak metamorphism for the high-P granulites has been estimated as 16 ± 2 Ma (Burg et al., 1998), 40 Ma (Ding et al., 2001), 37–32 Ma (Zhang et al., 2010b) or 24 Ma (Xu et al., 2010). An ~24 Ma metamorphic event is also recorded by a Ca-rich granulite-facies leucosome likely generated by melting of the host metapelite at high pressure (Zeng et al., 2012). Palin et al. (2015) present a summary of most of these data along with an additional P–T–t path within the margin of the syntaxis. As of yet there is no definitive geochronological evidence of uppermost

amphibolite facies metamorphism persisting into the Plio-Pleistocene, but this has yet to be thoroughly investigated.

Retrograde mineral assemblages overprinting the high-P prograde paragenesis of the Namche Barwa massif granulites provide constraints on the exhumation path towards the surface of these rocks (Liu and Zhong, 1997; Ding et al., 2001; Xu et al., 2010; Guilmette et al., 2011). Guilmette et al. (2011) modelled, for an anatectic kyanite-bearing paragneiss from the Zhibai Group west of the Namche Barwa peak, an ~isothermal path from lower crustal conditions higher than 14 kbar and ~825 °C to middle crust conditions at ~9 kbar and 800 °C. The peak metamorphic event was accompanied by biotite-dehydration melting in the kyanite stability field. This decompression is thought to be Miocene in age.

A much younger phase of volumetrically-limited melt production is recorded by 3–10 Ma U–Pb dates of granitic dykes and leucosomes occurring in the Namche Barwa–Gyala Peri massif (Booth et al., 2004; Zeitler et al., 2014). Zircon rims as young as ~1 Ma occur in granitic, pegmatitic and aplitic glacial float from the Layo glacier on the northern flank of the Gyala Peri (Zeitler et al., 2014). These rims correspond to a series of oscillatory cathodoluminescence (CL)-zones within each crystal indicating multiple <10 Ma episodes of zircon growth and have been interpreted to have formed in response to fluid infiltration and/or partial melting during decompression. The timing of emplacement of these granitic melts overlaps the ~5–8 Ma U–Th–Pb dates (weighted averages) of monazites separated from the matrix of metapelitic rocks (Booth et al., 2009). U–Pb titanite dates from the core of the syntaxis are 4.9 ± 3.9 and 2.8 ± 1.4 Ma (lower intercepts with Concordia of alignments of datapoints with variable common Pb content), whilst titanite and monazite outside of the syntaxis are 20 Ma and older. Booth et al. (2009) estimated a pressure decrease of ~5 kbar during growth of garnet north of the Gyala Peri peak over a period of several million years, as indicated by P–T estimates for the core (8.3 kbar and 800 °C) and the rim (3.5 kbar and 670 °C) of the garnet and in situ U–Th–Pb dates of monazite (~11 to 6 Ma) included in the garnet. This is in agreement with ~11 Ma concordant zircon rims (with a 17 Ma core) from mafic granulite boudins occurring within garnet–kyanite gneiss in the Zhibai Complex west of the Namche Barwa (Ding et al., 2001), corresponding to a moderate pressure (8–10 kbar and ~800 °C) high-grade metamorphic event. As we will report later (Section 4), rutile U–Pb dates range from ≥9 Ma in the southern part of the syntaxis antiform to as young as ~1.4 Ma within the area of youngest cooling ages.

Additional geochronological evidence for <10 Ma metamorphic events in the eastern syntaxis is provided by: 6–11 and 4–5 Ma monazites from migmatites respectively sampled north of the Gyala Peri peak and in the Yarlung Tsangpo gorge at an elevation of 2400 m (Liu et al., 2011); ~10 and 5 Ma zircon rims from mylonitic gneisses respectively north of the Namche Barwa peak and south of the Nam–La thrust (Xu et al., 2012); ~8 Ma rims of Paleozoic zircons from a calc-silicate rock metamorphosed under dominant amphibolite facies conditions west of the Namche Barwa peak (Zhang et al., 2012a).

2.4. Thermochronology of the eastern Himalayan syntaxis

The first recorded time constraints pointing to a very recent evolution of the Namche Barwa antiform were biotites as young as 1.2 Ma (determined by K–Ar dating) from migmatite gneisses within the inner Yarlung Tsangpo gorge, as opposed to biotites 18 Ma and older outside of the syntaxis (Zhang et al., 1981). Further studies by Burg et al. (1997, 1998) reported 3.9–3.3 Ma xenotime and 2.9 Ma thorite crystals from a leucosome layer interpreted to date the last anatectic event (~600–700 °C) in the syntaxis. Additionally, statistically equivalent FT zircon and apatite ages (central ages of ~2.5 and ~1.1 Ma) were determined in migmatites sampled at different elevations (2900 and 4100 m) within the Namche Barwa antiform. The lack of FT age variation with altitude, and the small range of crystallization ages indicated by xenotime and thorite were taken as evidence for very rapid exhumation at cooling rates of 100 °C/Myr or more. With the additional constraint of peak metamorphic conditions estimated for a garnet metapelite at 8–10 kbar and 720–760 °C and the 16.0 ± 2.5 Ma Sm–Nd isochron date for the garnet, Burg et al. (1998) proposed a decompression history associated with the growth of the Namche Barwa antiform. The modelled P–t path required a decrease of the exhumation rate from ~10 mm/yr between 3.5 and 3.2 Ma to 3–5 mm/yr since 2.2 Ma. As the antiform developed, a positive feedback between folding and erosion may have caused an acceleration of fold amplification, resulting in localised lithospheric uplift and exhumation under near-isothermal conditions and allowing for decompression melting (Whitney et al., 2004). The model was further refined by envisaging pure shear thickening and symmetric buckling as a means to accommodate shortening until, at a certain strain, an asymmetric thrust occurs on a crustal to lithospheric scale (Burg and Podladchikov, 2000) based on numerically modelled viscous shear heating (Burg and Schmalholz, 2008). The change to the thrusting mode within a few % shortening inhibits further fold amplification and lateral propagation that may account for the isolation of crustal-scale folds in continental lithosphere.

Seward and Burg (2008) integrated the earlier FT dataset of Burg et al. (1997) with new data from within and outside the core of the antiform. The new bedrock data showed that the young cooling was not limited to the core of the antiform, but zircon and apatite FT ages younger than 4 Ma and as young as 0.5 Ma occurred in a wider area delimited to the NW and the NE by the Milin–Tungmai and Jiali–Parlung Faults, respectively (Fig. 4A). Outside these fault bounds, the FT ages were systematically older (Fig. 2 of Seward and Burg, 2008; our Supplemental Fig. A4). This led to estimates of exhumation rates of ~2 mm/yr for the last 2 Myr for the whole area inside the fault bounds. Based on this finding and the earlier geochronological constraints on the vertical growth of the syntaxis via folding and efficient metamorphic decompression since 4 Ma, Seward and Burg refined their evolution model to include the Asian plate in the growth of the syntaxis. This was achieved via lateral expansion and associated erosion of the growing antiform towards and limited by the Jiali–Parlung Fault, as shown by the FT data. As a consequence, according to the authors an antecedent Yarlung Tsangpo–Brahmaputra was displaced, along with the suture, in a left-lateral sense along the exhuming north-plunging dome. This was thought to explain the U turn of the Yarlung Tsangpo course in the Namche Barwa–Gyala Peri massif area.

The bedrock thermochronology of the syntaxis is well represented in its erosion products, with ~45% of the detrital zircons in the modern river sediment load downstream from the Yarlung Tsangpo Gorge (at Pasighat in Arunachal Pradesh; cf. location S in our map of Fig. 5) belonging to a FT age population averaging 0.6 Ma (Stewart et al., 2008).

In Fig. 4 we infer the thermal state of the syntaxial area at <1 Ma (panel B) and <3 Ma (panel C) by drawing contour lines of equal T based on the spatial distribution of published thermochronological data (plotted on the maps of Supplemental Fig. A4) and the closure/annealing temperature (T_c) of the corresponding isotopic system. For the contour lines we took into account the following thermochronometers: fission tracks in apatite ($T_c \approx$ 75–125 °C; Wagner and Reimer, 1972; Laslett et al., 1987; Ketcham et al., 2007); (U–Th)/He in zircon ($T_c \approx$ 170–190 °C; Reiners et al., 2004); fission tracks in zircon ($T_c \approx$ 250 °C; Tagami et al., 1996) and Ar–Ar in biotite ($T_c \approx$ 350 °C; McDougall and Harrison, 1999). We note that with the exceptionally high cooling rate documented in this region in excess of 100 °C/Myr, the closure temperature applicable may be higher than listed above by up to 20–30 °C.

The closure temperature of rutile U–Pb has been estimated empirically (Mezger et al., 1989) and experimentally (Cherniak, 2010), but there is disagreement (>600 °C for experiments, ~500 °C for empirical studies in slowly-cooled terranes), as recently discussed on the basis of depth of Pb in rutile in the Ivrea zone by Smye and Stockli (2014), as well as the complication that cooling rate and grain size issues will influence closure temperature. Because this remains unresolved, we use a

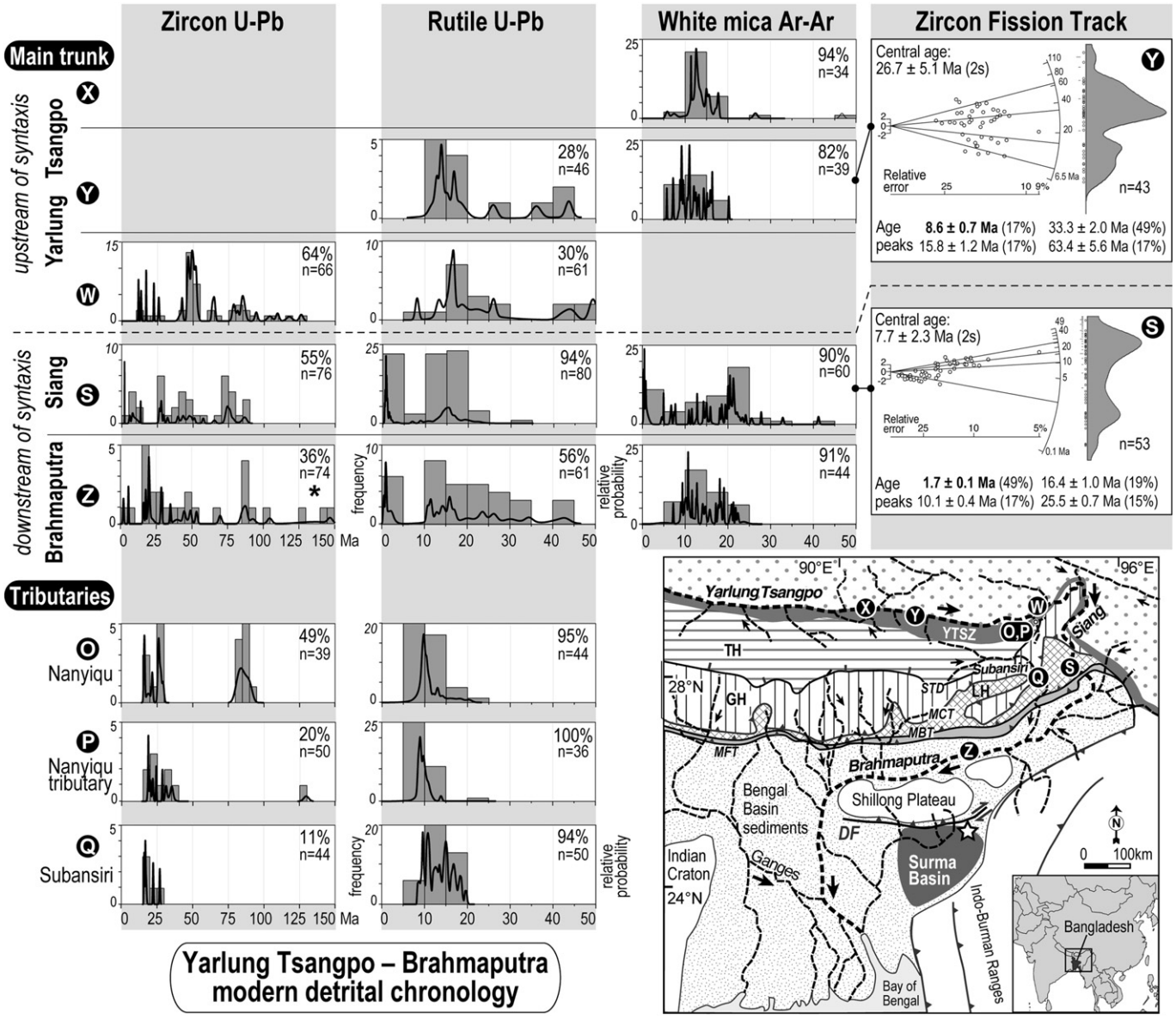

Fig. 5. New single grain detrital chronology of sand samples from the Yarlung Tsangpo–Brahmaputra modern drainage. U–Pb and Ar–Ar data are plotted as relative probability and frequency plots in the age range 0–150 Ma and 0–50 Ma; ZFT data are plotted as radial plots and kernel density estimate (KDE) plot, with central age and main age peaks ($\pm 1\sigma$) indicated for each sample. * indicates zircon U–Pb data of sample Z, from Bracciali et al. (2015). In U–Pb and Ar–Ar diagrams percentages indicate the proportion of grains younger than 150 and 50 Ma compared to n, the total number of: individual ablations after rejection of discordant zircon datapoints, individual ablations after the common Pb correction of discordant rutile datapoints and individual Ar–Ar ages of white mica grains. In ZFT diagrams n indicates the total number of grains per sample; percentages refer to the grains contributing to each age component (or "age peak"). U–Pb Concordia diagrams and relative probability–frequency plots showing the full age range of the samples are shown in Supplemental Figs. A2 and A3. The bottom-right panel locates the samples on a schematic geological map of the eastern Himalaya–Tibet region (inset locates main figure in eastern Asia). Locations of samples O and P are indistinguishable at this scale (cf. Figs. 9 and 2C). Black arrows indicate river flow direction. MBT: Main Boundary Thrust; MFT: Main Frontal Thrust; YTSZ: Yarlung Tsangpo Suture Zone; DF, CCF, KF, KaF and SF: Dauki, Chittagong Coastal, Kaladan, Kabaw and Sagaing Faults. The star locates our sampling area in the Surma Basin (bedrock sandstone samples of Fig. 6).

wide T range of 575 ± 75 °C when discussing the temperature significance of rutile in this study.

In Fig. 4C we also plotted bedrock data of the following higher-T chronometers to further constrain the thermal history of the syntaxial area: U–Pb in rutile (new data from this study, see Section 4; $T_c \approx 575 \pm 75$ °C, see summary of published studies in Bracciali et al., 2013 and Smye and Stockli, 2014); Ar–Ar in hornblende ($T_c \approx 525$ °C; McDougall and Harrison, 1999); U–Pb in titanite ($T_c \approx 600$–700 °C; Cherniak, 1993; Scott and St-Onge, 1995); U–Pb in xenotime and zircon (T the same as formation temperature, i.e. >700 °C; Dahl, 1997; Cherniak and Watson, 2000; Cherniak, 2006).

One of the interesting geological questions is whether the late Neogene (<10 Ma) metamorphism and limited partial melting within the syntaxis is related/caused by the rapid syntaxial exhumation or whether it is the youngest phase of the Himalayan metamorphism affecting the GH farther in the Himalayan hinterland, that in the syntaxis has been brought to surface "prior to its time" by an independent exhumation mechanism (i.e. Himalayan metamorphic rocks of this age occur elsewhere, but have not yet been unroofed by surficial or other processes). We will address this question later in Section 7.

2.5. The palaeo-Brahmaputra sedimentary record (Surma Basin)

The Surma Basin (Figs. 2A and 5), a sub-basin of the Bengal Basin in north-eastern Bangladesh, consists of sediments transported by the Brahmaputra and its ancestral river system to the margin of the Indian

continental margin since the Eocene (Lietz and Kabir, 1982; Johnson and Alam, 1991; Reimann, 1993; Uddin and Lundberg, 1998, 1999; Najman et al., 2008; Bracciali et al., 2015). The Surma Basin is bordered to the north by the Shillong Plateau, the only raised topography in the foreland of the Himalaya, consisting of Indian plate Precambrian basement partially overlain by Cenozoic sediments (Yin et al., 2010b). To the east the basin is bordered by the Cenozoic westward-propagating IBR fold and thrust belt which is responsible for the north–south trending folding in the Bengal Basin (Maurin and Rangin, 2009).

Our study focuses on both modern river sands along the course of the Brahmaputra and its tributaries (Fig. 5) and the Neogene Surma Basin deposits, for which a schematic stratigraphic section is presented in Fig. 6, where the samples are arranged in stratigraphic order with the exception of Dupi Tila sample 35 (from a different locality) whose stratigraphic position is not known relative to the other two Dupi Tila samples. A selection of images of sampling locations and key features of both modern and ancient deposits is presented in Fig. 7.

The Surma Basin is affected by ~N–S trending folding (Johnson and Alam, 1991) related to the frontal deformation zone of the IBR which propagated as far west as this location in the Pliocene (Maurin and Rangin, 2009; Najman et al., 2016). The anticline structures are evident in subsurface 3D map of top seismic reflector and thickness map of the Tipam Formation showing thinning of strata over anticlines (Najman et al., 2016). As a result of the folding, the Neogene deposits are exposed as a tilted succession in the sampling area (e.g. Figs. 7A and B).

In order to overcome the early lithostratigraphic correlation approach to dating (Evans, 1932) that proved problematic within a deltaic system with high rates of subsidence and rapid facies changes, the Neogene succession has been divided into biostratigraphically dated, seismically distinct, unconformity-bounded and regionally correlatable Megasequences (MS in Fig. 6; Najman et al., 2012). MS1 is equivalent to the Bhuban and Bokabil Formations (Surma Group), MS2 to the Tipam and Dupi Tila Formations.

In the Surma Basin the boundary between the marine-deltaic MS1 and the fluvial MS2 has been constrained by magnetostratigraphy at 3.5 Ma (Worm et al., 1998) in agreement with nannoplankton data (Najman et al., 2012). Magnetostratigraphy also constrains the top of MS2 at 1.4 Ma in the study area (Worm et al., 1998). The Early Pliocene age for the upper Bhuban Formation is indicated by stratigraphic (Lietz and Kabir, 1982) and magnetostratigraphic data (Worm et al., 1998). Below MS1, the Eocene–Early Miocene deltaic sandstone of the Barail Formation records the first major clastic influx from the Himalaya (Najman et al., 2008). The lower boundary of MS1 is constrained at <18 Ma by the occurrence of detrital white mica in uppermost Barail and lowermost Bhuban samples dated by Ar–Ar at 21 ± 3 (Najman et al., 2008) and 14 ± 4 Ma (this study), respectively. This is in agreement with prominent modes of Ar–Ar white mica ages of 16–18 Ma in Bhuban samples from well penetrations (Uddin et al., 2010), in which the youngest mica grains in three Bhuban samples of increasing stratigraphic depth are dated at 12.3 ± 0.6 Ma (upper Bhuban, well Beani–Bazar-1X; cf. well stratigraphy in Reimann, 1993), 16.8 ± 0.6 Ma and 19.3 ± 0.8 (lower Bhuban, well Fenchuganj-2; cf. well stratigraphy in Deb et al., 2014).

The clay mineralogy of the Paleogene to Neogene deposits in the Surma Basin indicates that burial temperatures were <200 °C (Najman et al., 2008). It follows that the isotopic clocks of our samples (ZFT and mica Ar–Ar ages) were not reset in the sedimentary basin and are indicative of thermochronological events in the source regions.

3. Samples and analytical methods

3.1. Sample details and preparation

This paper presents new U–Pb (zircon and rutile), Ar–Ar (white mica) and ZFT data on eight sand samples from modern rivers and streams belonging to the Brahmaputra drainage (Fig. 5). We also present new Ar–Ar and ZFT data from samples of the Surma Basin whose petrographic and whole rock isotopic composition, U–Pb zircon and rutile U–Pb provenance signatures were presented in Bracciali et al. (2015). (see Supplemental Table A1 for the geographic coordinates of all samples and Supplemental Fig. A1 for a map of sampling localities and schematic geology of the study area).

All the modern river sand samples from this study are variably enriched in a range of minerals (e.g. apatite, titanite, magnetite, tourmaline, epidote, allanite, monazite, garnet, kyanite) that reflect the erosion of the Himalayan orogen on the Indian Plate and/or the Transhimalayan Arc and Lhasa Terrane of the Asian plate (Bracciali et al., 2015). In addition to the detrital samples, we analysed rutile grains from two bedrock samples from the west of the Namche Barwa massif (location R in Fig. 4C). These are a mafic granulite (sample T604) from a boudin of mafic lithologies and a pelitic gneiss (sample T602) from the host rocks of the mafic granulite. Further metamorphic and geochronological details on the two samples can be found in Xu et al. (2010).

Zircon, rutile and white mica grains were isolated from the samples by mineral separation techniques at the NERC Isotope Geosciences Laboratory, Keyworth, making use of standard crushing, milling, dense liquid separation and Frantz magnetic separation. The subsequent analytical work focussed on grains larger than 0.1 mm and, for white mica, up to 2 mm.

Zircon and rutile samples were mounted in 25 mm epoxy resin discs and polished to expose the interior of the mineral grains. All zircons were CL-imaged prior to LA U–Pb work using a FEI Quanta 600 environmental scanning electron microscope (ESEM) equipped with a Centaurus CL detector at the British Geological Survey, Keyworth.

3.2. LA U–Pb dating of zircon and rutile

Laser ablation U–Pb data were collected at the NERC Isotope Geosciences Laboratory (NIGL), Keyworth, using either a 193 nm or a 213 nm wavelength laser ablation system coupled to a Nu Plasma HR multi-collector inductively coupled plasma mass spectrometer (MC-ICP-MS). U–Pb data are tabulated in Supplemental Tables A2 and A3 and the instrument parameters used during analysis are detailed in Supplemental Table A4.

The MC mass spectrometer has a specially designed collector block to allow simultaneous detection of all masses in the range 202–207, 235 and 238. The instrument was tuned at the start of each analytical session whilst aspirating a 500 ppt solution containing Tl (with isotopes 203 and 205) and ^{235}U introduced via a Nu Instruments DSN-100 desolvating nebuliser to assist with inter-element ratio normalisation. Ion counter(IC)-Faraday gains were determined for each of the three ICs using a weaker 100 ppt Tl–^{235}U solution, jumping the ^{205}Tl peak through each ion counter (IC) and comparing the equivalent Faraday signal.

Ablated sample material was transported from the laser cell into the MC-ICP-MS using a continuous flow of 0.6 l/min of He gas. Analysis was performed using the Time Resolved Analysis (TRA) mode of the Nu Plasma software with signals integrated excluding the first 3–5 s of data and the data normalised and uncertainty propagated offline using an in-house Excel spreadsheet. After an initial 30 s instrument baseline measurement and 30 s gas blank, individual analysis ablation times were 40 s for a run of 10–15 ablations. The simultaneous measurement of the ^{202}Hg signal allows correction for the isobaric interference of ^{204}Hg on ^{204}Pb during the ablation (assuming $^{204}Hg/^{202}Hg = 0.229887$). The Tl–$^{235}U$ solution was simultaneously aspirated in order to correct for mass spectrometer-related mass bias (Pb/Pb ratios using $^{205}Tl/^{203}Tl$, Pb/U ratios using $^{205}Tl/^{235}U$) at the time of analysis.

Uncertainties for the $^{207}Pb/^{206}Pb$ ratios were propagated using quadratic addition to combine the measurement uncertainty with a reproducibility component modelled to reflect increasing uncertainty with decreasing signal size. A minimum uncertainty of 0.5% (2σ) was

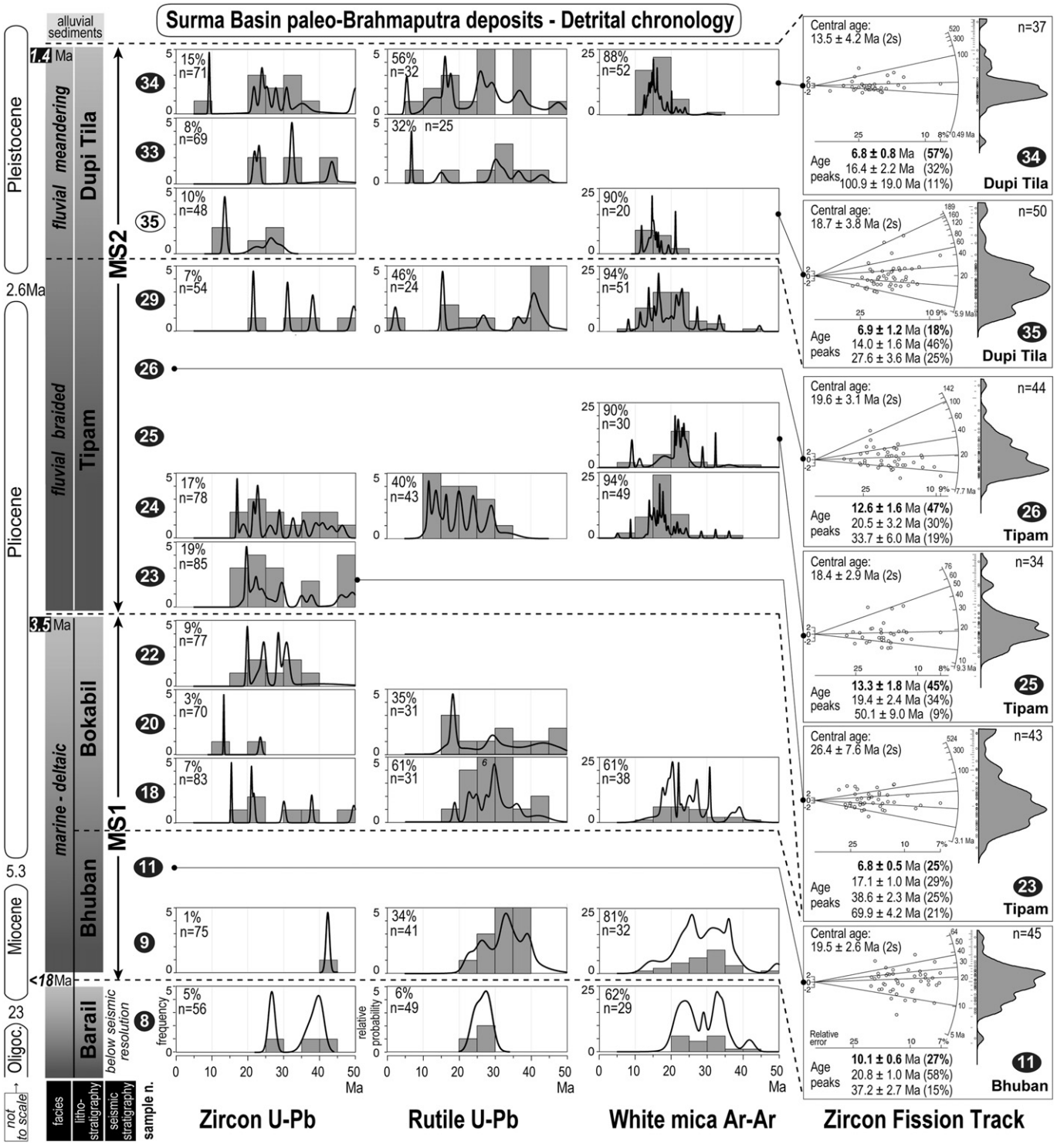

Fig. 6. Schematic stratigraphy and detrital single grain chronology of palaeo-Brahmaputra deposits from the Surma Basin. U–Pb zircon and rutile data from Bracciali et al. (2015); Ar–Ar data (with the exception of sample 8 from Najman et al., 2008) and ZFT data from this study (Supplemental Tables A5 and A6). Sample details can be found in Table A1. The stratigraphic boundaries are constrained with variable degree of confidence by biostratigraphy, magnetostratigraphy and detrital mineral dates (Bracciali et al., 2015). MS: Megasequence. Relative probability plots and frequency diagrams of zircon and rutile U–Pb data and Ar–Ar white mica data are plotted in the range 0–50 Ma. In U–Pb and Ar–Ar diagrams percentages indicate the proportion of grains younger than 50 Ma compared to n, the total number of: individual ablations after rejection of discordant zircon datapoints, individual ablations after the common Pb correction of discordant rutile datapoints and individual Ar–Ar ages of white mica grains. Relative probability and frequency plots showing the full age range of the samples are shown in Supplemental Fig. A5. ZFT data are plotted as radial plots and kernel density estimate (KDE) plot; n indicates the total number of grains per sample; central age and main age peaks ($\pm 1\sigma$, with percentages referring to the grains contributing to each peak) are also shown.

assigned to the $^{207}Pb/^{206}Pb$ ratio by default for ablations with high ^{207}Pb ion beams, to reflect the confidence in the ability of the multi-ion counting (MIC) set-up to accurately reproduce any one value. $^{206}Pb/^{238}U$ uncertainties were propagated in a similar way utilising the measurement uncertainty and the reproducibility of the ablation reference material used.

During each analytical session both zircon and rutile reference materials were measured between each group of unknowns to verify

that $^{207}Pb/^{206}Pb$ ratios were correct, to determine the degree and matrix effect of elemental fractionation and to assess more generally instrumental accuracy (Supplemental Table A4).

Where zircon thin rims <10–5 μm were identified on CL images, the grains were removed from mount and the outer surface ablated (following the approach of Bracciali et al., 2015). Discordant zircon data (Supplemental Fig. A2) were not included in the probability plots (Supplemental Table A2, column: "data for probability plot"; Fig. A3, A5 and 5). Discordant rutile data (Supplemental Fig. A2) were common Pb-corrected as described in Bracciali et al. (2013) and are shown in italics in Supplemental Table A3 (column: "data for probability plot"). When two zircon or rutile dates from the same grain overlapped within uncertainty, only the one determined with the lower uncertainty was included in the final probability plot (Figs. A3, A5 and 6).

3.3. Ar–Ar dating of white mica

$^{40}Ar–^{39}Ar$ single fusion experiments (Supplemental Table A5) were carried out in the geochronology laboratory at the Vrije Universiteit, Amsterdam. For each sample >100 grains varying in diameter from 0.1 to 2 mm were packed in 9 mm diameter Al-foil packages. Sample packages and Al packages containing ca. 5 mg aliquots of a mineral reference material (DRA-2 sanidine, 25.26 Ma; Renne et al., 1998) were stacked into a 10 mm diameter quartz glass tube. The glass tube was irradiated in a standard Al-irradiation capsule for 7 h in a Cd-lined rotating facility (RODEO) of the NRG-Petten HFR facility in The Netherlands. The neutron flux profile across the reactor is optimised such as to give a negligible flux gradient across the central part of the tube. Rotation of the tube during irradiation helps to minimize the horizontal flux gradient in the tube.

Upon return to the laboratory the samples and reference materials were loaded in two Cu sample trays (diameter 66 mm) each containing 185 sample holes (depth 3 mm, diameter 2 mm) and placed in a low volume vacuum UHV gas sample purification line. The single grains were fused with a CO_2 laser (Synrad 48-5, 25 W + 25 W dual plasma tube instrument, 10.5 μm wave length). The laser power can be adjusted through a 0–5 V analogue signal from Eurotherm 900 series controller to the laser control/power supply units. Positioning of the laser beam was achieved using an analogue Raylease scanhead fitted with a dual mirror system (X-axis and Y-axis adjustment) and a ZnS 300 mm focusing lens. The beam delivery system achieved a beam diameter of ca. 300 μm at the focal point. At these settings a 5% laser power setting was sufficient to fuse the samples. Complete heating of even larger grains was achieved by using a computer controlled motor stage that moved the sample in 4 circles with increasing radius. Ca. 40 grains per sample were measured in sequence, and before, during and after each run system blanks were measured. System blanks were found to be stable and predictable during the runs.

The five isotopes of Argon (m/e 40–36) and their low mass side baselines (at half mass distance) were measured sequentially by magnet field controlled peak hopping on a MAP 215-50 double focusing noble gas mass spectrometer. The beam signals on all 10 mass steps were measured on a Balzers 217 SEM detector. Aliquots of air and of ^{38}Ar spiked air are measured routinely during the measurement program to monitor the mass discrimination. For off-line data reduction, we used ArArCalc2.2c (Koppers, 2002). The ages are reported with uncertainties at 2σ uncertainty level.

The main difficulty with measuring micas with the single fusion technique is sample beam intensity. Younger and smaller grains become progressively more difficult to measure, and it was found empirically that when sample to blank ratios were lower than ca. 10, uncertainties in the calculated age became very high, preventing the use of these grains. Accepted analyses all yielded ages that are reproducible.

In addition to single-grain fusion experiments, we carried out step-heating experiments on a few grains (per sample) larger than 0.5 mm, in order to check for potential age zoning. All grains resulted to be homogeneous, and for each grain we used a plateau age (Supplemental Table A5) as the individual date for that grain to use in the probability density plot (Fig. A3, A5, 5 and 6) along with the single fusion dates from the same sample.

3.4. Zircon fission track dating

Zircon concentrates were mounted, polished and etched following standard procedures at the London Fission Track Research Group using KOH–NaOH at 225 °C with multiple Teflon mounts each etched for different durations up to 48 h. Mounts were irradiated with muscovite external detectors and dosimeter glass CN-2 in the FRM 11 thermal neutron facility at the University of Munich, Germany. FT densities were measured using an optical microscope at 1250× magnification (Supplemental Table A6). Ages were calibrated by the zeta method (Hurford, 1990) using a zeta factor of 127 ± 5 for dosimeter glass CN2, determined by multiple analysis of zircon reference materials following the recommendation of Hurford (1990). Data were plotted as radial plots and kernel density distributions (Figs. 5 and 6) using the Radial Plotter software (Vermeesch, 2009). The central age is a modal age, weighted for different precisions of individual crystals (see Galbraith and Laslett, 1993). Mixed age data were deconvolved into age peaks using the method of Galbraith and Green (1990).

Although every effort is made to sample the range of FT ages in a sample, due to the nature of zircon etching and associated bias (Malusà et al., 2013) the ZFT datasets cannot give a robust definition of the true constituent age components and their proportions, regardless of the numbers of analysed grains. For example some grains can be uncountable due to high spontaneous track densities. The deconvolved data may also be affected by low numbers of grains within an age mode that does not adequately capture the natural Poisson variation hence we focus our interpretations on those age modes with the largest numbers of grain ages and the youngest exhumation ages (Sections 4 and 5). References to the proportions of grains belonging to an age mode in following sections are provided in order to describe the data rather than indicate the natural proportions present in the sample.

4. The isotopic fingerprint of the eastern Himalayan syntaxis in the modern detritus

In the following sections we present the results of the application of our four-fold chronometer approach, described in the Introduction, aimed at tracking the erosion of the eastern syntaxis (Section 4.1), compare our data with previously published detrital data from the eastern Himalaya (4.2) and with new U–Pb rutile bedrock data from Namche Barwa (4.3). A list of detrital samples (our new chronometry and compiled from previous studies) is presented in Table 1.

4.1. New detrital chronology from the modern Brahmaputra drainage

The new U–Pb, Ar–Ar and FT data presented in this section (Fig. 5) complement our previous U–Pb work carried out on other zircon and rutile samples from the modern Brahmaputra drainage (Bracciali et al., 2013, 2015). References to the proportions of grains belonging to certain age intervals are here provided in order to describe the data, keeping in mind that the measured age distributions can only approximately represent the natural proportions present in the sample.

In the Yarlung Tsangpo upstream of the syntaxis (sample W, Fig. 5) more than 60% of the sample is characterised by Cretaceous and younger zircons (as young as 12 Ma, U–Pb data), with the main age population around 50 Ma, reflecting the erosion of the Cretaceous–Paleogene granitoids of the Gangdese Batholith in the Lhasa Terrane (Chu et al., 2006; see Fig. 4 of Bracciali et al., 2015 for a summary of known >40 Ma igneous sources across southern Tibet). A few zircons in sample W are between ~12 and 25 Ma and were likely contributed from southern tributaries of the Yarlung Tsangpo draining Cenozoic metamorphic

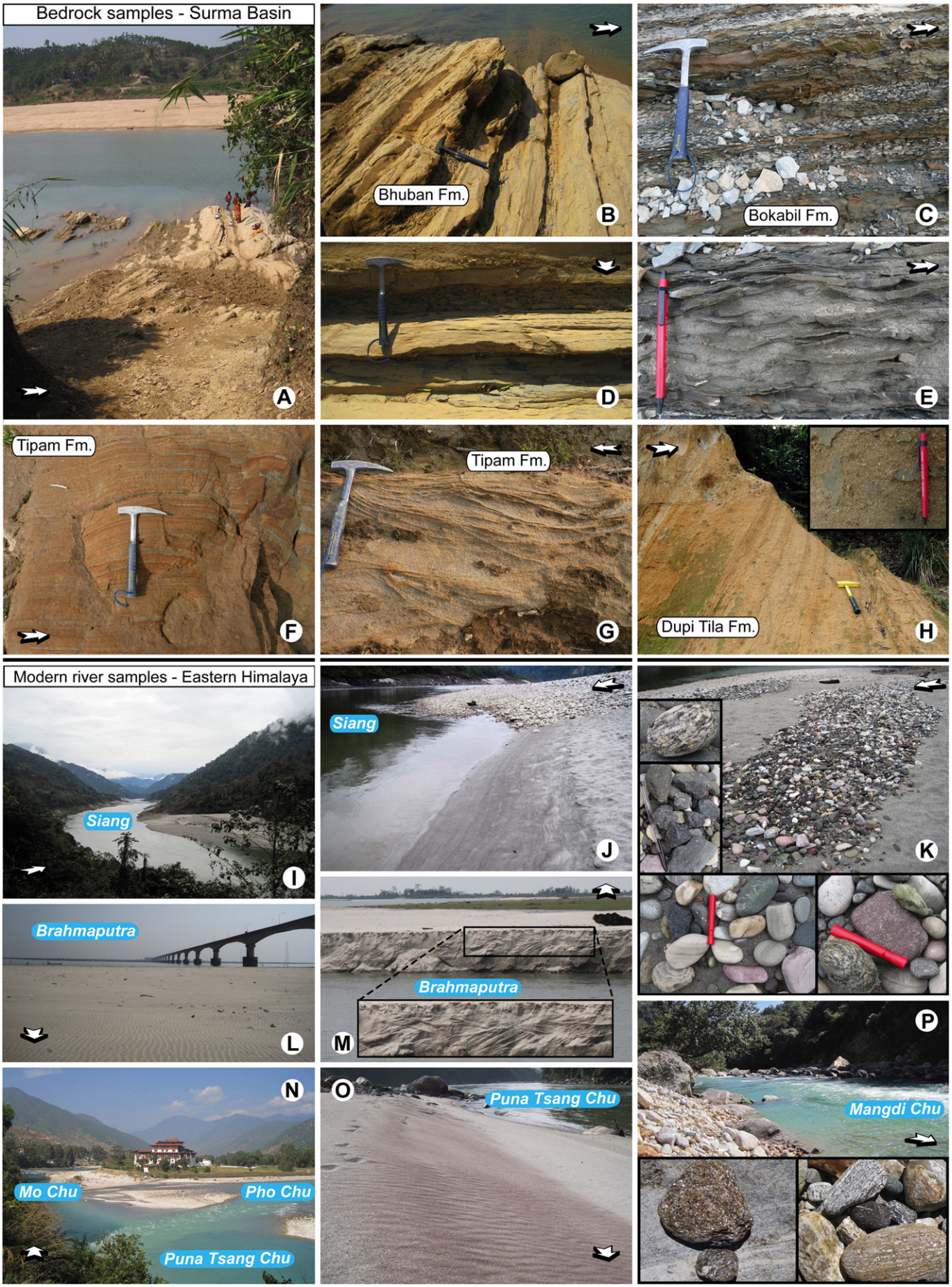
Bedrock samples - Surma Basin
A
Bhuban Fm.
B
Bokabil Fm.
C
D
E
Tipam Fm.
F
Tipam Fm.
G
Dupi Tila Fm.
H
Modern river samples - Eastern Himalaya
Siang
I
Siang
J
K
Brahmaputra
L
Brahmaputra
M
P
Mangdi Chu
N
Mo Chu
Pho Chu
Puna Tsang Chu
O
Puna Tsang Chu

or igneous (post-collisional) Himalayan sources or from northern tributaries draining 30–9 Ma adakites of the southern Lhasa Terrane (Chung et al., 2009), although these are of limited extent compared to Himalayan sources. Similar (15–30 Ma) populations occur in the Nanyiqu River (sample O) that joins the Yarlung Tsangpo SW of the syntaxis just upstream of location W, and in a tributary to the Nanyiqu River (sample P). We interpret the 80–90 Ma age population in the Nanyiqu sample as derived from the erosion of amphibolite facies rocks from the Lhasa Terrane, similar to those that ca. 30 km to the NW of location O yielded 85 to 95 Ma zircons (Zhang et al., 2010c).

The same two samples (O and P, from tributaries draining only the Indian plate) are dominated by rutile Miocene grains as young as ~8–9 Ma (Fig. 5). This is the same age as the youngest rutile grain in the Yarlung Tsangpo at location W, downstream of the junction with the Nanyiqu, whilst in the Yarlung sample further upstream (Y) rutile grains are older than 18 Ma.

Rutile grains as young as 0.4 ± 0.1 Ma in the Siang downstream of the syntaxis (locality S, in the vicinity of Pasighat) readily identify the distinct input from the syntaxis to the modern detritus. Similarly, white micas in the same sample are as young as 0.3 ± 0.1 Ma, in contrast to samples X and Y upstream of the syntaxis yielding white mica age distributions dominated by 6–20 Ma grains, with no younger grains (Fig. 5).

Importantly, in our zircon samples we identified (by CL-imaging) and U–Pb dated very thin (<5 μm) zircon rims. This allowed to track the latest growth events of the grains (that otherwise would be missed due to the difficulty in analysing these narrow zones of zircon) such as a few zircon rims determined by this "thin rim" dating approach (Section 3.2) in the Siang sample S younger than 10 Ma (Fig. 5; youngest: 2.0 ± 0.1 Ma), similar to those from the Namche Barwa–Gyala Peri massif (Fig. 4C). These <1–2 Ma rutile and zircon grains alone prove that cooling in the source area progressed at rates >250 °C/Myr.

The ZFT data of sample S (described in terms of main age groups, or age peaks, in Fig. 5) yield a central age of ~8 Ma and youngest age peak of 1.7 ± 0.1 Ma (corresponding to ~50% of the sample), in sharp contrast with the ZFT data of sample Y upstream of the syntaxis, characterised by a central age of ~27 Ma and youngest peak of 8.6 ± 0.7 Ma.

To better represent the different provenance signatures across the drainage basin, we plotted in Fig. 8 the detrital data of samples from the main trunk of the Yarlung Tsangpo–Brahmaputra as cumulative age distribution diagrams (the cumulative distribution of the measured dates; Vermeesch, 2007).

The cumulative age distribution curves show the increase of old zircons downstream (U–Pb data), as quantitatively indicated by <70 Ma grains being ~50% of the sample in both the Yarlung Tsangpo and the Siang but only ~25% in the Brahmaputra. This likely reflects the dilution of the Transhimalayan juvenile zircons in the Brahmaputra sediment load (at location Z) following the addition of older (inherited) components by the Siang–Brahmaputra and its tributaries draining the southern flanks of the Himalaya, where the Indian crust of TH and GH is exposed (as observed by Cina et al., 2009 and further discussed by Zhang et al., 2012b). The diagram also shows that the <10 Ma detrital zircons derived from the syntaxis account for a 10% component in the Siang and 5% in the Brahmaputra. All curves exhibit a sharp break in slope around 500 Ma, reflecting the input from late Pan-African granites intruding GH (Cawood et al., 2007; see also Zhang et al., 2012b).

The two Yarlung Tsangpo rutile samples (Y and W) show strikingly similar curves despite their locations being ~300 km apart, indicating that the Yarlung Tsangpo drainage basin upstream of sample W is characterised by a fairly homogeneous cooling history through ~575 ± 75 °C and also through ~300–450 °C (T_c of white mica; Hames and Bowring, 1994; Harrison et al., 2009), as indicated by the white mica cumulative age distributions of sample X and Y overlapping by ~80%. The <2 Ma rutile age population corresponds to ~10% of the sample in the Brahmaputra and ~25% in the Siang.

We interpret the prominent 500–600 Ma rutile population in the two Yarlung Tsangpo samples upstream of the syntaxis (corresponding to the steep portion of the W and Y curves accounting for more than 50% of the sample in Fig. 8) as derived from a metamorphic rock source in the Lhasa Terrane basement. A derivation of this ~500 Ma population from a GH source in the Indian plate drained by the southern tributaries of the Yarlung Tsangpo is unlikely because Himalayan metamorphism and exhumation of GH units has reset the U–Pb isotopic clock in rutile (e.g. samples O and P; Fig. 5). Even in the Subansiri sample (Q) that for most of its upper course drains TH, we only found 2 rutile grains older than 23 Ma (340 and 550 Ma). Grains of similar age occur in both the Siang (sample S, two grains 490–500 Ma) and in the Brahmaputra sample (sample Z: 25% of the population between 480 and 590 Ma).

The U–Pb rutile data plotted as cumulative age distribution diagrams highlight the effectiveness of this isotopic tool in capturing differences in provenance related to the T–t evolution of the rock sources at upper crustal levels. The rutile age distribution of the Brahmaputra sample, whose curve plots between the Siang and the Yarlung Tsangpo curves, indeed effectively visualizes how the Brahmaputra rutile detrital signature results from the integration of the extremely young syntaxial component that dominates the Siang and the variably older components contributed by the Lhasa Terrane and the Himalayan units as in the Yarlung Tsangpo.

In agreement with the other chronometers, the ZFT main age components plotted as cumulative age distribution diagrams (Fig. 8) permit to sharply distinguish the upstream and downstream (with respect to the syntaxis) isotopic signature of the modern detritus.

Remarkably, our zircon and rutile data show that the unique thermo-chronological features of the fast-exhuming syntaxis in the context of the eastern Himalaya can be successfully tracked even hundreds of km downstream of the syntaxis in the Assam plains (locality Z). We note however that the distinctly young white mica population of the Siang (~15% of the grains <1 Ma) is lacking in our Brahmaputra sample, where the youngest grain is ~5 Ma (Fig. 8). This could be due in part to: i) white mica being less abundant in the high grade lithologies of the syntaxis resulting in a limited proportion of datable mineral grains in

Fig. 7. Photographs of a selection of sampling localities from the Surma Basin (sandstone samples) and the eastern Himalayan modern drainage network (sand samples). Complete list of samples and locations is in Table 1, Supplemental Table A1 and Fig. A1. White arrows point towards the north. A: View of the palaeo-Brahmaputra deposits (Surma Group) cropping out along the Shari River in north-eastern Bangladesh. In B to H note the intense weathering affecting the outcrops. B: Decimetric sandstone beds alternating to silty to muddy layers, upper part of Bhuban Formation (Surma Group, location of sample 15, Fig. 6). C: Intercalations of centimetric fine-sand and mud layers, top of Surma Group (upper Bokabil Formation, location of sample 22). D: Close-up of the same outcrop shown in B. E: Close-up of the same outcrop shown in C. F: Layering in Tipam Sandstone (location of sample 29). G: Cross-bedding in medium-grained Tipam sandstone (location of sample 23). H: Poorly consolidated Dupi Tila sandstone (location of sample 33). I: Siang River ca. 40 km upstream of the town of Pasighat, Arunachal Pradesh, India. J: Sandy-pebbly beach along the Siang River (location of sample S, Fig. 5). K: Centimetric pebbles of igneous, (meta-)sedimentary and high-grade metamorphic lithologies (same location as J). L: Right bank of the Brahmaputra River (location of sample Z) below the ca. 3 km bridge crossing the river south of the town of Tezpur, Assam, India. M: Cross-bedding along the side of one of the several sandy islands of the up-to-20 km wide Brahmaputra River as it flows in the Assam plain, NE of Dibrugarh. N: The Puna Tsang Chu, one of the right tributaries of the Brahmaputra, at the confluence of the Mo Chu and Po Chu (Bhutan; Punakha Dzong in the centre of image). O: Sandy beach along the left bank of the Puna Tsang Chu (location of sample E); the purple-brown colour of the sand results from enrichment in garnet, a major constituent of the sand along with other heavy minerals (zircon, rutile, kyanite, sillimanite, titanite); P: boulders and centimetric pebbles along the Mangdi Chu, a Bhutanese tributary of the Brahmaputra; the high grade metamorphic lithologies testify to the erosion of GH rocks comprising most of the Mangdi Chu drainage basin (Bracciali et al., 2013).

Table 1
Summary of new and published modern detrital geo- and thermo-chronology from the Eastern Himalayan region.

Sample label (this study)	River name (location)	Sample short label	Sample full label	Latitude (° N)	Longitude (°E)	Reference	Zircon U–Pb	Rutile U–Pb	White mica Ar–Ar	Zircon FT
Yarlung Tsangpo main trunk upstream of the eastern syntaxis (draining both the Lhasa terrane + Gangdese Batholith and the northern slopes of the eastern Himalayan orogen)										
X	Yarlung Tsangpo	X	TG05-40A	29.35468	90.726483	This study			x	
Y	Yarlung Tsangpo	Y	TG05-41A	29.25882	91.66515	This study		x	x	x
W	Yarlung Tsangpo	W	NB13C08	29.27728	94.313389	This study	x	x		
y1	Yarlung Tsangpo (Quxu)	b	AY09-08-08-(7)	29.3193	90.6864	Zhang et al. (2012b)	x			
y2	Yarlung Tsangpo (Gonggar)	1	AY06-28-06-(1)	29.3228	91.0921	Cina et al. (2009)	x			
y3	Yarlung Tsangpo (Gyaca)	d	AY09-10-08(12)	29.0747	92.7748	Zhang et al. (2012b)	x			
y4	Yarlung Tsangpo (Pai)	302	302	–	–	Stewart et al. (2008)	x			x
Tributaries draining the Lhasa terrane + Gangdese Batholith and Eastern Batholiths										
a1	Lhasa River Tributary	–	HKT-10a	29.83775	91.39925	Henderson et al. (2010, 2011)	x			
a1	Lhasa River Tributary	A	HKT-10a	29.83775	91.39925	Bracciali et al. (2015)		x		
a2	Lhasa River	–	HKT-11a	29.67256	91.38481	Henderson et al. (2011)			x	
a3	Lhasa River	2	AY09-08-08-(3)	29.4426	90.9315	Zhang et al. (2012b)	x			
a4	Niyang	B	NB09A-08	29.69086	94.34836	Bracciali et al. (2015)	x	x		
a5	Niyang	G	G	29.86966	93.66360	Enkelmann et al. (2011)				x
a6	Niyang	5	AY09-11-08-(6)	29.4333	94.4543	Zhang et al. (2012b)	x			
a7	Yigong	3	NB0404	30.0967	95.0647	Lang et al. (2013)	x			
a8	Yigong	D	D	30.14160	95.00467	Enkelmann et al. (2011)				x
a9	Parlung	7	AY09-12-08-(3)	29.9084	95.4606	Zhang et al. (2012b)	x			
a10	Parlung tributary	303	303	–	–	Stewart et al. (2008)				x
a11	Parlung	304	304	–	–	Stewart et al. (2008)				x
a12	Parlung	305	305	–	–	Stewart et al. (2008)				x
a13	Parlung	309	309	–	–	Stewart et al. (2008)				x
a14	Parlung	310	310	–	–	Stewart et al. (2008)				x
a15	Burhi Dihing (Assam)	H	LI10-04	27.30881	95.70864	Bracciali et al. (2015)	x			
Detrital input from the eastern syntaxis										
O	Nanyiqu	O	NB11A08	29.14671	94.20913	This study	x	x		
P	Nanyiqu tributary draining the SW syntaxis only	P	NB11B08	29.14719	94.20908	This study	x	x		
sy1	Yarlung Tsangpo tributary draining the Namche	P	P	29.60737	94.93648	Enkelmann et al. (2011)				x
sy2	Barwa massif tributary draining the Namche	5	NB0904	29.60642	94.93687	Lang et al. (2013)	x			
sy2	Barwa massif	H	NB0904	29.60642	94.93687	Enkelmann et al. (2011)				x
sy3	Gyala Peri glacial float; leucogranite	–	GP-10-03	29.92347	94.88394	Zeitler et al. (2014)	x			
sy4	Gyala Peri glacial float; pegmatite	–	GP-12-03	29.92347	94.88394	Zeitler et al. (2014)	x			
sy5	Gyala Peri glacial float; aplite	–	GP-15-03	29.92347	94.88394	Zeitler et al. (2014)	x			
sy6	Gyala Peri glacial float; pegmatite	–	GP-02-03	29.90861	94.89092	Zeitler et al. (2014)	x			
sy7	Gyala Peri glacial float; granite	–	GP-04-03	29.90861	94.89092	Zeitler et al. (2014)	x			
sy8	Gyala Peri glacial float; pegmatite	–	GP-06-03	29.90861	94.89092	Zeitler et al. (2014)	x			
sy9	Gyala Peri glacial float; pegmatite	–	GP-07-03	29.90861	94.89092	Zeitler et al. (2014)	x			
Siang and its tributaries downstream of the syntaxis										
S	Siang (upstream of Pasighat)	Z	LI10-03b	28.16606	95.04391	This study	x	x	x	x
d1	Siang (Kapu)	A	Siang @ Kapu	29.04867	94.91080	Lang et al. (2016)			x	
d2	Siang (Nubo)	B	Siang @ Nubo	28.57666	95.07020	Lang et al. (2016)			x	
d3	Siang (Pasighat)	C	Siang @ Pasighat	28.09866	95.29384	Lang et al. (2016)			x	
d4	Siang	6	3280836	29.04847	94.91079	Lang et al. (2013)	x			

Table 1 (*continued*)

Sample label (this study)	River name (location)	Sample short label	Sample full label	Latitude (° N)	Longitude (°E)	Reference	Zircon U–Pb	Rutile U–Pb	White mica Ar–Ar	Zircon FT
d5	Siang	7	TUTING	28.99628	94.90344	Lang et al. (2013)	x			
d6	Siang	8	3250816	28.57666	95.07020	Lang et al. (2013)	x			
d7	Siang	Q	Q	29.04938	94.91017	Enkelmann et al. (2011)				x
d8	Siang tributary	I	I	28.96166	94.86376	Enkelmann et al. (2011)				x
d9	Siang tributary	J	J	28.90998	94.7740	Enkelmann et al. (2011)				x
d10	Siang tributary	K	K	28.97833	94.90471	Enkelmann et al. (2011)				x
d11	Siang	R	R	28.57713	95.07036	Enkelmann et al. (2011)				x
d12	Siang tributary	L	L	28.33640	94.95766	Enkelmann et al. (2011)				x
d13	Siang tributary	M	M	28.21978	94.85535	Enkelmann et al. (2011)				x
d14	Siang tributary	N	N	28.18498	95.22018	Enkelmann et al. (2011)				x
d15	Siang	S	S	28.09970	95.29385	Enkelmann et al. (2011)				x
d16	Siang (Pasighat)	301	301	–	–	Stewart et al. (2008)	x			x
d17	Siang tributary	Y	Yang Sang River	28.97737	94.90473	Lang et al. (2016)			x	
d18	Siang tributary	X	Siyom River	28.21933	94.86589	Lang et al. (2016)			x	
d19	Siang tributary	Z	Yamne River	28.18604	95.22274	Lang et al. (2016)			x	
Tributaries draining the southern slopes of the eastern Himalayan orogen and the Indo-Burman Ranges										
Q	Subansiri (Arunachal Pradesh)	Q	LI10-02b	28.00542	94.20242	This study	x	x		
b1	Subansiri (Arunachal Pradesh)	7	AY01-05-09-(1A)	28.0054	94.2028	Cina et al. (2009)	x			
b2	Mo Chu (Bhutan)	C	BH0108	27.72219	89.75536	Bracciali et al. (2013, 2015)	x	x		
b3	Pho Chu (Bhutan)	D	BH0208	27.58825	89.87000	Bracciali et al. (2015)	x			
b4	Puna Tsang Chu (Bhutan)	E	LB09-03b	27.03051	90.07346	Bracciali et al. (2013, 2015)	x	x		
b5	Mau Khola (Bhutan)	F	LB09-02b	26.94194	90.51898	Bracciali et al. (2013, 2015)	x	x		
b6	Mangdi Chu (Bhutan)	G	LB09-01b	27.14777	90.68972	Bracciali et al. (2013, 2015)	x	x		
b7	Dhansiri (Assam)	I	LI10-05b	26.62281	93.74142	Bracciali et al. (2015)	x	x		
b8	Kameng	–	KAM 20	–	–	Chirouze et al. (2013)				x
b9	Kameng	–	KAM 30	–	–	Chirouze et al. (2013)				x
Brahmaputra main trunk in the Assam plain										
Z	Brahmaputra	Z	LI10-06b	26.609694	92.85569	This study		x	x	
Z	Brahmaputra	Z	LI10-06b	26.609694	92.85569	Bracciali et al. (2015)	x			
b10	Brahmaputra	3	AY02-21-06-(2)	26.6108	92.8536	Cina et al. (2009)	x			

the detritus (fertility bias; Malusà et al., 2015); and/or ii) a preservation bias: micas could be less preserved in the sampled bar sands compared to rutile (cf. the ~15% of <2 Ma white mica grains and ~25% of <2 Ma rutile grains in sample S), resulting in a relative proportion of very young white mica grains smaller than very young rutile in the first cycle detritus. We will further discuss the potentially limited ability of white mica Ar–Ar detrital data in representing its hinterland source(s) in Section 4.2.3.

4.2. Review of published modern detrital chronology from the eastern Himalaya

In this section we review (and compare to our new data presented in Section 4.1) published modern detrital chronology from the eastern Himalayan region (see: Table 1 for sample details and references; Fig. 9 for sample locations). All data are plotted as cumulative age distribution diagrams to allow for easy comparison of the detrital samples.

4.2.1. Detrital U–Pb zircon data

The detrital zircon U–Pb signature of the Yarlung Tsangpo sampled at various locations (up to 400 km apart) upstream of the syntaxis is strikingly homogeneous (Fig. 10A). Tributaries draining the southern Lhasa Terrane (Lhasa and Niyang Rivers: a1, a3, a4; Fig. 10B) typically contribute a large proportion of 50–70 Ma Gangdese zircons of the Transhimalayan Arc as well as older zircons. The Yigong and Parlung Rivers (a7, a9) draining the Eastern Batholiths are enriched in 110–130 Ma zircons. (see Zhu et al., 2011 and Liang et al., 2008 for a review of pre-collisional igneous rocks of the southern Tibet–Burma region, and Fig. 4 of Bracciali et al., 2015 for a visual summary of U–Pb data and their spatial distribution).

Various Siang samples downstream of the syntaxis (Fig. 10C) exhibit similar cumulative curve patterns, with our Siang sample S (n = 75) yielding ~20% of the data in the range 2–30 Ma as a results of our "thin rim" dating approach (see Methods Section 3.2). In samples from other studies (with n up to 150) the youngest dated zircons are

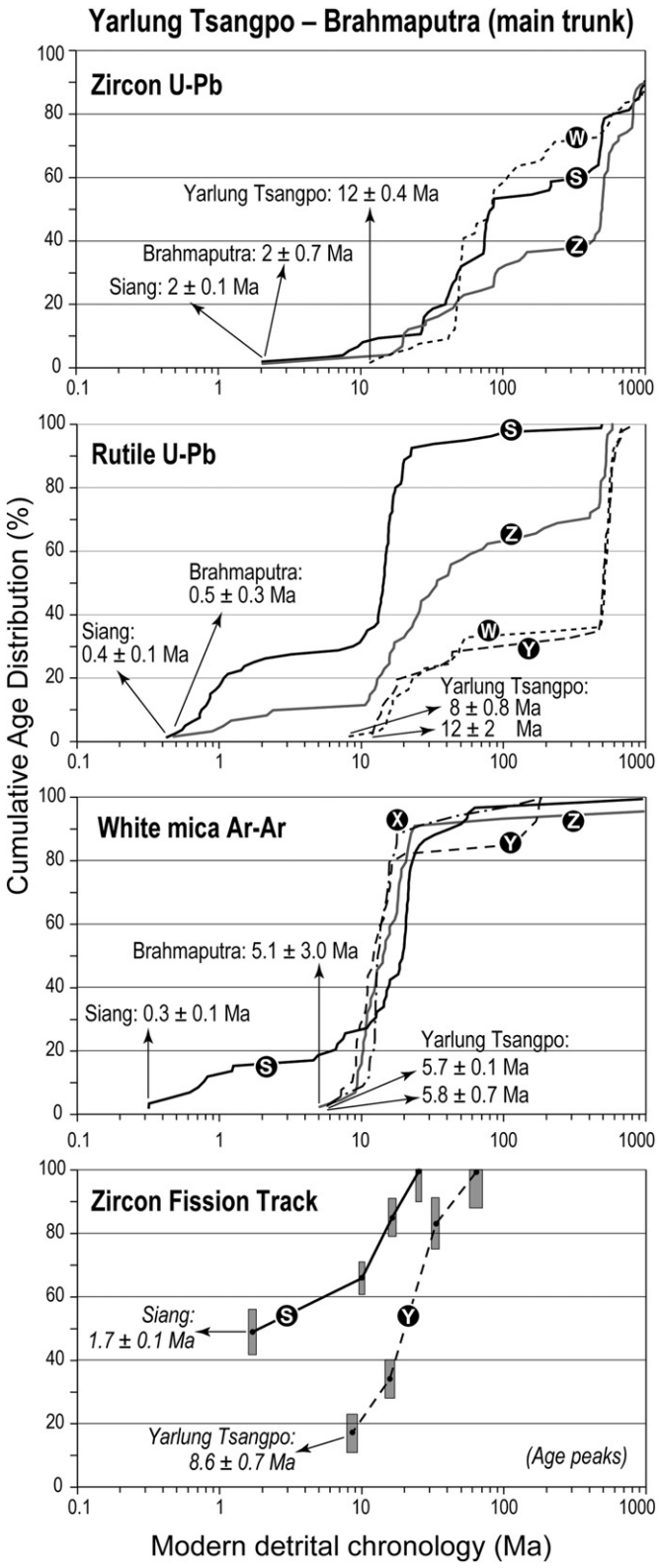

Fig. 8. Cumulative age distribution of detrital mineral age data from the Brahmaputra modern drainage (main trunk only). Samples and data as in Fig. 5. Arrows indicate the youngest grain in each sample (±2σ uncertainty). ZFT data are plotted as main age peaks (±1σ uncertainty, with youngest age peak indicated for each sample). Note the logarithmic scale for the horizontal axis.

>10 Ma and zircons <30 Ma constitute only a few % of the sample. The source of <10 Ma zircons (spatially subordinated to all other rock sources, hence diluted in the detritus) can be readily identified as the core of the syntaxial antiform, as shown by both bedrock data (Fig. 4C) and the age of zircons from igneous clasts recovered as glacial float west of the Gyala Peri peak (sy3–sy9, Fig. 10D). A minor tributary draining the NB massif (sy2; Fig. 10E) clearly exhibits this young age component, which is absent in our sample P draining the SW flank of the syntaxial antiform. Apart from this component, the cumulative curves of the two samples (P and sy2) are nearly indistinguishable (note the different n).

Tributaries in the Assam plain (b7, a15; Fig. 10F) mainly contribute to the Brahmaputra 500 Ma and older zircons. In our Brahmaputra sample (Z), in analogy with the Siang sample S, 15% of the data is <30 Ma, in contrast with Brahmaputra sample b10 from the literature totally lacking this young age component.

Generally, U–Pb zircon age spectra of detritus derived from the erosion of TH and GH units exhibit main peaks at ~0.5 and 0.8–1.2 Ga, whilst in LH detritus the dominant U–Pb zircon age range is 1.7–2.0 Ga (DeCelles et al., 2000; Gehrels et al., 2011, and references therein; cf. the coloured vertical bands in Fig. 10). The ~500 Ma peak (the reported age of granitoids intruding GH and corresponding to the intrusion of late Pan-African granites, Cawood et al., 2007) is prominent in all tributaries draining TH and/or GH rocks (Fig. 10G) in the southern slopes of the Himalaya (cf. Fig. 9). In these samples (Bhutanese rivers: b2–b6; Subansiri River: Q, b1) the 50–70 Ma population that is distinctive of the Gangdese Batholith in the Asian plate is lacking and 15–30 Ma zircon rims (up to 30% of the sample, with ~15 Ma being the youngest zircons) testify to Cenozoic Himalayan metamorphism affecting GH (HM in Fig. 10). The uniform signature of GH-derived detritus across an area stretching for ~600 km is shown by the striking similarity (allowing for some variability in the relative abundances of the different components) of the cumulative curve patterns of the Puna Tsang Chu (b4), the Subansiri (Q) and the two small tributaries draining the syntaxis (P and sy2; Fig. 10H).

4.2.2. Detrital rutile U–Pb data

U–Pb detrital rutile data for the Himalayan–Tibet region are currently limited to this and our previous studies (Bracciali et al., 2013, 2015).

Similar to zircon, the rutile U–Pb data show striking differences between tributaries draining the Lhasa Terrane, in which 15 to 0% of the sample is <50 Ma (samples a1 and a4, respectively, with youngest grains 18 and 55 Ma; Fig. 11A), and tributaries that drain only the Indian plate (Fig. 11B and C). The occurrence in a tributary of the Lhasa River (a1; Fig. 9) of a prominent 500–600 Ma population supports our interpretation (Section 4.1) of derivation of the same population in the Yarlung Tsangpo upstream of the syntaxis (samples Y and W) from metamorphic rock source(s) in the Lhasa Terrane basement. Interestingly, a rutile population of similar age (500–550 Ma) occurs in the modern Dhansiri River that drains the IBR (b7; Fig. 11D).

For the main part of the eastern Himalaya of Bhutan (samples b2–b6, Fig. 11C) rutile is dominated by late Miocene ages (youngest grains: ~9–13 Ma), with some older components as old as Paleozoic probably coming from Tethyan sedimentary sources. Clearly none of these and other Indian plate samples (Q, P, O; Fig. 11C) contributes the very young (<~3 Ma) rutile component to the Brahmaputra (Z) and the Siang (S), not even sample P from the tributary draining the SW flank of the syntaxial antiform (Fig. 11B). The available data thus show that rutile grains younger than ~9 Ma do not occur outside of the eastern syntaxial area, except perhaps in the far west of the Himalaya in the western syntaxis of Pakistan coincident with Nanga Parbat (although no rutile U–Pb data from the western syntaxis have been collected yet). We will further discuss this is Sections 4.3 and 7 as it gives a clue as to the tectonic setting of the eastern syntaxis rocks prior to their recent exhumation.

Interestingly, the Miocene age of rutile from these samples draining the southern slopes of the Himalaya (b2–b6 in Bhutan to Q, O and P) becomes younger towards the syntaxis, as indicated by the shift towards a younger age of the main peak of the probability curves as well as the youngest rutile grain (Fig. 11C).

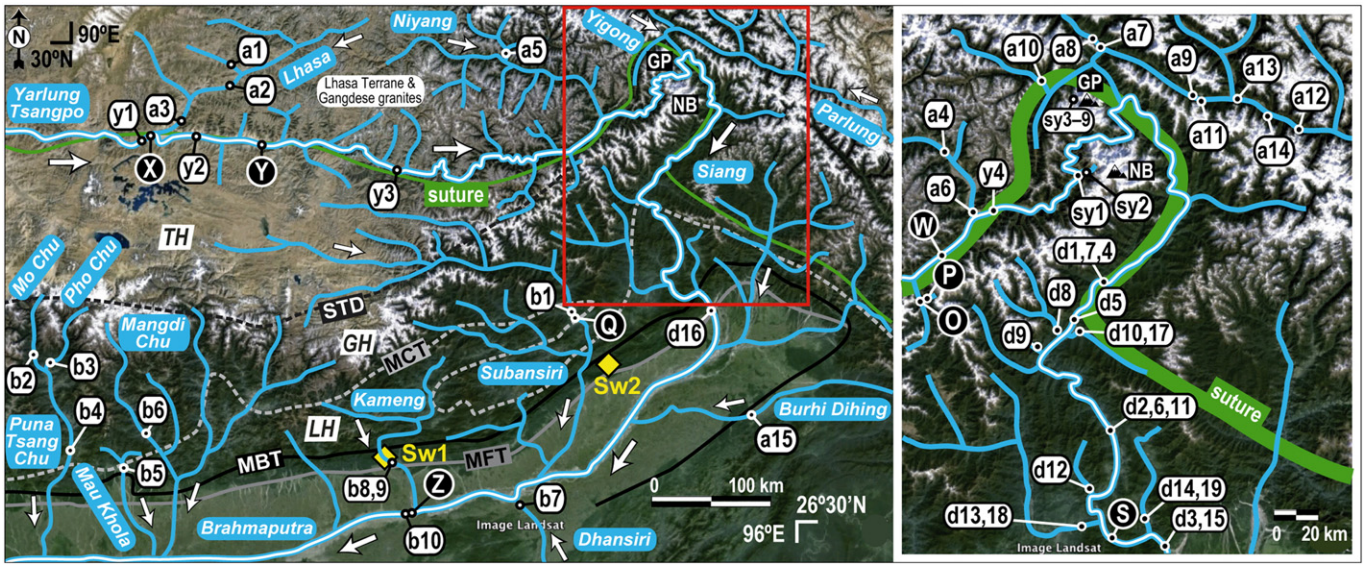

Fig. 9. Map showing the modern Yarlung Tsangpo–Brahmaputra drainage network in the eastern Himalaya superimposed on a Google Earth Landsat image and locations of modern river samples from the literature (Table 1). The red boxed area in left panel is showed in more detail in right panel. Also shown for comparison are locations of samples for which new data are provided in this study (capital letters on black background, cf. Fig. 5) and foreland Siwalik deposits from published studies (Sw1: Kameng section of Cina et al., 2009 and Chirouze et al., 2013; Sw2: Siji River section of Lang et al., 2016; see text for discussion). White arrows indicate river flow direction. Abbreviations for Himalayan lithotectonic units (TH, GH, LH) and their bounding faults (STD, MCT, MBT, MFT) are the same as in Fig. 2.

4.2.3. Detrital white mica Ar–Ar data

The Lhasa River draining a portion of the southern Lhasa Terrane in the western part of the eastern Himalaya (Fig. 9) contributes to the Yarlung Tsangpo Cenozoic white mica grains in the range 4–15 Ma, with no younger grains (sample a2; Fig. 12A). A <10 Ma age component, prominent in this sample (>50%), also occurs in the Yarlung Tsangpo upstream of the junction with the Lhasa River (X) and ~100 km downstream (Y; Fig. 9), although it is less abundant (10 and 30% of the samples, respectively). Both samples X and Y are dominated by 10–20 Ma grains, with some older (Mesozoic) grains that also occur in the Lhasa River.

Siang samples from four localities along an ~200 km reach downstream of the syntaxis exhibit very similar cumulative curve patterns, with 25 to 40% of the white mica grains <10 Ma and as young as 0.3–0.4 Ma in all samples (Fig. 12B). In contrast, the youngest dated white mica grains in three Himalayan tributaries south of the syntaxis (d17–d19 draining GH, LH and Transhimalayan units across the suture; Fig. 12C) are 13 to 25 Ma, with main age peaks at ~16 Ma (d18, west of the Siang) and ~29 Ma (d17 and d19, east of the Siang).

We disagree with Lang et al. (2016) arguing for derivation of all white micas <9 Ma in the Siang exclusively from the Namche Barwa massif, since 5–10 Ma white mica are not unique to the syntaxial area but occur elsewhere in the eastern Himalaya. We have shown above that 4–10 Ma white micas are abundant in southern Lhasa drainages and also occur in the main trunk of the Yarlung Tsangpo upstream of the syntaxis. Grains in this age range are also reported from modern rivers draining the southern slopes of the Himalaya (Subansiri and Kameng, Gemignani et al., 2016). This is consistent with our finding of 8–9 to 13 Ma main rutile age peaks in rivers also mainly draining GH rocks exposed on the Indian plate (samples b2–b6, Q, O, P; Fig. 11). What is distinctive of the Siang are the <2 Ma white mica grains. In the age distribution pattern of the composite Siang sample plotted as frequency and probability plots (total n = 325; Fig. 12D) the <2 Ma grains define a distinct population corresponding to 11% of the sample with a main peak around 0.4 Ma. We suggest that this population is derived entirely from the core of the syntaxial antiform, in agreement with our detrital rutile data (Fig. 11) and the published bedrock data (Fig. 4C). We provide additional evidence in support to this interpretation in Section 4.3.

As to the lack of the <2 Ma population in our Brahmaputra sample (Z), we argue that downstream dilution due to the input of tributaries draining older sources or to hydrodynamic sorting effects (e.g. Garzanti et al., 2009) significantly reduces the relative proportion of this very young population in the Brahmaputra detritus. We suggest that the analysis of a larger number of grains would allow the identification of this population in the sample. This is supported by the recent work of Gemignani et al. (2016) reporting the occurrence of the <2 Ma white mica population in three main trunk Brahmaputra samples (n ~50 to 100) downstream of the syntaxis in the Assam plains.

4.2.4. Detrital zircon fission track data

Siang ZFT samples from the literature plotted as cumulative age distribution of main age peaks (Fig. 13A) compare well to our Siang sample, although the youngest age peak (1.7 ± 0.1 Ma) in our study is slightly older than the ~0.6–1.1 Ma youngest peaks reported by other studies. The cumulative curves of the five Siang samples are significantly younger than the two Yarlung Tsangpo samples upstream of the syntaxis (see Fig. 9 for sample locations) that yield youngest peaks of ~7–9 Ma.

Two samples from the Kameng River mainly draining LH rocks exposed along the southern slopes of the Arunachal Himalaya (b8, b9; Fig. 9) have youngest peaks of 4–6 Ma (Fig. 13B). Tributaries downstream of the syntaxis lack the youngest FT signature of the Siang (Fig. 13B) with the exception of sample d8 from a western tributary of the Siang draining the SE flank of the syntaxis, with a youngest peak of 1.6 ± 0.3 Ma.

All tributaries draining the Asian plate north-west to the north-east of the syntaxis (Fig. 13C) are characterised by cumulative age patterns similar to the Yarlung Tsangpo further to the west, with youngest peaks ~4 to 12 Ma. The Niyang River (sample a5), draining the Lhasa Terrane and the Gangdese Batholith NW of the syntaxial region exhibits a pattern almost coincident with that of our Yarlung Tsangpo sample Y. Samples a8, a10, a11 located within a few km and to the N–NE of the

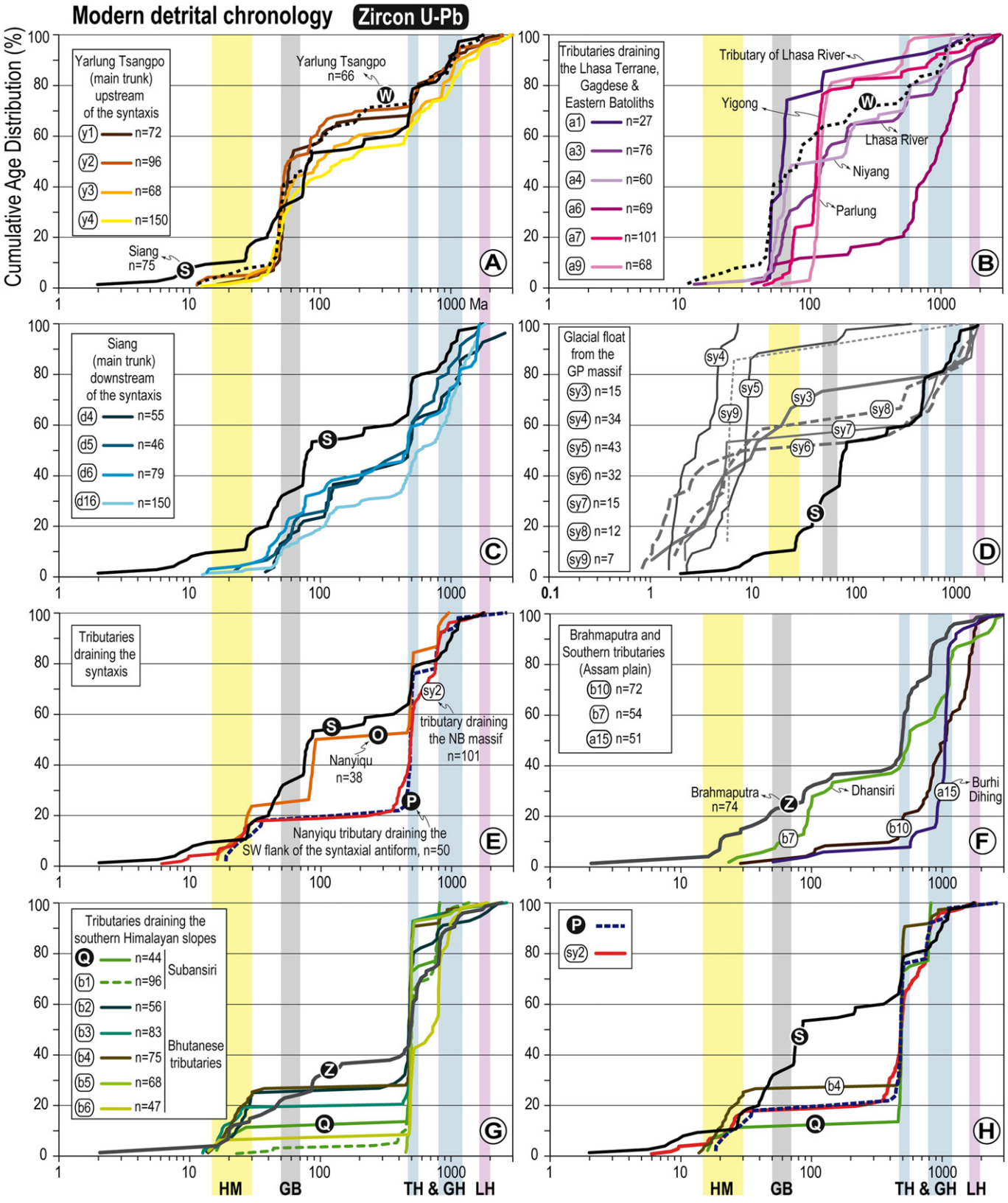

Fig. 10. Cumulative age distribution of U–Pb zircon data from the modern Yarlung Tsangpo–Brahmaputra and some of its tributaries. Samples are from this study and the literature (Table 1). Sample locations are shown Fig. 9. Less than 10% discordant and <5% reversely discordant data are plotted (never resulting in rejection of the youngest component of the sample as presented in the original publication); discordant young data (generally younger than ~100 Ma) but concordant within their individual uncertainty are also included in diagrams; best ages as indicated in the original publication are plotted for samples y4, d16, sy3–sy9. Coloured vertical bands: main age peaks of Himalayan metamorphism of GH units (HM); the Gangdese Batholith of the Transhimalayan Arc in southern Lhasa Terrane (GB); detrital zircons in Tethyan (TH), Greater (GH) and Lesser Himalaya (LH) based on literature data. See text for discussion and references.

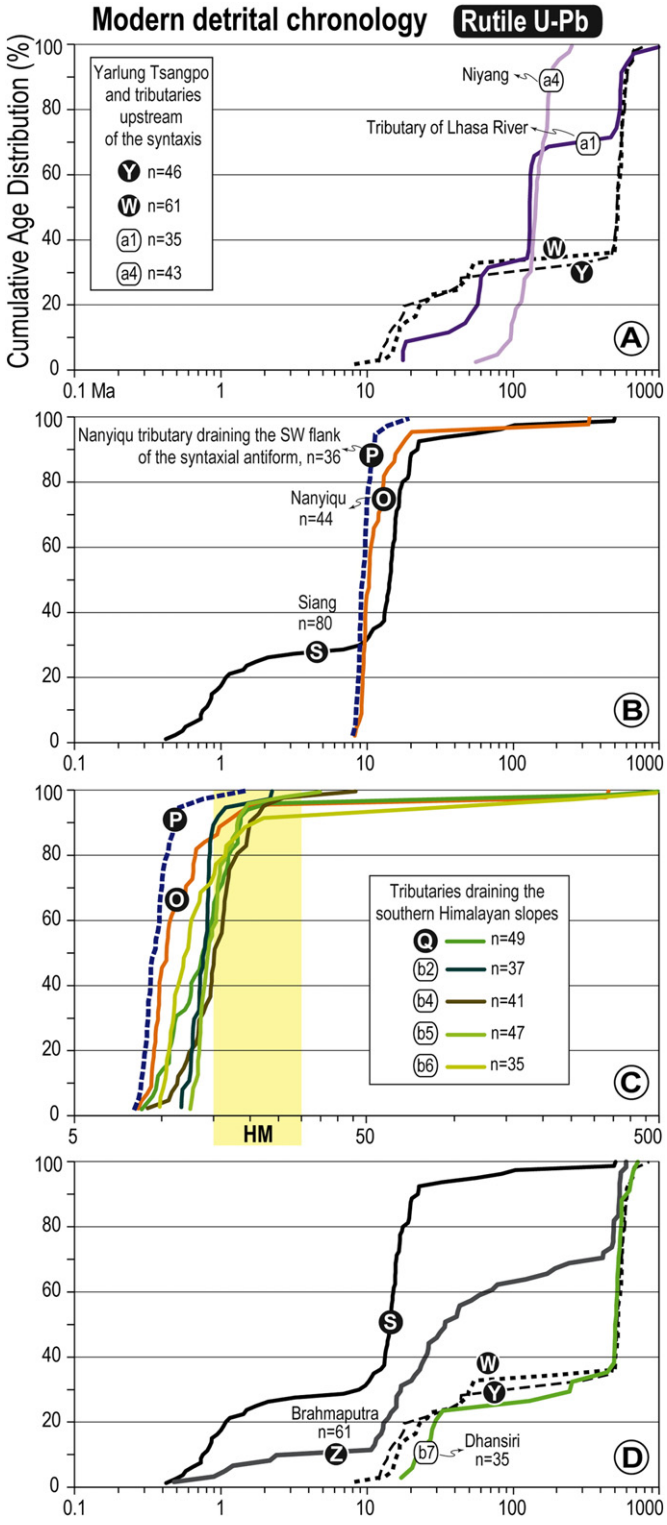

Fig. 11. Cumulative age distribution of U–Pb rutile data from the modern Yarlung Tsangpo–Brahmaputra and some of its tributaries. Samples from this study and Bracciali et al. (2013, 2015). Sample locations are shown in Fig. 9; n indicates the total number of datapoints plotted for each sample. Yellow vertical band: main age peaks of Himalayan metamorphism of GH units (HM; cf. Fig. 10). See text for discussion.

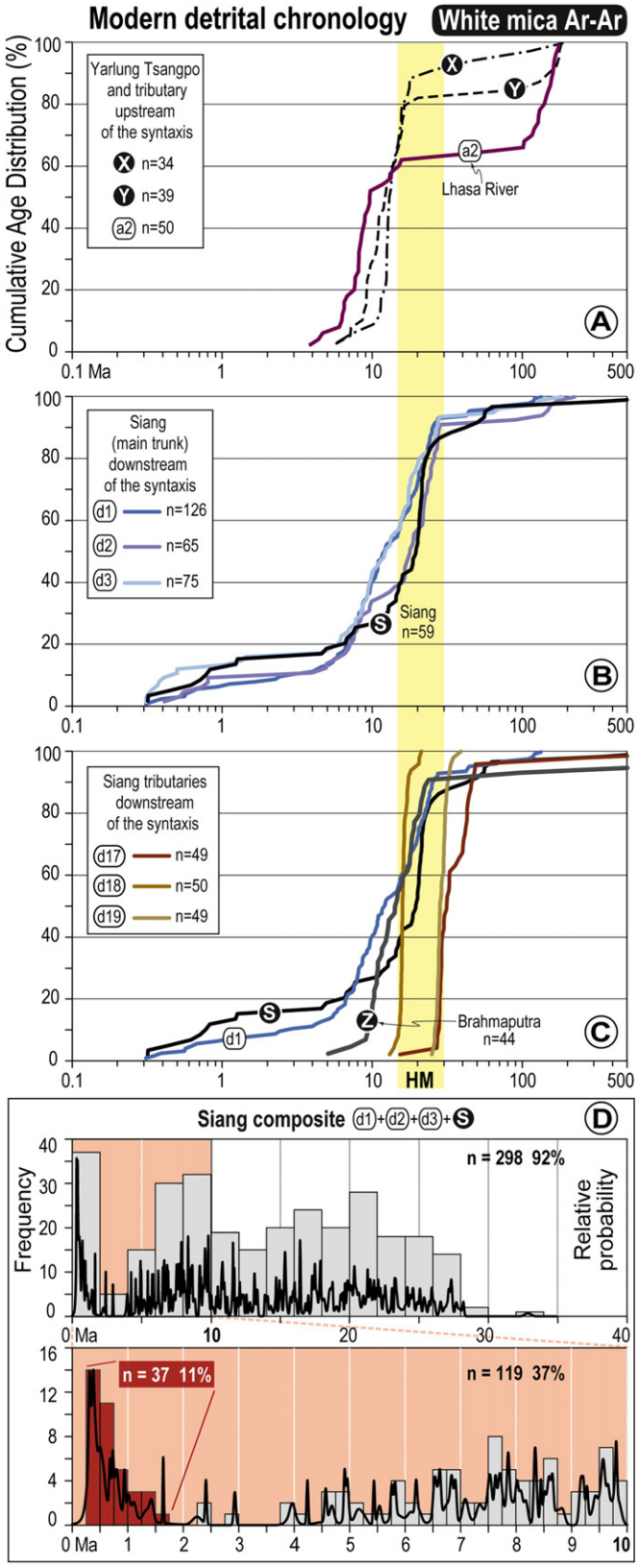

Fig. 12. Cumulative age distribution and probability plots of Ar–Ar white mica data from the modern Yarlung Tsangpo–Brahmaputra and some of its tributaries. Samples from this study and the literature (Table 1). Sample locations are shown Fig. 9; in A to C n indicates the total number of datapoints plotted for each sample; yellow vertical band: main age-range of peak Himalayan metamorphism in GH units (HM; cf. Figs. 10 and 11). In D n indicates the number of plotted datapoints; percentages indicate the relative amount of n compared to the total number of grains analysed. See text for discussion.

suture bounding the GP–NB massifs (Fig. 9) have the overall youngest cumulative curves.

The youngest detrital ZFT peak age of the entire dataset is ~0.3 Ma from a stream draining a high cirque on the NW side of the Namche Barwa massif (sy2, Fig. 13D). Remarkably, the Yarlung Tsangpo (sy1)

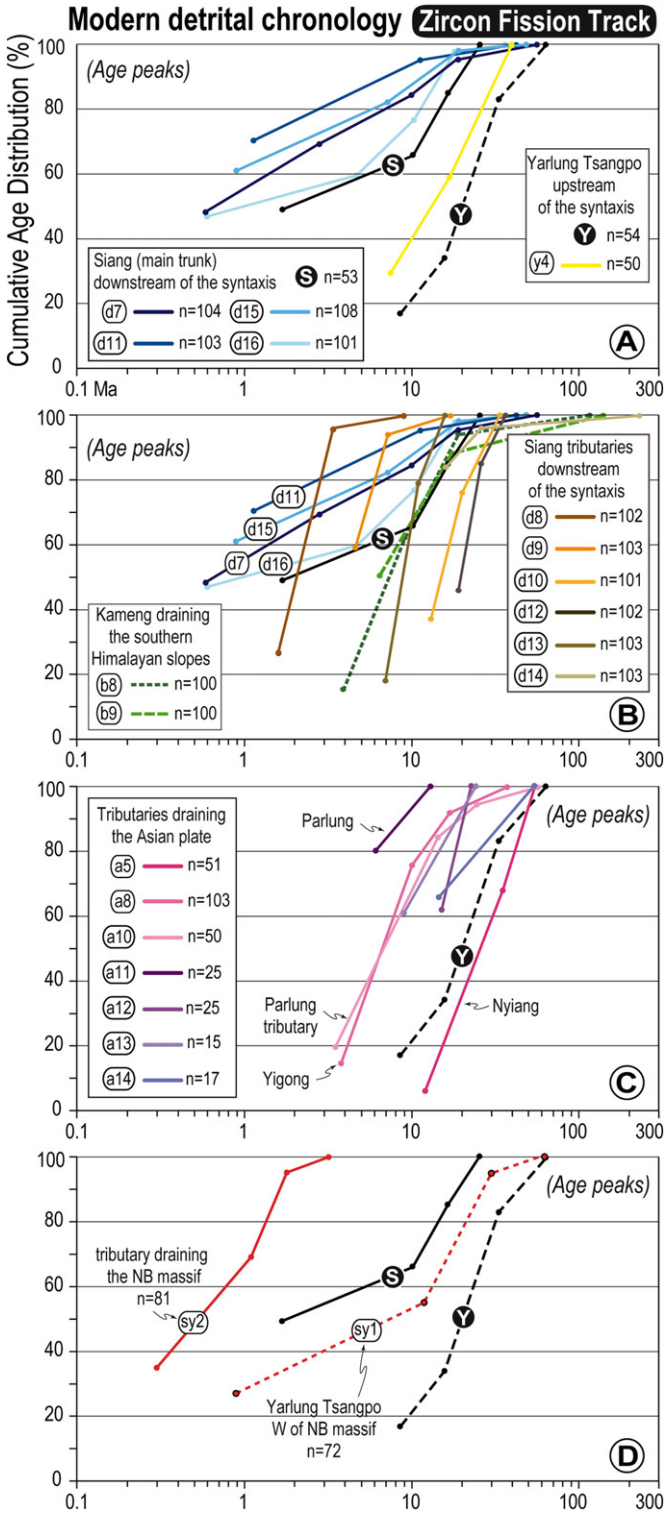

Fig. 13. Cumulative age distribution of ZFT data (plotted as main age peaks; n = total number of grains for each sample) from the modern Yarlung Tsangpo–Brahmaputra and some of its tributaries. Samples from this study and the literature (Table 1). Sample locations are shown Fig. 9. See text for discussion.

downstream of the junction with this stream and upstream of the gorge carries this very young isotopic signature in its youngest peak of 0.9 ± 0.1 Ma.

The available detrital ZFT data from the eastern Himalaya confirm that the northernmost part of the syntaxis (with the Namche Barwa–Gyala Peri massifs at its core) is characterised by a unique isotopic signature in agreement with the other higher-T chronometers, and that this distinctive fingerprint is preserved and detectable in its erosion products (even in Brahmaputra samples further downstream, as shown by the ongoing work of Gemignani et al. (2016), not shown here, accounting for <2 Ma ZFT populations in several Brahmaputra samples from the Assam plains).

As a general comment on the data discussed in this whole Section 4.2, we note the striking similarity of cumulative age patterns of detrital samples draining source areas apparently homogeneous in terms of their isotopic signature. This is even the case for samples collected from locations several hundreds of km apart (e.g the Yarlung Tsangpo –main trunk– upstream of the syntaxis, all the four chronometers). We also note the effectiveness of the detrital multi-chronometer approach in effectively representing the thermal state of any given source area (e.g. the Namche Barwa–Gyala Peri massifs vs. the GH rocks from Bhutan to Arunachal Himalaya). Finally, although in general the number of analysed grains per sample is clearly important to identify all age components in the case of complex provenance or downstream dilution effects, in more than one case presented in this study the variable number of analysed grains did not seem to be the key parameter affecting the ability of the data of effectively characterising the provenance of the samples (cf. the Ar–Ar white mica cumulative curves of the four Siang samples, with n ranging from 59 to 126).

4.3. Comparison of detrital data with new U–Pb rutile bedrock data from Namche Barwa

In Sections 4.1 and 4.2 we have shown that both the Siang and the Brahmaputra modern sand samples yielded a <3 Ma rutile population that we interpret to derive entirely from the erosion of the northern core of the syntaxis.

This interpretation is supported by our new U–Pb bedrock rutile data determined on two high grade rocks from the west of the Namche Barwa metamorphic massif: a mafic granulite from a boudin and its host rock, a pelitic gneiss (respectively samples T604 and T602; Xu et al., 2010). The U–Pb data of both samples (Supplemental Table A3; Fig. 14) are characterised by a cluster of concordant data within their uncertainty and one array of discordant data intercepting the cluster of concordant data at its lower end. The discordant data reflect a variable proportion of common Pb within the analysed grains. The regression of all data (plotted respectively on a Tera–Wasserburg and a Wetherill Concordia diagram, Fig. 14) for sample T602 yielded a lower intercept of 1.39 ± 0.13 Ma and for sample T604 gave 1.31 ± 0.96 Ma. The weighted average of the youngest population of sample T602 (of the two samples the one affected by lower variability in the common Pb relative content of the data) is 1.38 ± 0.05 Ma (eight concordant datapoints overlapping within uncertainty; MSWD = 0.76). Our best estimate for the age of these rutile bedrock samples from the Namche Barwa massif is therefore 1.4 ± 0.1 Ma.

As described previously (Sections 4.1 and 4.2) a small drainage in the south-western half of the syntaxis entirely within GH (sample P, see location in Figs. 2C and 9) has a uniform rutile population of 9.3 ± 0.2 Ma (cf. the main peak in its detrital age distribution, Fig. 5). A regression through all the data gave for this sample a lower intercept of 9.90 ± 0.64 Ma (Fig. 14). The comparison between samples T602–T604 and sample P provides evidence that rutile ages young dramatically towards the northern core of the syntaxis, though it is not known if there is a continuous gradient or an abrupt change. Additionally, the rutile cumulative age distributions of the Brahmaputra and the Siang (Fig. 8) show that 2–8 Ma grains are rare, with none in the range 4–6 Ma (Fig. 14). This indicates that the source of the very young rutile grains is distinct in age and that if intermediate age (3–8 Ma) grains are present in the drainage they are very subordinate in terms of source apportionment. A distinct <2 Ma detrital white mica population

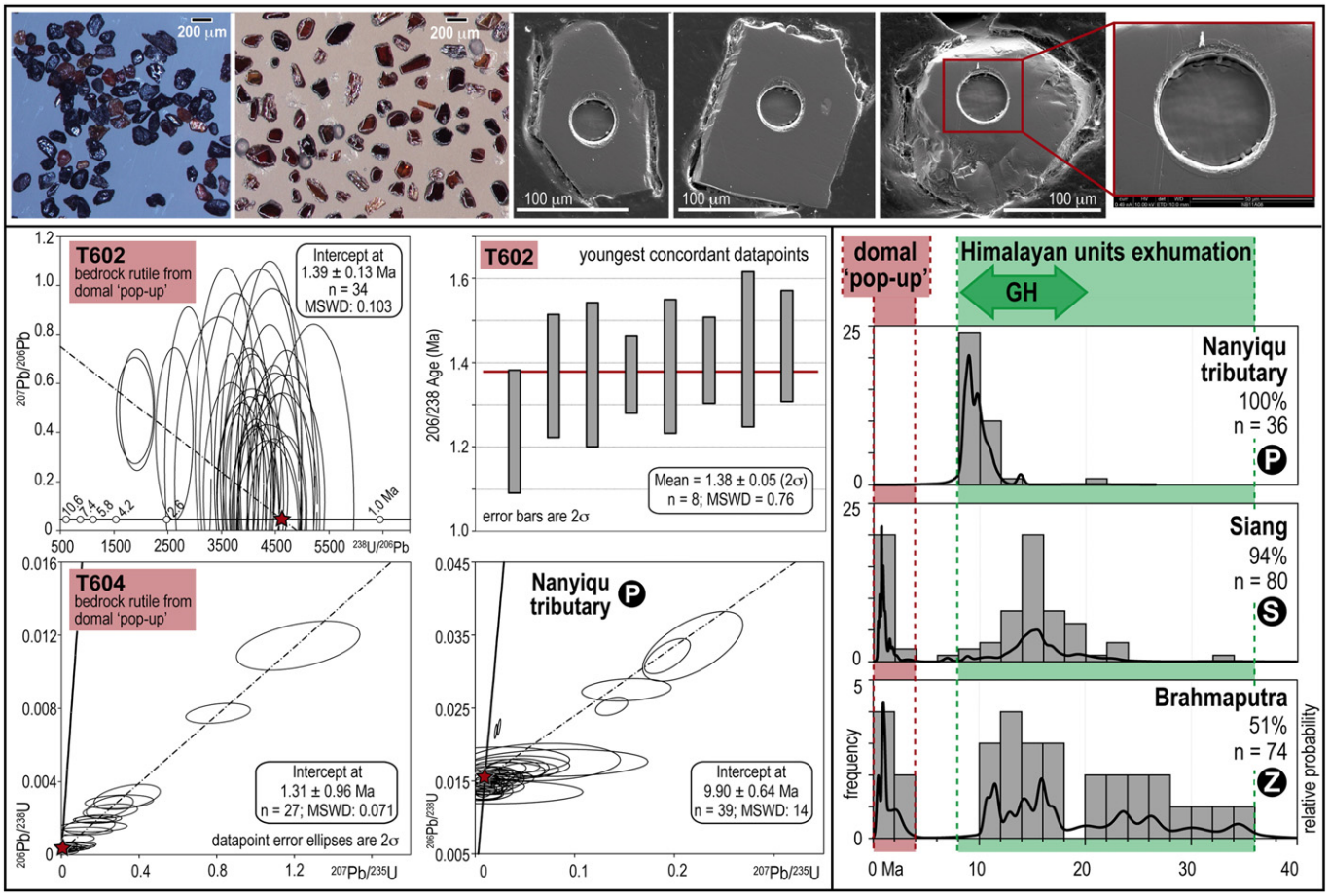

Fig. 14. Images and U–Pb data of key rutile samples. Top panel (left to right): rutile grains before (sample O) and after sample mounting and polishing (sample W); SE (secondary electron) images of ablated rutile grains, with detail of a 50 μm ablation pits (measured pit depth: 20 μm). Bottom left panel: Tera–Wasserburg diagram of rutile from gneiss T602, Namche Barwa massif; weighted average diagram of the youngest 206/238 age population in T602; Concordia diagrams of rutile from granulite T604 (Namche Barwa massif) and detrital sample O (tributary of the Nanyiqu river, draining exclusively the south-western flank of the syntaxis; Fig. 2C). Bottom right panel: probability density plots of rutile U–Pb data showing the occurrence of a <~3 Ma age component exclusively in the modern detritus downstream of the syntaxial domal 'pop-up' (samples S and Z); this component is absent south-west of the Nam–La Thrust as shown by the detrital age distribution of the Nanyiqu river (sample O) and its tributary (sample P), with rutile being >9 Ma. The erosion of GH is mainly reflected in detrital rutile in the range 9–20 Ma (Bracciali et al., 2013).

similarly characterises the Siang at various locations downstream of the syntaxis (Fig. 12D).

5. Detrital chronology of Neogene Himalayan sedimentary deposits

5.1. Neogene palaeo-Brahmaputra deposits from the Surma Basin

U–Pb zircon data from a recent study (Bracciali et al., 2015) documented the first influx of Transhimalayan Arc-derived zircons in the uppermost Barail Formation of the Surma Basin,.thus constraining the timing of the capture of the Yarlung Tsangpo by the palaeo-Brahmaputra as Early Miocene (~18 Ma). Additionally, increasingly dominant and upwards-younging Cenozoic zircon and rutile from the same samples (plotted in Fig. 6 of this study) testify to progressive erosion of the metamorphosed Himalayan units (in agreement with petrographic and isotopic evidence; Bracciali et al., 2015). Consistently, the new Ar–Ar data determined in this study on the same samples and presented in Fig. 6 show a general proportionate increase of Cenozoic white mica grains and younging of their ages at higher stratigraphic levels.

The published U–Pb and new Ar–Ar and ZFT data of these Neogene Surma Basin samples are plotted as cumulative age distributions in the range 1 Ma–1 Ga in Fig. 15. We indicate for each U–Pb and Ar–Ar sample the youngest grain, and we compare the detrital chronology of the samples with their depositional age (cf. Fig. 6).

A marked steep section of the cumulative age distribution of all zircon samples at ~500 Ma (Fig. 15) suggests the contribution from TH or GH rocks (in the latter case likely from late Pan-African granites intruding Indian crust of GH), in analogy with the modern river data (Figs. 8 and 10). The zircon data also show the general increase up-section of Cenozoic grains, as indicated for example by the increase of the <40 Ma grains from none in the Bhuban Formation, to 5–10% in the Bokabil and up to 15% in the Tipam and Dupi Tila. The youngest grains of these samples generally confirm this younging trend, with the youngest grain of the whole dataset (9 Ma) found in the uppermost Dupi Tila sample (sample 34). However we observe a certain degree of variability, as shown for example by the youngest grain in the Bokabil Formation (13 Ma) being younger than the youngest grain in the Tipam Formation (17 Ma). In part this could be due to the relatively small number of data <50 Ma (up to 20%) compared to the other zircon age populations of the samples. Additional analytical work, particularly aimed at targeting the zircon rims, would certainly allow better resolution of the Oligo-Miocene and younger zircon growth events in the source areas

The rutile U–Pb data show the occurrence in all samples of a 500–600 Ma population (Fig. 15 and probability plots of Supplemental Fig. A5). We identify the Lhasa Terrane metamorphic basement as the likely source for these grains, in analogy with the same interpretation for the modern Yarlung Tsangpo–Brahmaputra (Figs. 8 and 11). We cannot rule

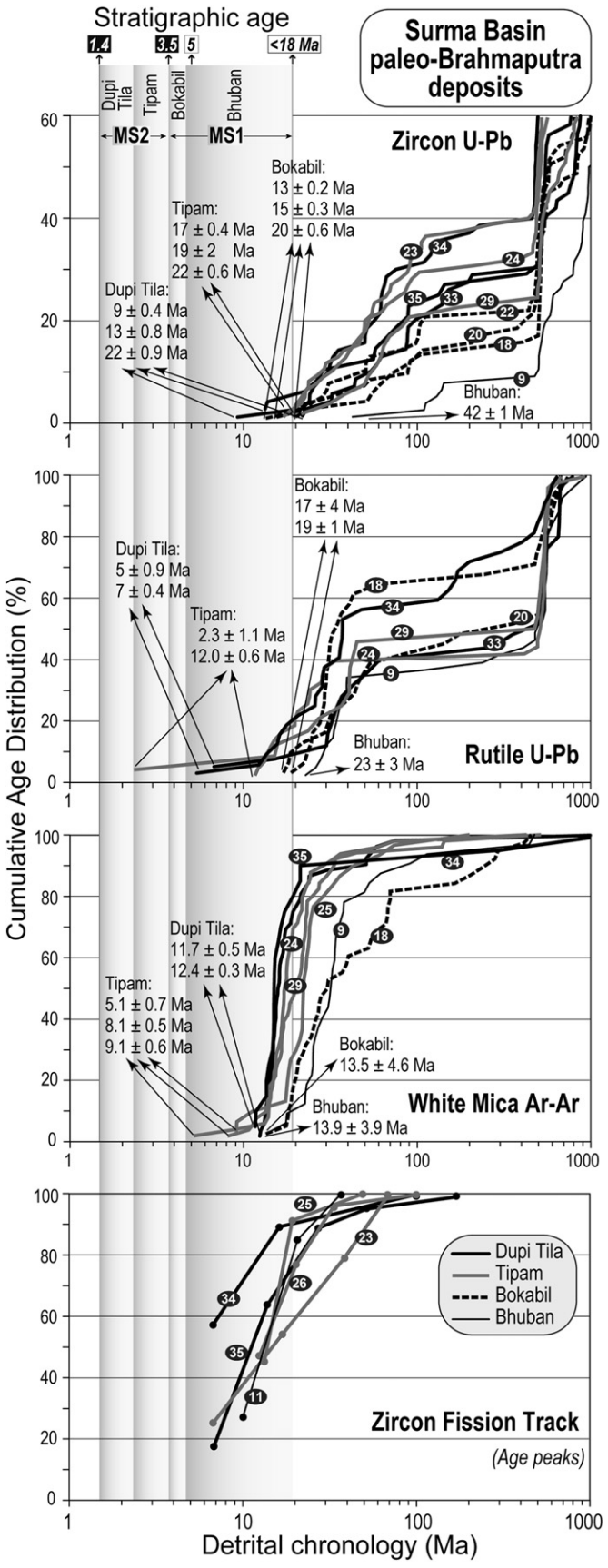

out however that part of these grains may be derived from a metamorphic source of similar age located to the east of the Surma Basin and contributed by a river draining the Cenozoic Indo-Burman Ranges (cf. the U–Pb rutile age peak at ~500 Ma of the modern Dhansiri River draining the IBR, Fig. 11D). In the Tipam Formation, we record the first appearance of an ~2 Ma date of rutile.

Detrital white mica grains in our samples are dominantly Cenozoic (60–80% of the sample in the uppermost Barail to Bokabil, >90% in the Tipam and Dupi Tila), with sporadic Jurassic–Cretaceous and rare Cambrian and Precambrian grains (Figs. 6 and 15).

All the ZFT samples (Bhuban to Dupi Tila) exhibit Late Oligocene–Early Miocene central ages overlapping within uncertainty at the 2σ level (Fig. 6). The data indicate an increasingly abundant Middle–Late Miocene detrital population up-section, corresponding to ~25% of the sample in Bhuban (sample 11) and lower Tipam (sample 23), and ~45% in upper Tipam (samples 25 and 26). The youngest age peak in all samples is older than the Miocene–Pliocene boundary (Fig. 15).

The general trend of decreasing ages up-section exhibited by the Oligo-Miocene zircon age populations in the Neogene Surma Basin deposits is confirmed by both rutile and white mica data (note the shifting of main age peaks towards younger detrital age in progressively stratigraphically younger samples in the probability plots of Fig. 6). However, the Tipam samples exhibit 5–9 Ma youngest white mica grains that are systematically younger than the ~12 Ma youngest Dupi Tila grains (Fig. 15). Similarly, the youngest rutile grain of the whole dataset (2.3 ± 1.1 Ma) is found in the highest stratigraphically Tipam sample 29 (stratigraphic age ~3.5–2 Ma), and the youngest age peak of one Tipam sample (23) is the same as the two Dupi Tila samples (34, 35; Fig. 15).

The Dupi Tila data need to be discussed in light of the recent work of Najman et al. (2016), showing that surface uplift of the Shillong Plateau bounding the Surma Basin to the north started during the deposition of the Tipam Formation. The rise of the plateau and the coeval westward encroachment of the Indo Burman Ranges resulted in the diversion of the palaeo-Brahmaputra away from the Surma Basin to the west of the plateau. As a consequence, sedimentation in the basin continued with the meandering facies of the Dupi Tila Formation, likely predominantly sourced by recycling of the Himalayan-derived sedimentary cover of the rising plateau immediately to the north, ± possible contributions from the IBR to the east (Najman et al., 2016). Recycling of Tipam deposits is compatible with rutile and white mica youngest grains and ZFT youngest peaks (allowing for the limitations of FT age modes defined by relatively small numbers of grains) in the Dupi Tila Formation being ca. same age or older than youngest Tipam grains. Importantly, these youngest grains and age peaks in Dupi Tila samples are never younger than the stratigraphic age of the Tipam Formation. Based on this evidence from detrital chronology and on the conclusions of Najman et al. (2016) we argue against derivation of the Dupi Tila deposits directly from the erosion of the syntaxis, hence we do not include Dupi Tila data further in the discussion.

We recognise and have discussed previously: i) the limited robustness of ZFT data in defining the true age components of a sample; ii) the potential biases (source fertility and dilution effects) that affect the ability of the white mica provenance proxy of tracking the syntaxial source in distal locations in the absence of a large number of analysed grains; and iii) the general dilution downstream of the syntaxial signature (all the four chronometers). Nonetheless we have shown (Sections 4.1 and 4.2) that not only the detrital isotopic signature of the modern fast exhuming syntaxis is unique within the eastern Himalayan region,

Fig. 15. Cumulative age distribution of detrital age data of palaeo-Brahmaputra deposits from the Surma Basin compared to their stratigraphic age. Data and stratigraphy as in Fig. 6. ZFT data are plotted as main age peaks. Arrows indicate the youngest grain in each U–Pb and Ar–Ar sample (±2σ uncertainty). In addition to the 1.4, 3.5 and <18 Ma key chronostratigraphic constraints for this basin (Section 2.3), the Miocene–Pliocene boundary (~5 Ma) is indicated as a reference (see main text for discussion).

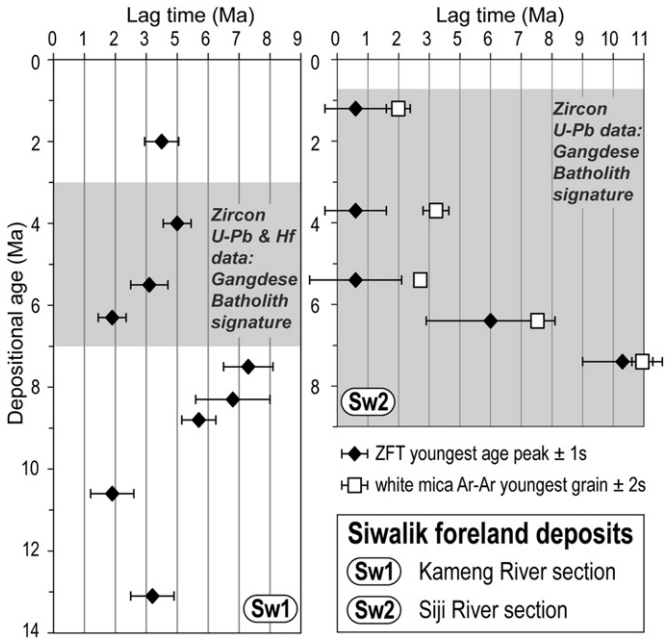

Fig. 16. Lag times plotted versus depositional age of Siwalik deposits from two stratigraphic sections in the eastern Himalayan foreland southwest and south of the syntaxis. Data from Cina et al. (2009), Chirouze et al. (2013), Lang and Huntington (2014) and Lang et al. (2016). Location of the stratigraphic sections Sw1 and Sw2 shown in Fig. 9.

but that it can be tracked in Brahmaputra sediments sampled at distal locations (with respect to the syntaxial source) in the Assam plains. Considering that zircon, white mica and rutile generally occur in our Surma Basin sandstone samples as abundant accessory phases (zircon and rutile) and framework grains (white mica), we conclude that it is plausible that a major phase of rapid syntaxial exhumation in the Early Miocene to early Pleistocene time interval would have been recorded as short lag time grains in its coeval erosion products (Bhuban to Tipam deposits) and that such a signature would be observable assuming that a sufficient number of grains were analysed per sample. In Section 7 we provide additional lines of evidence (based on bedrock and modern detrital chronology as well a simple numerical model) to constrain the initiation of the rapid exhumation of the syntaxis.

5.2. Neogene Siwalik foreland deposits in the easternmost Himalaya

We summarise here detrital chronology from magnetostratigraphically dated Neogene foreland deposits of the Siwalik Group (see Chirouze et al., 2012 for a review of Siwaliks deposits along the Himalayan foreland) from two stratigraphic sections respectively south-west and south of the syntaxis (locations Sw1 and Sw2 in Fig. 9). In Fig. 16 we summarise lag times calculated for the two sections based on detrital ZFT (youngest age peak in the sample) and Ar–Ar data (youngest grain) from Chirouze et al. (2013) and Lang et al. (2016).

Based on U–Pb and Hf zircon data, Cina et al. (2009) reported the occurrence of Gangdese Batholith-derived detrital zircons in 7–3 Ma Middle to Upper Siwalik deposits from the Kameng section (Sw1) in the Arunachal Himalaya (Bhalukpong area; base of section ~13 Ma; Chirouze et al., 2012). For the same 7–3 Ma stratigraphic interval Chirouze et al. (2013) determined whole rock ε_{Nd} values diagnostic of rocks from the suture zone (Fig. 16). These data indicate a connection between the Lhasa Terrane and the foreland basin at the Sw1 location between 7 and 3 Ma via a large, transverse river system variably interpreted to be either the Kameng or Subansiri directly draining through the suture zone or an integrated palaeo-Yarlung Tsangpo–Brahmaputra (Cina et al., 2009; Chirouze et al., 2013).

Chirouze et al. (2013) used the ZFT lag times of sediments deposited between 13 and 8 Ma and after 3 Ma to constrain exhumation rates of eastern Himalayan sources (in their interpretation not including the eastern syntaxis for these time intervals) of 1.8 mm/yr for the most rapidly exhuming source areas. They suggest that this indicates exhumation dynamics similar to those of the central Himalaya, also based on the similarity of ZFT age peak trends between this Siwalik sedimentary section and other sections in Nepal. For the 7–3 Ma Siwalik sediments (deposited by the palaeo-Brahmaputra draining through the eastern syntaxis in the interpretation favoured by Chirouze and coauthors) lag times of youngest ZFT peaks were on average shorter (Fig. 16). Nonetheless, exhumation rates of 1.5–2.0 mm/yr were estimated for the eastern syntaxis (interpreted to be the main zircon source to these deposits) that were similar to those estimated for the eastern Himalaya. Such significantly lower rates than the modern rates (>10 mm/yr) suggest that rapid exhumation in the eastern syntaxis did not begin before 4 Ma (Chirouze et al., 2013).

Lang and Huntington (2014) interpreted the U–Pb detrital zircon signature of Siwalik foreland deposits from the Siji River section (Sw2) to indicate a direct connection of this part of the foreland Himalayan basin to Gangdese rock sources in the Asian plate via the eastern syntaxis. In the same samples, Lang et al. (2016) observe a decrease up-section in lag times of both youngest ZFT peaks and white mica Ar–Ar youngest grains starting between 5 and 6 Ma (Fig. 16), interpreted and numerically modelled to reflect a 5 to 10-fold increase of syntaxial exhumation rate at this time. Exhumation rates are estimated as >5 km/yr since 5 Ma, an order of magnitude unique to the two syntaxes across the Himalayan orogen based on a compilation of lag times in Siwalik foreland deposits based on published data (Lang et al., 2016). These results will be discussed and compared to our detrital chronology and thermal modelling results in Section 7.

6. Initiation and pace of rapid exhumation within the syntaxis, as determined from the Surma Basin palaeo-Brahmaputra deposits

We showed in Section 5.1 that the thermochronological data from the marine-deltaic Early Miocene–Pliocene Bhuban and Bokabil formations have no signal characteristic of a rapidly-eroding syntaxis. Considering that the whole Bokabil Formation has been attributed to the Pliocene, the current data would indicate lag times of at least 8 Myr between the lowest T cooling event that we are able to track in the source (~300–450 °C based on Ar–Ar detrital white mica data as we have not collected ZFT data for this sample) and the deposition of the sediment. This is consistent with derivation from sources typical of GH and the Transhimalaya.

Additionally, in our Neogene Bhuban to Tipam Formation samples the Late Cretaceous–Cenozoic zircon populations become increasingly dominant and young up-section (Bracciali et al., 2015). Cina et al. (2009) interpret dilution of Gangdese-age zircons (from the Transhimalayan Arc in the Asian plate) in the modern Brahmaputra drainage downstream of the syntaxis as due to the high erosion rates across the syntaxis (although they fail to recognise any syntaxis-derived (i.e. <10 Ma) zircon in their Siang sample; their Fig. 3) and to the addition of Himalayan detritus further downstream. They suggest that, prior to the strong coupling between erosion and exhumation at the Namche Barwa massif, the concentration of Gangdese detritus would have been less affected by dilution because of the rapidly exhuming syntaxial source. Hence, in agreement with Cina et al. (2009), we suggest that the persistence and increase of Late Cretaceous–Cenozoic zircon populations in our Surma Basin samples likely indicate the lack of an extreme phase of exhumation and erosion of the syntaxis during Bhuban–Tipam times.

In the ~3.5–2 Ma Tipam Formation, we record the first appearance of ~2 Ma date of rutile which indicates very short lag time between cooling and deposition. By contrast, the abundance of syntaxis-derived very young grains in modern river sands is much higher, though there is clear dilution of this signal downstream (compare samples S and Z in Fig. 8). Tipam time is also the time of rapid rise of the Shillong Plateau facilitated by thrusting basement over the Surma Basin along the Dauki Fault and causing re-routing of the Brahmaputra River to its present course to the west of the Shillong Plateau at the end of Tipam deposition (Najman et al., 2016).

The sporadic occurrence in the Tipam Formation of a short lag time rutile grain suggests rapid uplift in the syntaxis in late-Pliocene time. The lack of grains indicative of short lag time lower in the sedimentary succession suggests that rapid uplift had not initiated significantly prior to this time.

An important question is how much time may have elapsed after initiation of rapid uplift and erosion but prior to first appearance of short-lag time detrital grains. In an abrupt and rapid uplift event, the first detrital indicators should be grains dated with the lowest-temperature threshold, i.e. U–Th–He and FT of apatite and zircon, since these retain either He or fission tracks once they cool below the ~70–200 °C temperature range, in the uppermost km of the crust. In the initial stage of rapid uplift, it is logical that surface uplift would precede substantial erosion, and that erosion (assuming the region was externally drained) would follow shortly. A period of perhaps 1–2 Myr is not an unreasonable time between initiation of rapid uplift and first appearance of detrital grains with short-lag times in the lowest temperature thermochronometers, since rates of erosion of several km/Myr are not uncommon in areas of high relief, such as the Himalaya (e.g. Finlayson et al., 2002). The abundance of such grains would increase with time as further uplift and erosion proceeded. Only with very substantial (>10 km) and rapid erosion would grains with short lag-times of high-temperature metamorphic thermochronometers, i.e. rutile U–Pb, ever appear in a sedimentary succession; indeed this paper is the first documentation of this in the sedimentary record to our knowledge, and indicates unusually rapid exhumation. With this situation in mind, it is likely that the initiation of rapid uplift and erosion may have begun prior to Tipam deposition in early Pliocene time ~5–4 Ma.

We suggest that the occurrence in modern river sands of extremely young grains (<1 Ma) within increasingly high thermal retentivities (i.e. ZFT, white mica Ar–Ar, rutile and zircon U–Pb), and the lack of grains with short lag times in the palaeo-Brahmaputra sedimentary record until the late Pliocene indicates substantial (>10 km) erosion in Quaternary time within the syntaxis, similar to conclusions initially published by Burg et al. (1997) using information from bedrock of the syntaxis.

The recent study by Wang et al. (2014) mentioned earlier is extremely pertinent as a complement to our data. They showed that the wide and sediment-filled Yarlung Tsangpo valley upstream of the gorge is filled with thick fluvial sediment extending upstream over several hundred km of longitudinal river distance. This sedimentary basin has buried an older incised canyon (characterised by an ~0.5% gradient), the infilling of which began at least 2.5 Ma based on cosmogenic dating of basal gravels upon bedrock within the buried gorge 150 km upstream of the syntaxis core. The infilling was caused by the rise of the bedrock floor of the ancestral canyon on the west flank of the uplifting syntaxial dome. The resulting reduction in eastward river gradient caused hundreds of metres of sediment to accumulate upstream, progressively burying the canyon and eventually reversing its palaeo-gradient, with an eastward rise in the former canyon level by at least 1 km over a 20 km distance upstream of the present gorge knickpoint. Wang et al. (2014) documented the apparent lateral gradient of the uplift to be approximately 5% on the far west part of what is regarded as the syntaxis domal uplift. This observation demonstrates that the position of the modern main knick-point within the syntaxis, often referred to as pivotal in the geomorphic evolution of the syntaxis (reviewed recently by

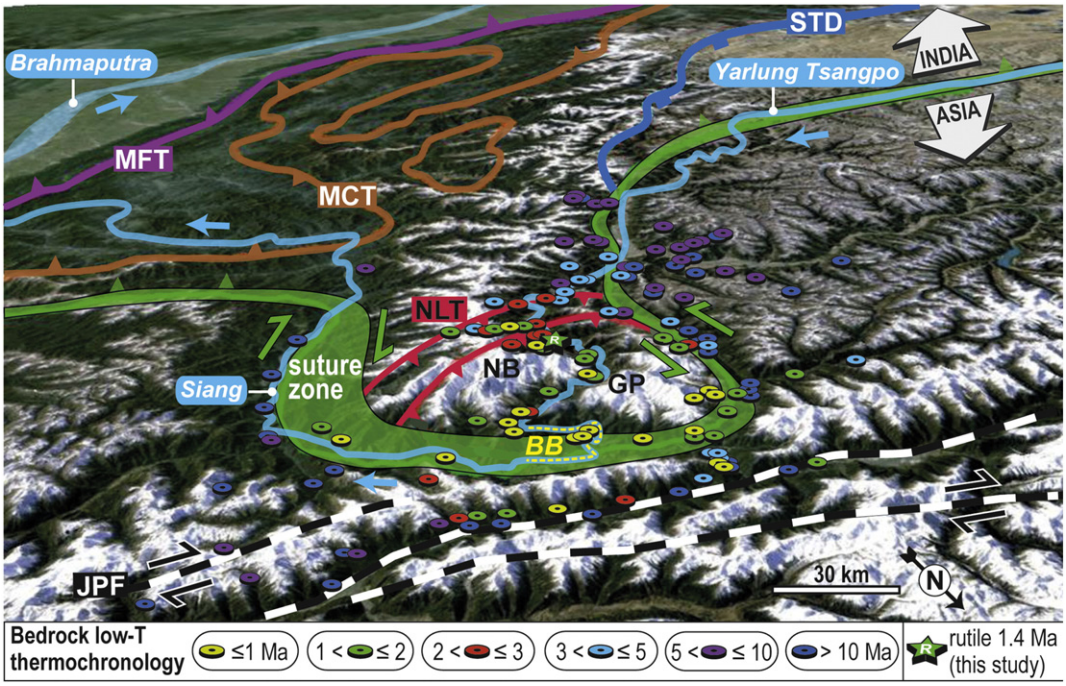

Fig. 17. Oblique image of eastern Himalaya and syntaxis looking southwest along the anticlinal trend of the syntaxis towards the Brahmaputra plain and the main part of the Himalaya in Arunachal Pradesh. Features shown (superimposed on a Google Earth Landsat Image) are: suture zone, Main Central Thrust (MCT), Main Frontal Thrust (MFT) South Tibetan Detachment zone (STD) and Nam–La Thrust (NLT) (cf. same features in Fig. 2C). BB: "Big Bend" of Zeitler et al. (2014). The youngest, exclusively Pleistocene, cooling ages for isotopic systems ranging from rutile U–Pb (~575 ± 75 °C T_c) to apatite U–Th–He and FT (80–120 °C Tc), are found within the domal 'pop-up' region bounded to the south by the Nam–La thrust and to the north by the suture and nearby portion of the Jiali–Parlung Fault zone.

Koons et al., 2013), is a coincidence of the emergence via erosional removal of Quaternary sediment of the deeply buried former canyon's bedrock floor as a result of uplift of the syntaxis 'dome'. The conclusion of Wang and coauthors is that the syntaxis domal uplift began at least ~2.5 Myr ago.

In summary, in the palaeo-Brahmaputra sedimentary record we have not found evidence consistent with the previous estimates of the inception of the syntaxis rapid uplift as being Miocene (Zeitler et al., 2001a). However, the latest Miocene and Pliocene ages of igneous and high temperature cooling events within the syntaxis, and the physical cause of the uplift, are yet to be fully explained. In Section 7 we address these issues and provide additional lines of evidence (based on bedrock and modern detrital chronology as well a simple numerical model) to constrain the initiation of the rapid exhumation of the syntaxis.

7. The syntaxial domal 'pop-up' and its cause

7.1. Coincidence of domal shape and youngest thermochronometry

As described in detail in Section 2, the northern end of the syntaxial antiform consists of an internally folded domal uplift defined on the three sides by the shear zones and suture zone rocks and on its south side by the N-dipping Nam–La Thrust (Figs. 2D and 16). Little is known of the structure of the Nam–La Thrust footwall other than it contains panels of paragneiss and orthogneiss in an overall elongate antiform extending to the south where it continues as the GH of the main part of the eastern Himalaya.

Very young metamorphic and cooling ages (Figs. 4, 17 and Supplemental Fig. A4) are largely spatially coincident with the syntaxial dome, with the <3 Ma low-T (T_c < 350 °C) cooling ages north of the Nam–La thrust, and our 1.4 Ma rutile U–Pb dates on the western side of the Namche Barwa massif (sample R in Figs. 4C and 17). On this basis, this paper refers to this area of young ages and domal geometry at the northern end of the syntaxis as the domal 'pop-up' on account of the exceptionally high rate of uplift required.

Burg and Podladchikov (2000) modelled in two-dimensions the syntaxis structure rheologically and produced pure shear thickening and symmetric buckling that then led to asymmetric thrusting with geometry not unlike to that seen in the syntaxis. Whilst there are limitations to this approach due to its important three-dimensionality, it demonstrates that a wholly structural origin for the feature is plausible. Like Burg et al. (1997), we consider the occurrence of very young ages with this northern domal part of the syntaxis is no coincidence, and assert that the pop-up dome north of the Nam–La thrust is intrinsically related to the origin of the syntaxis as we observe it today.

7.2. Reconciling the metamorphic, cooling and tectonic evolution of the syntaxis

The young (10–1 Ma, mainly 6–1 Ma) ages of both geochronometers and thermochronometers documented by various authors (initially by Zeitler et al., 1993 and by Burg et al., 1997 for the western and eastern syntaxis, respectively) are unique to the syntaxes of the Himalaya. The eastern syntaxis is not solely characterised by these young ages (summarised in Fig. 4C), but has widespread evidence for Miocene (~24–16 Ma) metamorphic and melting events within GH type rocks not dissimilar to the main part of the Himalaya (Burg et al., 1998; Zhang et al., 2010a, 2012a; Palin et al., 2014). However what is unique is that the youngest ages of metamorphic and igneous events persist into the latest Miocene and Plio-Pleistocene (Burg et al., 1997, 1998; Booth et al., 2009), with the youngest ages being broadly spatially coincident with the northern domal pop-up structure.

The rocks within the elongate anticline of the syntaxis have the lithological, geochemical, and metamorphic hallmarks of GH metamorphism (Section 2.3), but with a progressively younger age and the *youngest* events having occurred in the northernmost part of the syntaxis. For example, granulites within the northern syntaxis with ~20–24 Ma high temperature equilibration, have zircon rims as young as 8–11 Ma, and rutile, titanite, and hornblende cooling ages as young as 1–2 Ma, suggesting that whilst the peak metamorphism may have been ≥20 Ma (or at least >8 Ma), the rocks remained hot and deep in the crust and did not cool below 575 ± 75 °C until Plio-Pleistocene time.

By contrast, ages of amphibolite facies post-peak metamorphic events within the southern syntaxis, well south of the domal pop-up, are generally older (24–10 Ma; Palin et al., 2014) and the rutile ages near the western side of the southern syntaxis are ≥9 Ma (sample P, Fig. 14). Late Miocene ages are observed in northern exposed parts of the GH in the main Himalaya (Mottram et al., 2015), where monazite metamorphic and muscovite cooling ages are as young as 12 and 8 Ma, respectively.

Burg et al. (1997, 1998) suggested, using metamorphic phase equilibria in pelite and geochronology of leucosome in migmatite and metamorphic minerals, that decompression from pressures of 8–10 kbar following uppermost amphibolite facies metamorphism did not substantially begin until Pliocene time, after 4 Ma. Many other P–T determinations of 'peak' assemblages within the northern core of the syntaxis converge on conditions of approximately 700 ± 100 °C and 7–11 kbar pressure prior to decompression (see summary in Section 2), not unlike that seen throughout the GH of the Himalaya. Zeitler et al. (2001a, 2001b) and Booth et al. (2009) suggested, based on U–Pb geochronology of accessory minerals, that decompression related to exhumation began perhaps 10 Myr ago rather than as late as 4 Ma. No studies published to date within the core of the syntaxis, however, have sufficiently detailed P–T–t path determination to resolve this difference in apparent inception of decompression. For example, the 3–4 Ma xenotime and thorite in leucosome were inferred by Burg et al. (1997, 1998) to have been generated at the P–T conditions of nearby pelites, >700 °C and 8–10 kbar, but the petrology to demonstrate this unequivocally has not been published. Rapid decompression may have begun earlier, but what is clear is that the pattern of recent ages coinciding with the northern part of the syntaxis was produced by a distinct initiation and/or acceleration of uplift and exhumation in the Plio-Pleistocene.

The existing bedrock datasets are consistent with this conclusion of a distinct initiation or acceleration of Plio-Pleistocene exhumation of the northern part of the syntaxis, but quantifying the Plio-Pleistocene uplift and exhumation is more challenging. Most of the young U–Pb dates that bear on the metamorphic history (as opposed to lower temperature cooling history) are from accessory minerals (zircon, monazite, xenotime, thorite) from small volume pegmatites, leucogranites, leucosomes and pelitic lithologies, with young rims of zircons being the most dated mineral occurrence (Ding et al., 2001; Booth et al., 2004, 2009; Liu et al., 2011; Xu et al., 2012; Zhang et al., 2012a; Zeitler et al., 2014; Palin et al., 2015). These dates range from >10 Ma to as young as ~1 Ma. Some authors ascribe these rocks to decompression melting (e.g. Booth et al., 2004) but Burg et al. (1997, 1998) suggested that these were mainly generated at near peak conditions.

High temperature thermochronometers (500–675 °C) including Ar–Ar hornblende, U–Pb titanite and rutile have been sparsely applied to this region with only a handful of determinations. Within the northern domal pop-up region, limited precision titanite U–Pb (Booth et al., 2009) and hornblende Ar–Ar ages suggest cooling below ~500–600 °C perhaps 2–5 Myr ago. U–Pb rutile ages on bedrock samples and detrital grains from the Siang and Brahmaputra Rivers downstream, presented in this paper (Fig. 14) are as young as 1.4 Ma (bedrock) and <1.0 Ma (detrital), suggesting that cooling below 575 ± 75 °C was exceptionally

recent in the syntaxis. The occurrence, unique across the eastern Himalaya, of a <2 Ma white mica detrital population in the Siang, with main peak at ~0.4 Ma (Fig. 11D) suggests rapid cooling of the same source through ~300–450 °C.

Of the rutile grains from the Siang and Brahmaputra (samples S and Z; Fig. 14) that are younger than 10 Ma, 21 of 22 grains are 0.5 to 2.0 Ma, one grain is 3.2 ± 1.1 Ma, and no grains fall between 4 and 8 Ma. Of all of the grains that are <35 Ma old (74 grains measured with robust ages), only two are between 4 and 11 Ma, with nearly 1/3 of these being ≤3 Ma, the rest mainly being 11–20 Ma in age. This implies that the source of the very young rutile grains is distinct and relatively sharply separated from the source of all other rutile grains, without a significant 'transitional' source with ages between 3 and 11 Ma. This conclusion refers both to the area of the pop-up but also to its ~5–7 km of topographic relief. The implication is that within the domal pop-up, there are no rocks being eroded with rutile ages older than ~3 Ma, even at higher elevations, implying much more rapid exhumation than adjacent areas outside of the domal pop-up.

It is therefore plausible that most of the northern pop-up dome of the syntaxis was at temperatures >575 ± 75 °C prior to 1–3 Myr ago. Unfortunately the lack of coverage of rutile U–Pb dates is far too sparse to use this proxy for the boundary of the pop-up, and until more data become available we assume it is near the boundary of the suture high-strain zone to the west, the Jiali Parlung fault to the N-NE and near the Nam–La thrust to the south. Whilst this is entirely consistent with the large body of lower temperature thermochronological data summarised in Figs. 4 and 17, this magnifies further the amount of erosion that is Pleistocene in age, suggesting that the domal pop-up of the northern syntaxis is an area of exhumation distinct from the older syntaxis rocks to the south/southwest that have late Miocene metamorphic and igneous events arising from earlier post-peak pressure decompression.

This conclusion is supported by Palin et al. (2015) who undertook detailed P–T–t work on GH rocks to the southwest margin of the syntaxis well south of the pop-up dome. In that work, ~24 Ma peak (~610 °C) conditions at staurolite grade, dated by monazite inclusions within zoned garnet, were followed by decompression and greenschist conditions during shearing and faulting between ~16 and 8 Ma that produced retrograde reactions in major and accessory minerals. This period of decompression was followed by more rapid average cooling in the last 8 Ma. The study demonstrated that in some samples, several kilobars of post-peak decompression took place prior to 8 Ma that cannot be ascribed to the pop-up domal structure of Plio-Pleistocene age. This may have been a more general characteristic within the syntaxis prior to the Plio-Pleistocene.

The elements that must therefore be reconciled in a general model are: (1) a GH metamorphic signature of Miocene age from ≥700 °C and 7–11 kbar peak conditions with equilibration from 24 to ~12 Ma; (2) structural continuity of the syntaxis rocks with those of the main Himalaya and its local disruption by the south-verging Nam–La thrust fault zone; (3) probable decompression of GH rocks within amphibolite and in part upper greenschist conditions during the period ~15–5 Ma including the generation of small volume melts; (4) the development of major shear zones on the boundary of syntaxis antiform within GH and the suture zone with movement consistent with relative northward transport of the GH 'antiformal' footwall along the elongate boundaries of the syntaxis; and (5) a superimposed very rapid uplift and exhumation event in the Pleistocene largely restricted to the ~40 km by 40 km area largely coincident with the northern part of the GH rocks within the syntaxis, from temperatures in excess of 575 °C.

The vexing question is: what produced the domal pop-up that defines the unique characteristics of the syntaxis and is distinct from the surrounding region or the GH rocks to the southwest in the main part of the Himalaya? Burg et al. (1997, 1998) and Burg and Podladchikov (1999, 2000) ascribed this very rapid exhumation to compressional crustal folding, as a trigger, and showed that its progression could sustain the continued uplift (and erosion). By contrast, Zeitler et al. (2001a, 2001b) suggested that very rapid erosion led to crustal feedback mechanism by removing stronger uppermost crustal rocks that led to rise of weak ductile rocks to near the surface, leading in turn to further uplift, without appealing to compressional folding. In spite of the difference in origins, the resultant geometry of the latter model could conceivably result in a domal-shaped uplift centred about the area of maximum erosion in the gorge.

7.3. Himalayan mid-crustal context of the syntaxis and its domal pop-up

In attempting to understand the thermochronology of the syntaxis, the position of the pop-up dome in the Himalayan orogen is significant, as it exposes the northernmost part of the high-grade GH metamorphic core within the eastern Himalaya, the Namche Barwa complex (Fig. 2C). This is continuous with the mainly east to east-northeast trending GH of north-eastern India (Sikkim and Arunachal Pradesh), Bhutan and Nepal. As Palin et al. (2014) suggested, the GH rocks in the syntaxis may not have been exposed without very young uplift. As such, they may represent exposures of GH rocks that were deeply buried within the orogen until the Pliocene–Pleistocene uplift that folded the suture zone and are analogous to similar GH rocks of the Indian plate underthrusted beneath southern Tibet well north of the South Tibetan Detachment within the central part of the Himalaya (and possibly well north of the current trace of the suture). In this position within the main part of the Himalaya where substantial, presumably much less rapid, exhumation of deep-seated GH rocks beneath Tibet has yet to take place, the metamorphic history is likely to consist of early to middle Miocene peak metamorphism (~24 to 10 Ma) followed by a protracted residence period within the crust at amphibolite facies. In this scenario and with continued convergence between India and Asia, some southward movement (via low angle channel flow – cf. Beaumont et al., 2001 – or other shearing) may have taken place accompanied by modest decompression potentially driving anatexis (producing pegmatites, leucosomes, limited volume hydrous melts), some retrograde mineral phase reactions, and limited growth of rims on zircon/monazite whilst all other thermochronometers remained open systems due to residence at temperatures >575 °C. We emphasize here the importance of the residence of the syntaxial rocks for some time in the mid–lower crust (at suprasolidus conditions), effectively priming the system prior to their eventual rapid exhumation by thrusting along higher angle faults at the mountain front, facilitated by rapid erosion of the southern Himalaya.

Events such as emplacement of the North Himalayan gneiss domes, for example, and a few other exposures of metamorphic rocks (Langille et al., 2012; Lee et al., 2000) have exposed such materials within the hinterland of the orogen and they record ages of igneous, structural, metamorphic and cooling events that are younger than the front of the Himalaya (as young as ~9–12 Ma). Similarly, the domal pop-up of the northern part of the syntaxis at Namche Barwa has exposed a deep-seated metamorphic zone of GH rocks "before its time", providing a window into processes within the deep crust of the Himalayan hinterland.

There are other analogues for this scenario. In the Sikkim Himalaya over a cross-strike distance of ~50 km there is a northward-younging of metamorphic ages within the sheared and metamorphosed footwall of the MCT and a northward-younging of cooling ages in both MCT footwall and the GH (Mottram et al., 2015). The determined gradient is approximately 1 Ma younger for every 10–20 km farther north, such that ~12 Ma metamorphic events are present in northernmost exposures with white mica cooling ages as young as ~8 Ma. Extrapolating this gradient to the eastern Himalaya, the syntaxial region can be considered as an exposed portion of the GH that may be equivalent to rocks approximately 100 km north of the most northerly exposures of GH in the main part of the eastern Himalaya in northern Bhutan and northern Arunachal Pradesh. This gradient in age plausibly translates into a thrust-related decompression involving late melts and retrograde

metamorphism within amphibolite facies about 5–10 Ma younger than what could be expected within the eastern GH Himalaya of Nepal, Sikkim, Bhutan or Arunachal Pradesh, i.e. with ages of melts and some decompression extending to perhaps 5–10 Ma (cf. 12–20 Ma for analogous events in the main Himalaya).

The current interpretation of the sense of shear of the mylonite zones bounding the syntaxis suggests northward transport of the GH footwall relative to the suture zone hanging wall along its southeast and northwest sides. Whilst this is likely to be a composite shear zone with both early pervasive shear of Miocene age (Palin et al., 2014) and later shear and faulting related to Pleistocene doming and accommodation, the overall pattern is consistent with northward underthrusting of the GH footwall beneath Asia, prior to the steep anticlinal arching to form the syntaxis observed today. This is opposite to the sense of shear present within the normal sense STD, and needs to be reconciled. Curiously, in the eastern Himalaya, the TH (Fig. 2C) appears to taper eastward and virtually disappear as a mappable unit within the south-western-most part of the syntaxis, though some of the metasedimentary rocks within the bounding mylonite zone may be of Tethyan affinity (Booth et al., 2009). In any case the Tethyan rocks are either greatly attenuated or absent. Channel flow within the GH beneath the STD is thought to have stopped by ~16 Ma (Harris, 2007). One explanation might be that subsequent shearing/underthrusting of GH beneath the overlying Asian plate may have recommenced in the Late Miocene to accommodate further contraction, overprinting any earlier normal sense of motion.

The 'pre-syntaxis' residence of GH within the deep crust to produce evidence of 'post-peak' metamorphic signatures, 'anaemic' small-volume late leucosomes, leucogranites, and pegmatites, and limited decompression may be a reasonable explanation for some of the features observed within the syntaxis that may have pre-dated the rapid domal pop-up rise of the syntaxis. This is at least an explanation for the latest Miocene evidence of melting and metamorphism that links it in terms of process to the main Himalaya, without it needing to be associated with the distinctive rapid exhumation of the domal pop-up of the northern syntaxis.

What is clear is that, prior to the inception of very rapid uplift, rocks of the 30–50 km wide core of the syntaxis domal pop-up were hotter than 575 °C in Plio-Pleistocene time and at significant depth within the crust. Their depth is difficult to determine but may have approached 20 km (>6 kbar according to Burg et al., 1997, although the data in that paper are not robust in terms of a depth estimation for the melting events). Given that rutile and hornblende cooling ages of <2 Ma are present within the syntaxis and that the Siang River sediment has a dominant <3 Ma age peak for rutile arising from modern erosion of the pop-up area, rutile cooling ages within the domal pop-up are likely to be <3 Ma over >5 km of topographic elevation difference of the Gyala Peri and Namche Barwa massifs. This implies a very large magnitude of erosion within the domal pop-up. If the pre-pop-up surface thermal gradient was ~35–40 °C/km as might be expected if the rocks had equilibrated ~3–4 Myr ago at 20 km depth and ~650 °C, the erosion produced by the Plio-Pleistocene uplift could have approached or exceeded 20 km. Combined with numerical solution of the thermal field, these thermochronological data can be used to constrain the permissible range of erosion rates and durations as it has been done by several authors, most recently by Zeitler et al. (2014) and Lang et al. (2016).

Table 2
Thermal model parameters.

Parameter	Value	Unit
Q_0, basal heat flow	48	mW/m^2
A_0, heat production at surface at start	5	$\mu W/m^3$
D, depth at which the heat production decreases by a factor of 1/e	8	km
k, thermal conductivity	2	W/m·°C
α, thermal diffusivity	25.3	km^2/Myr
ρ·Cp, product of density and heat capacity	2.5 E6	$J/m^3 \cdot$ °C

	Single stage	Two stage	
Duration of model	7	24	Ma
Stage 1 rate of exhumation	4	0.381	km/Myr
Time of change of exhumation rate (after start)	–	21	Ma
Stage 2 rate of exhumation	–	7	km/Myr

The initial geotherm is defined by: $T(Z) = a + (Q_0 \times Z/k) + (D^2 \times A_0/k) \times (1 - \exp(-Z/D))$, where T(Z) is the temperature at depth Z and a is the surface temperature.

Table 3
Thermochronological constraints for modelling.

Thermochronometer	Mean date for modelling (Ma)	Range over 6 km elevation (Ma)	Lag times (Myr)	
			for 1–5.4 Ma Siwalik deposits	for >6 Ma Siwalik deposits
Rutile U–Pb	1.4	0.4–3.0[a]	–	–
Biotite Ar–Ar	1–2	0.2–2.0	–	–
White mica Ar–Ar	–	0.4–1.5[a]	2–3	>6
Zircon fission track	0.8–1.5	0.2–1.0	<1	>4
Zircon (U–Th)/He	~1	0.1–1.0	–	–

[a] Inferred from modern river sands.

7.4. Thermal modelling of uplift and erosion: methods, parameters, constraints

Models for the origin of the extreme exhumation in the syntaxis (discussed in the Introduction) although propose a range of different explanations from structural buckling, river capture, erosion–deformation feedbacks and subduction geometry in the indentor region, all predict very rapid erosion and uplift in the syntaxis. In this section we aim to place clear bounds on the time of initiation and rates of rapid exhumation by investigating permissible combinations of erosion rate and intensity that satisfy the aforementioned thermo- and geochronological constraints of the thermal–tectonic evolution of the eastern syntaxis with a thermal model. Importantly, our new U–Pb rutile data permit to further constrain model parameter space (i.e. permissible rates and timing of erosion) and hence to go beyond previous modelling.

Erosional exhumation of >15 km in the last 4–6 Ma, would have advected heat upwards, elevating the near surface geothermal gradient. Given the ~5 km of current topographic relief and rapid implied erosion rates, isotherms <~200 °C would be perturbed on amplitudes governed by topography (Stüwe et al., 1994) with highest gradients in deep valleys. However, as will become clear, the key constraint on the magnitude and rate of exhumation is the highest temperature thermochronometer, rutile U–Pb. Within the centre of the dome in the temperature realm of ~575 ± 75 °C, isotherms are initially deep enough to be unaffected by surface topography. With this in mind, like other authors, we adopt a simplified thermal modelling approach in which we solve the heat equation with advection and radiogenic heat production using standard finite difference methods on a 1-D mesh. Successful heat flow solutions must satisfy the thermochronological and geochronological data that have been discussed previously. Salient parameters used in the model are presented in Table 2.

We solve the heat equation using a fully implicit discretization, predefined surface and basal temperatures and an exponential distribution of heat production with depth. Numerical accuracy is verified through comparison with available analytical solutions (equation 15.2 of Carslaw and Jaeger, 1959). The initial geotherm is a solution to the non-transient heat equation with fixed surface temperature, exponential distribution of heat producing elements and a specified mantle heat flux; these parameters are optimised to fit a P–T point derived from peak metamorphic conditions (see below; 820 °C, 28 km). Thermal histories for three samples are considered, simulating the cooling history of syntaxis rocks with elevations of 2, 5, and 8 km elevation

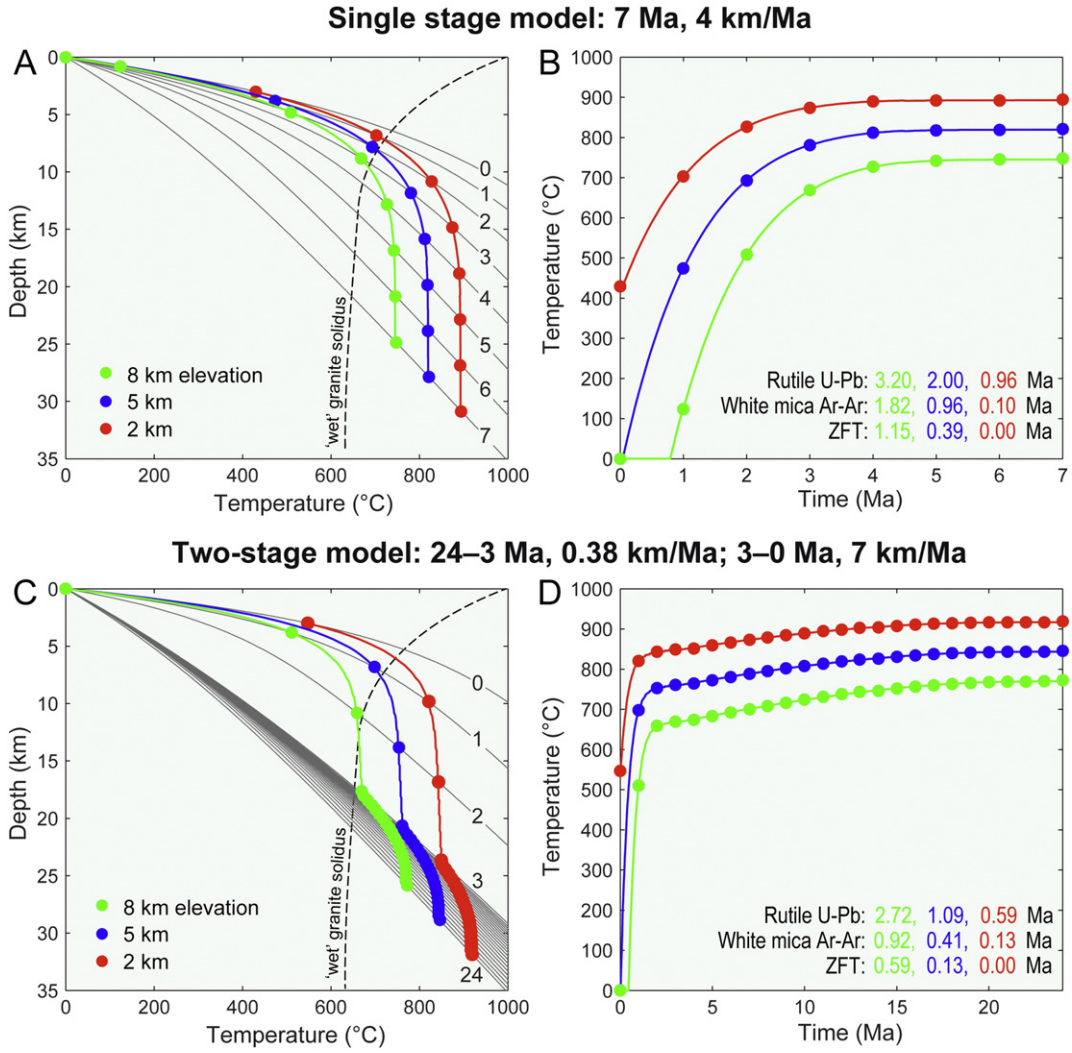

Fig. 18. Results of numerical modelling of heat flow and erosion in the domal 'pop-up'. Two different models (single stage and two stage) are shown as depth temperature plots (A, C) and temperature time plots (B, D). The duration and exhumation rates are listed above each set of diagrams. Green, blue and red dotted lines connect the paths of nominal samples at 8, 5, and 2 km elevation above sea level for the Namche Barwa–Gayla Peri massif. In A) and C) the wet granite solidus and the evolving geotherms at 1 Ma time intervals are also shown (the latter labelled as black numbers within the plots). The calculated dates of three thermochronometers are shown in the lower right part of panels B and D. The equilibrium mean geothermal gradients for the upper 1 and 5 km of the crust are ~40 °C/km and 36 °C/km, respectively; at 20 and 28 km depths the temperatures are ~630 °C and 820 °C, respectively. The sample initially at 820 °C and ~28 km depth is assigned to the 5 km elevation sample in the massif.

today in the Namche Barwa–Gyala Peri massif. The 2 and 5 km samples' thermochronological constraints are provided by existing published data and new data from this paper (Table 3). The erosion of the upper part (>5 km elevation) of the syntaxis has few thermochronological data but its rutile dates are unlikely to be older than 3 Ma, given our interpretation of the rutile age and other dates of grains in the Siang River sediments downstream (Section 7.2). The cooling history for each of the sample nodes is used as input to a forward kinetic model that calculates single-grain ages for the U–Pb and $^{40}Ar/^{39}Ar$ (K–Ar) systems. For the U–Pb rutile system we employ the Cherniak Pb diffusion law (Cherniak, 2000), 20 ppm U concentration and rectangular grain dimensions (150 × 100 × 100 μm). For the white mica $^{40}Ar/^{39}Ar$ forward model, we used the Ar diffusion law of Harrison et al. (2009), 10 wt.% K_2O and a sheet-like geometry (300 × 300 × 50 μm). Grain dimensions were recast into equivalent sphere dimensions. Due to the uncertainty over the kinetics of FT annealing, we chose to record the timing at which a sample traversed the 220 °C isotherm as representing closure of the ZFT system.

We explored a range of candidate erosion histories and compared calculated ages to both bedrock (using in part a summary of data from the pop-up dome from Zeitler et al., 2014) and detrital thermochronological constraints presented in Table 3. Specifically, we used detrital thermochronological data of Lang et al. (2016) from 1 to 6 Ma Siwalik foreland deposits (Fig. 16) to assess if our solutions are also consistent with the ages and lag times resulting from past erosion recorded in these foreland Plio-Pleistocene sediment archives.

Our starting point was to assume a "peak" P–T condition that defines the depth and temperature of the highest grade rocks of the syntaxis so that the maximum exhumation does not exceed the maximum depth of burial. An initial "Himalayan" geothermal gradient was used that is consistent with the P–T paths of GH rocks and peak P–T conditions inferred from the metamorphic studies, which include migmatite and granulites. We have set the initial geotherm to be consistent with ~28 km depth at ~820 °C at 24 Myr ago, based on consistency with P–T–t data that has been summarised recently by Palin et al. (2015). This is not dissimilar to pre-uplift P–T estimates as discussed earlier in Section 2.3.

7.5. Thermal modelling: results and discussion

Results for two plausible erosion scenarios are shown in Fig. 18 as depth–temperature curves (panels A and C) and temperature–time curves (panels B and D), respectively. The first model has the initial

condition at 7 Myr ago followed by a constant 4.0 km/Myr exhumation rate, whilst the second model has erosion from 24 Ma to 3 Ma at 0.381 km/Myr (8 km exhumation total) followed by 21 km exhumation in the last 3 Ma at a rate of 7.0 km/Myr. Samples dated in the syntaxis domal pop-up have very young, but non-zero, low temperature cooling ages and are more proximal to major valleys than peaks.

Both of these model solutions are consistent with the range of available thermochronological constraints for the bedrock ages. For example the predicted dates shown in Figs. 18B and D include primarily rutile dates <3.2 Ma and as low as 0.6 Ma, Ar–Ar mica dates of 0.1–2.0 Ma, and ZFT dates mainly 0–1 Ma. Models similar to the two stage model but with a later initiation of rapid exhumation (i.e. 1–2 Ma vs. 3 Ma) could explain the data provided that the rates in the second stage were higher (>10 km/Myr) with the same time-integrated amount of exhumation (~20 km) during the second stage, though predicted ages would be skewed to even younger ages. The key requirement of the modelling prior to ~2–3 Ma is having the samples from the pop-up reside in the crust at temperatures above the rutile closure temperature for each of the tracked samples, even though the depth of the 575 ± 75 °C closure isotherm can vary considerably depending upon the prior history of exhumation. The two stage model is a better fit to the bedrock cooling ages than the single stage model, and it better explains the common <0.4–1.0 Ma ages of rutile within the Siang River modern sediments. Both models predict rutile ages of no more than ~3 Ma at the highest elevation of the massif, consistent with <3 Ma dates of rutile from modern erosion of the massif as recorded in the Siang and Brahmaputra sediments, as inferred from the gap in rutile dates from 3 to 8 Ma (Fig. 14). Therefore, these models indicate that a wide range of Pleistocene exhumation rates (~4 to ≥7 km/Myr) can explain the observations within the syntaxis. The single stage model remains broadly consistent with the observations, even with a rate as low as 4 km/Myr because prior exhumation from 7 to 3 Ma has advected and compressed isotherms towards the surface, allowing rocks >575 °C to be at shallower depths. This model also shows that in terms of the observed data, the initiation of the rapid exhumation could have begun at any time from ~7 Ma to 3 Ma.

There are several reasons why we have produced the two contrasting model solutions. First, they show that quite different scenarios can explain the observed bedrock data from the syntaxis pop-up and that there is no unique exhumation rate or time of initiation required to explain it.

Second, the two stage model illustrates that having a reasonably long period (24–3 Ma) of slower (~0.4 km/Myr) decompression prior to the Quaternary, is also permissible. Other variations (not shown) were modelled that had stage one of shorter duration but higher rate (i.e. 14–3 Ma vs. 24–3 Ma with rates of ~0.8 vs. 0.38 km/Myr) prior to the Pleistocene. The output from these other permutations is largely the same for the cooling history of the pop-up. These two stage models serve to show that a period of moderate rate decompression following peak metamorphic conditions is permitted, allowing the pre-Pleistocene evolution of these GH rocks within the hinterland of the Himalaya to have a portion of their post-metamorphic peak history similar to the main part of the Himalaya (cf. that observed in northern Sikkim, northern Bhutan, or the North Himalayan domes).

Third, we wanted to present two contrasting models to discuss the extent to which either could explain the Siwalik lag time data summarised in Fig. 16 and Table 3. These Siwalik data have as their main feature a significant drop in lag time for both the white mica Ar–Ar mica and ZFT ages between 7–8 Ma and ~5 Ma, with subsequent lag times for Ar–Ar being around 2 Myr, approaching but not as short as the modern river sands of the Siang River downstream of the syntaxis pop-up dome. This has been assumed by Lang et al. (2016) to result from erosion of the syntaxis and its pop-up dome, with modelled exhumation rates suggesting an ~5-fold increase beginning about 6 Myr ago. In the models of Fig. 18, the predicted lag time output for white mica Ar–Ar, ZFT and rutile U–Pb (if the latter data were available) can be estimated by calculating the difference in time between erosion at the land surface and the time when these samples cooled below their closure isotherm. This can be done for various times during the model so that lag times can be estimated as a function of time for progressive surface erosion during the modelling. Both models predict decreasing lag times with younger age of erosion in the interval 6–1 Myr ago. This arises because, with such high rates of erosion, the advection of isotherms toward the surface does not abate and thermal gradients continue to rise, even though the majority of radioactive heat-producing elements are removed by erosion. For example, for the single stage model, lag times in 5 Ma sediment would be >4 Myr, 2–3 Myr and ~2 Myr for rutile U–Pb, white mica Ar–Ar and ZFT, respectively but would decrease in 2 Ma sediment to <2 Myr, ~1 Myr, and <1 Myr, respectively. In contrast, the two stage model with inception of rapid exhumation at 3 Ma has short lag times in the last 1–2 Ma of erosion: in 2 Ma sediment lag times for rutile U–Pb, white mica Ar–Ar and ZFT would be >5 Myr, >4 Myr and 0.8–1 Myr, respectively. Only for 1 Ma sediment do the lag times in either model closely match approximately what is observed in Fig. 16.

Although the Siwalik deposits data of Fig. 16 (section Sw2) indicate a decrease in lag times starting at ~6 Ma, the pattern of 1–5 Ma Siwalik sediments more closely resembles a relatively constant lag time value for each chronometer, rather than having a more obvious gradual decrease. The decrease at ~6 Ma suggests that some rapid exhumation, possibly near to or partly coincident with the domal pop-up, but within the existing larger NE-trending syntaxis, took place with rates of at least several km/Myr. However, the observation that the lag times are relatively constant from ~5 to 1 Ma rather than decreasing could be explained by i) having exhumation beginning prior to ~6 Ma but *decreasing* in rate with time, or ii) by an artefact of erosion of two, perhaps adjacent, areas of the syntaxis experiencing rapid exhumation sequentially or partly overlapping in time, combining their erosion products to result in the pattern observed. Overall our two models can both broadly produce a reasonable fit to the observed in situ and modern data from the Siang River sediment, but the two-stage model with *only* Pleistocene rapid exhumation fails to explain the lag time data in 1–5 Ma Siwalik deposits.

The exhumation path in P–T space falls within the melt-present field of wet granite (Fig. 18), quenching only below about 8–10 km depth, which today could be only ~5 km below the river level within the pop-up where temperatures may be as high as 600 °C. Rocks seen at the surface were at conditions allowing granitic melt production prior to ~1.5 Ma. This helps to explain the very young ages of observed pegmatites documented within the syntaxis by various workers and suggests that they are the product not of peak conditions but were accompanied by rapid decompression.

7.6. Synthesis: the pop-up dome in the context of the Himalaya

We have shown via new rutile U–Pb, white mica Ar–Ar, and ZFT data and heat flow modelling, that a Pleistocene exhumation of the north-easternmost part of the syntaxis took place at rates of at least 4 km/Myr and that 12–21 km of rock have been eroded there in the last 3 Ma. The modelling and data suggest that no single numerical heat flow model can explain all the data (bedrock, modern and Neogene thermochronology and lag times), which suggests a scenario for the syntaxis involving a migration of very high erosion over the course of the last ~7 Ma towards the northeast. This could be facilitated by one or more south-verging back thrusts, with the locus of maximum uplift stepping north-eastwards. In any case, to explain the thermochronology of the pop-up dome, 40% to >75% of the total exhumation happened in the last 3 Ma, and the 'gap' in dates of mica and rutile in modern river sand of the Siang suggests that the current dome was exhumed mainly in the Pleistocene.

The apparent plunge of the syntaxial anticline on the south side of the pop-up dome appears to decrease from moderately steeply south

to a sub-horizontal orientation over the ~100 km length of the syntaxis to be consistent with its thermochronological signature, although the density of dating in the south-western two-thirds of the syntaxis is sparse (Fig. 17). From numerous existing studies, cited earlier, the area comprised of Pleistocene mineral cooling ages for low temperature thermochrometers (apatite FT, zircon U–Th–He, ZFT and biotite Ar–Ar) is restricted to ~40 km by 40 km, bounded by the suture zone (and the associated strike-slip faults) on its west and southeast sides, the Jiali–Parlung Fault zone on its north-north-western side and the north-dipping, south-verging Nam–La thrust on the south side (Fig. 17).

The amplitude of the Pleistocene pop-up dome is ~20 km across an anticlinal width of ~40–50 km, on the north side of the Nam–La thrust. Because the internal structure of the dome is not well documented, its shape is only generally known. Similarly, as it is not possible to establish a footwall-hanging wall match across the Nam–La thrust, its displacement is similarly not well-constrained. The relatively steep shear zones corresponding to its ~eastern and western boundaries are defined by the suture zone such that most of the width of the dome may have come from depths approaching 15–20 km. However, because the shear zones and suture zone mylonitic rocks do not encircle the pop-up dome, these mylonites likely pre-date the Pleistocene uplift, as demonstrated by Palin et al. (2014).

Burg et al. (1997, 1998) showed that crustal scale folding, buckling, and subsequent failure along faults can account for the geometry of the domal pop-up. Seward and Burg (2008) suggested that both the suture and the Jiali–Parlung Fault exerted some structural control on the growing (and progressively NE-wards migrating) dome, based on the distribution of the zircon and apatite bedrock FT data (summarised in Fig. 17 along with U–Th–He zircon and Ar–Ar biotite data; see also Supplemental Fig. A4). The data also suggest that the syntaxial dome has not yet fully spread north-eastwards over the Jiali–Parlung Fault because a jump in ages is evidence for ongoing vertical displacement along this active fault (Seward and Burg, 2008; Fig. 1B of Zeitler et al., 2015).

We agree with Zeitler et al. (2015) pointing out that the bedrock cooling age transition across the Nam–La thrust zone is not marked by a sharp cooling age discontinuity as the one represented by the Jiali–Parlung Fault to the NE of the syntaxis. Nonetheless, as apparent from Fig. 17, the Nam–La Thrust acts as the southern boundary of both the pop-up structure and the area where all thermochronometers (including rutile) yield <3 Ma dates. This youngest area, that includes the Namche Barwa–Gyala Peri massifs but extends beyond the suture and abruptly terminates against the Jiali–Parlung Fault, appears to be structurally limited by mapped discontinuities. Hence we disagree with Zeitler et al. (2014, 2015) that in the last ~4 Myr rapid and possibly accelerating cooling only occurred within the Namche Barwa–Gyala Peri metamorphic massif at the location of the supposedly stabilized knickpoint. Zeitler and coauthors interpret the young bedrock cooling ages external to the Namche Barwa–Gyala Peri massif (in the Lhasa Terrane south-west of the Jiali–Parlung Fault) as the result of lateral heat flow from the massif. According to their interpretation, this would have raised the geotherm in Lhasa Terrane rocks immediately adjacent to the massif and made it possible for much modest degrees of incision to set low-T cooling ages system.

We note that several publications from Zeitler and coauthors (mentioned earlier in this paper) supporting and elaborating on the aneurysm model did not provide evidence or arguments to counter the structural explanation of Burg and coauthors for how the syntaxis was produced. Indeed Booth et al. (2009) stated that the structural explanation was consistent with their data.

South-vergent tight folds of km-scale (Fig. 2 in Burg et al., 1997) and the Nam–La Thrust on the south side of the Namche Barwa massif (our Fig. 2D) suggest a southerly vergence for the domal structure, whilst being largely upright in form, consistent with upright folds on Namche Barwa (Fig. 3B). This is consistent with a model of the deeply buried thick Indian crust indentor, comprised of the GH and lower structural panels (LH, cratonic basement of India), finally resisting further underthrusting against the Lhasa and other terranes of southern Tibet. The jamming of this narrow indentor against the Asian buttress is suggested to have led to thickening of this indenting crust and failure via south-vergent folding and thrust failure, with geometry similar to that shown by Burg and Schmalholz (2008) but with steeper aspect and not dissimilar to the general model shown by Palin et al. (2014).

An interesting twist on this model is suggested from our attempt to model lag time data. The type of domal structure observed north of the Nam–La thrust may have an earlier analogue, possibly adjacent to but further southwest along the syntaxis (where detailed mapping and thermochronology have yet to be clearly resolved) and that could have been the source of the grains with ~1–2 Myr lag times in Siwalik sediment 1–5 Ma. As the most recent dome is the farthest northeast in the syntaxis, if there were older structural dome features or thrusts to the southwest of the current one, they would resemble out-of-sequence structures, having propagated away from the foreland of the orogen.

We thus suggest that the Plio-Pleistocene failure and deformation of the syntaxis involved major vertical uplift and south-vergent structures in its northern part, forming the pop-up dome, and may have postdated the Latest Miocene–Pliocene anticlinal structure in GH rocks and the suture zone in the southern portion of the syntaxis. Such an uplift would lead to high topography, possibly migrating north-eastwards, a rapid acceleration in river erosion, and probable isostatic uplift arising from the removal of the upper crust, on the assumption that the elastic thickness permitted this. The consequences of this structural event are major erosion and addition of detritus from the syntaxis and dome with its distinctive Pleistocene thermochronological signature into the sedimentary record of the current and palaeo-Brahmaputra River. Finally, as already suggested by Seward and Burg (2008), the developing syntaxial antiform would have distorted an antecedent Yarlung Tsangpo–Brahmaputra producing the peculiar drainage pattern we observe today.

8. Pleistocene climate-tectonic feedbacks in the eastern Himalayan syntaxis

In this section we review several studies that have addressed the geomorphic evolution of the syntaxial region in the Pleistocene in the wider evolution of the Himalaya–Tibet region, showing evidence for surficial erosive processes that likely enhanced the Pleistocene exhumation of the domal pop-up.

Along the southern margin of the Tibetan plateau, Montgomery et al. (2004) and Korup and Montgomery (2008) observed evidence for repeated Holocene and Pleistocene glacial damming of the Yarlung Tsangpo and its tributaries Yigong Tsangpo and Parlung Tsangpo upstream of the eastern syntaxis. According to Korup and Montgomery (2008) the equilibrium line altitude of glaciers in the region (ELA, where annual accumulation equals annual ablation) was depressed enough with respect to present-day during both the Pleistocene and Holocene glacial maxima to allow the development of moraine dams capable of blocking the three river courses in the area. Upstream of the glacial dams, river incision into bedrock was dramatically impeded by impoundment during glacial occupancy, with further upstream interglacial aggradation, infill of meltwater lakes with sediment and burial of valley floors under glacio-fluvial sediments long after the dams were breached and the glacier melted off. Conversely, the river below the dam continued to incise bedrock efficiently, thus contributing to maintenance of a steep river profile below the existing knickzone. Repeated glacier-controlled damming upstream and fluvial bedrock incision downstream may have retarded or prevented the migration of the knickpoints upstream.

The occurrence of hundreds of breached dams upstream of the Yarlung Tsangpo Gorge suggests outburst floods as a frequently-occurring process in the area, with extreme events as those reported by Lang et al. (2013). These floods, especially when extreme, would result in lateral river erosion that in turn would trigger landslide erosion of

threshold hillslopes (Larsen and Montgomery, 2012). The spatial association between highest landslide erosion rates and maxima in unit stream power occurring on the Yarlung Tsangpo knickzone and its tributaries Po Tsangpo and Parlung suggests that river incision drives erosion on threshold hillslopes by both the vertical incision mechanism and lateral erosion mechanism (driving landslide erosion of threshold hillslopes) in the eastern syntaxial region (Larsen and Montgomery, 2012).

In the north-western Himalaya Brozović et al. (1997) found that the distribution of slope minima over the highly elevated area extending from northern Karakoram to the western syntaxis follows trends in the altitude of the snowline, taken as a proxy for regional ELA. Overall, mean regional elevation, hypsometry and slope distributions appear to be controlled by the extent of glaciation regardless of rock uplift rates as estimated from thermochronometry. Any (tectonically or isostatically induced) surface uplift will tend to cause an increase in the glacier-covered area that in turn will increase erosion rates, thus establishing a negative feedback mechanism returning the landscape towards its previous hypsometry. The high peaks of the region (e.g., Nanga Parbat, 8125 m) represent remnants of topography that surface processes were not able to remove. This mechanism of glacial erosion, with glaciers acting as long-term "buzz-saws" capable of effectively posing a limit on orogenic topography, has been suggested for other glaciated and uplifting orogens of the planet (the St. Elias Orogen, Spotila et al., 2004; the Cascade Range, Mitchell and Montgomery, 2006; the Andes, Montgomery et al., 2001). Its exceptional erosional efficiency has been numerically modelled and confirmed at the global scale by Egholm et al. (2009).

Another climate-dependent factor that has been suggested to promote focused denudation at the southern edge of the Tibetan Plateau is orographic precipitation. As such, it was included in the thermo-mechanical model of Beaumont et al. (2001) in which erosion is the dynamic link between channel flow in the middle to lower crust and ductile extrusion of the high grade metamorphic rocks of the GH. Spatial coincidence between focused rapid exhumation of the steep southern Himalayan front since at least the Pliocene (as indicated by young mineral cooling ages) and orographic precipitation has been observed in northwest India along an ~120 km wide NE–SW Himalayan transect spanning the Sutlej region (Thiede et al., 2004, 2005). The monsoonal precipitation controlled by topography is here interpreted as exerting a strong control on erosional processes (landsliding, debris-flow activity, mass removal by streams), whilst fluvial erosion unloading appears to be focused on high mountainous areas. Furthermore, a direct link between monsoon-driven sustained erosion at the foot of the GH and Pliocene–Holocene sustained out-of-sequence thrusting has been suggested in Nepal south of the MCT (Wobus et al., 2003; Hodges et al., 2004). Other studies (e.g., Burbank et al., 2003; Adlakha et al., 2013; Godard et al., 2014) based on fission-track and cosmogenic radionuclide dating challenge this coupling between spatial gradients in precipitation and variations in long-term denudation in the Himalayas.

In the modern syntaxes the water budget is dominated by moisture influxes by the Westerlies (western syntaxis) and the East Asian Monsoon (eastern syntaxis), whilst in the Central Himalaya precipitation is dominated by the Indian summer monsoon (Burbank et al., 2012). Above ~4 km altitude across the Himalaya, 40% of the annual precipitation arrives as snowfall, with snow accumulation steadily increasing from ~2 km to 4.5–5 km altitude, before levelling off and then dramatically decreasing above ~6 km. Hence, whilst the Central Himalaya receives >70% of its annual precipitation during the Indian summer monsoon, in the highly elevated syntaxial regions, snowfall, and subsequent melting in the Himalayan rain shadow makes a far larger contribution to annual discharge (65 and 35% in the western and eastern syntaxis, respectively) than in Central Himalaya.

The mean ELA position in northwest Himalaya during the Quaternary has been estimated to be ~400 to 500 m lower than at present (and up to 1000 m lower during the Last Glacial Maximum, ca. 20k yrs. ago, Brozović et al., 1997). Similarly, if modern glaciers in the eastern syntaxial region are advanced to the position of tens of large moraines that in the Holocene blocked or constricted the Yarlung Tsangpo and its tributaries, the resulting ELA is depressed by 470 ± 170 m (1σ; Korup and Montgomery, 2008). It is estimated that such a glacial advance impounded between 30% and 55% of the length of the Yigong and Parlung Tsangpo during the Holocene, and commensurately higher for the greater ELA depression (inferred to be ~1 km) during earlier Pleistocene advances (Korup and Montgomery, 2008, and references therein). This supports the inference that surface processes operating in the eastern syntaxial region during the Pleistocene–Holocene were influenced by climatic conditions, with glacial processes dominating over and directly influencing fluvial and hillslope erosive processes.

In summary we argue that glacial erosion, supported by frequent mass wasting in landslides, with detritus carried downstream by a major river with a steep gradient, likely enhanced focused erosion in the eastern syntaxial region to keep pace with the rapid rock uplift caused fundamentally by buckling of the crust, the surface expression of which is the syntaxial antiform with its ~20 km amplitude domal pop-up centred on the Namche Barwa–Gyala Peri massif.

As reported by Wang et al. (2014), ponding of sediment upstream (west) of the syntaxial dome began prior to 2.0–2.5 Myr ago and was caused by the rise of the bedrock floor of the ancestral canyon on the west flank of the uplifting syntaxial (pop-up) dome. The resulting marked change of the pre-existing river gradient on the west side of the dome appears to have created a 'palaeo-knickpoint' at the eastern termination of the ponded sediment. This 'palaeo-knickpoint' may have migrated along the river depending upon the pace of uplift and erosion but it is possible that it was relatively near the position of the current knickpoint, as both are logically on the west upstream flank of the domal uplift.

9. Summary and conclusions

The rocks of the domal pop-up of the northern third of the antiformal eastern Himalayan syntaxis are characterised by Pleistocene thermochronological ages involving a wide range of minerals and isotopic systems. These ages demonstrate that rocks were >575 °C only 1–2 Myr ago within the dome and that present geothermal gradients of >100 °C are expected.

Detritus within the Neogene Surma Basin of Bangladesh, representing deposits of the palaeo-Brahmaputra River, does not record evidence of rise and erosion of this dome with its distinct thermochronological signature until late Pliocene time at the earliest. Strikingly, the record of syntaxis erosion is much more dramatic in modern sediments downstream of the syntaxis than in any Plio-Pleistocene deposits, although the Plio-Pleistocene Siwaliks proximal to the Siang river do record unusually short lag times for Ar–Ar mica and FT zircon data compared to the main part of the Himalaya, suggesting that rapid exhumation within the syntaxis may have begun earlier.

The domal zone of the syntaxis is comprised of GH rocks that equilibrated metamorphically at typical GH conditions of about 700–800 °C and 20–30 km depth, and there is evidence that they were at these conditions into the latest Miocene and perhaps Pliocene time, residing deep in the Tibetan crust and possibly undergoing modest decompression prior to the Pleistocene. This decompression may have arisen from gradual southward extrusion of the middle crust and mountain front erosion, similar to the main part of the Himalaya.

In the interval of latest Miocene to Pleistocene time, the northern part of the syntaxis, consisting of the domal pop-up bounded by the suture zone on north, east, and west sides, and by the Nam–La thrust on its south side, began to buckle, fold, and fail via south-vergent thrust faulting, creating an ~20 km amplitude antiformal dome coincident with an antecedent Yarlung Tsangpo River flowing through the area of the future syntaxis. The rise of this dome impounded sediment upstream, folded the suture zone and its mylonitic basal boundary into a

steep anticline, distorted the course of the Yarlung Tsangpo and reversed the gradient of the former river bedrock gorge, creating a buried canyon prior to ~2.5 Myr ago. The river successfully maintained its main course and steepened its gradient downstream of the Pleistocene ponded sediment above the palaeo-knickpoint.

In the Pleistocene between ~12 and 21 km of rock were uplifted and eroded within the core of the syntaxis, exposing rocks at amphibolite facies conditions to surface erosion as shown by some of the youngest U–Pb and other thermochronological mineral cooling ages anywhere on Earth at rates of at least 4 km/Myr. This changed dramatically the characteristics of the sediment delivered downstream of the gorge to comprise, as it is observed today, up to 50% of the sediment load derived from the domal uplift. The lag time data of 1–5 Ma foreland Himalayan deposits, interpreted to be derived from erosion of the syntaxis and decreasing between ~7 and 5 Ma, recorded a period of rapid exhumation of a source within the syntaxis near to or along strike to the southwest of the current domal pop-up. This source could be a migrating domal feature produced by the indentation process of the Indian plate progressing north-eastwards.

The data collected in this study and in other related studies of this region are consistent with: antecedence (to the development of the syntaxis) of the Yarlung–Tsangpo River; gradual exhumation of up to ~8 km in Late Miocene–Pliocene time linked to typical Himalayan processes; antiformal development of the broader syntaxis region and the late Pliocene–Pleistocene pop-up dome of ~20 km amplitude in the north-easternmost part of the syntaxis exhuming rocks to the surface that were in excess of 575 °C just 1.4 Myr ago; inception of high sustained exhumation rates with at least 12 km of material removed by erosion in the last 3 Ma.

10. Future work

The area of the syntaxis remains seismically very active, eroding at very high rate, and needs to be better investigated geophysically and geologically to fully understand how these discrete syntaxial features originate and evolve.

In particular, improved knowledge of the structure and thermobarometric evolution of the domal pop-up and in general the eastern syntaxial antiform would allow existing thermomechanical numerical models to be better constrained and as such to shed light on mechanism and processes generating and currently sustaining the syntaxial antiform and its domal pop-up. If there has been a migration of the site of the pop-up dome and its high rate of exhumation, this can be tested by tectonic studies and geo- and thermochronology in the much less studied region of the syntaxis to the southwest of the Nam–La thrust towards the foreland. Although the bedrock and detrital thermochronology acquired so far in this remote region has led to several significant studies, more systematic spatial and vertical thermochronology datasets, including rutile U–Pb data, would greatly improve our ability to constrain and model the exhumation history of this region, and to track its erosion products in the past sedimentary archives and in the present-day Bengal Basin sink.

We also appeal to better structural geological investigations both within and at the margins of the domal pop-up, especially on the north and south sides, to evaluate the history of displacement and the extent to which the northern boundary is a fault/shear zone with normal sense displacement, as it would be predicted from its exhumation history.

Recently, the IODP expedition Leg 354 drilled seven sites along on a proximal (°8N) east–west transect in the Bay of Bengal covering the Late Paleogene to present time interval (France-Lanord et al., 2015). Ongoing post-expedition studies are expected to test variations in accumulation rates generated by the Tibet–Himalayan erosion and thus to shed new light on the complex relationships between this source and its sink.

Acknowledgements

The authors wish to thank Tim Horscroft at Elsevier for inviting us to submit a review article on this topic. Special thanks are due to S.H. Akhter for logistical support and advice during sampling of Surma Basin deposits. L. Bracciali warmly thanks: Matt Horstwood (NIGL) for numerous and valuable “five minute” discussions on analytical issues and approaches, Vanessa Pashley (NIGL) for precious technical support with the U–Pb work and Francesca Cigna (British Geological Survey) for helping with geospatial data visualization in the GIS environment. Hongfei Zhang is thanked for allowing access to two granulite facies samples dated in this study. The manuscript greatly benefited from the constructive comments of two anonymous reviewers. This research was supported by NERC (UK Natural Environment Research Council) through grants NE/F01807X/1 to Y. Najman and NE/F017588/1 to R. Parrish.

Appendix A. Supplemental data

Supplemental material to this article can be found online at http://dx.doi.org/10.1016/j.earscirev.2016.07.010 and includes: list and location of samples from the Surma Basin (Table A1), zircon U-Pb data (Table A2), rutile U-Pb data (Table A3), LA-MC-ICP-MS instrument parameters (Table A4), white mica Ar–Ar data (Table A5) and ZFT data (Table A6). Supplemental figures show: the geographic location of samples and schematic geology of the Surma Basin (Fig. A1), U–Pb Concordia diagrams (Fig. A2) and relative probability plots – frequency diagrams of zircon U–Pb, rutile U–Pb and white mica Ar–Ar data (in the 0–2.5, 0–0.8 and 0–1.0 Ga age range, respectively) from modern river sands (Fig. A3), bedrock thermochronology data from the literature used to draw the contour lines of Fig. 4 (Fig. A4), relative probability plots – frequency diagrams of zircon U–Pb, rutile U–Pb and white mica Ar–Ar data (in the 0–2.5, 0–0.8 and 0–1.0 Ga age range, respectively) from the Surma Basin (Fig. A5).

References

Adlakha, V., Lang, K.A., Patel, R.C., Lal, N., Huntington, K.W., 2013. Rapid long-term erosion in the rain shadow of the Shillong Plateau, Eastern Himalaya. Tectonophysics 582, 76–83.

Andò, S., Garzanti, E., Padoan, M., Limonta, M., 2012. Corrosion of heavy minerals during weathering and diagenesis: a catalog for optical analysis. Sediment. Geol. 280, 165–178.

Beaumont, C., Jamieson, R.A., Nguyen, M.H., Lee, B., 2001. Himalayan tectonics explained by extrusion of a low-viscosity crustal channel coupled to focused surface denudation. Nature 414, 738–742.

Bendick, R., Ehlers, T.A., 2014. Extreme localized exhumation at syntaxes initiated by subduction geometry. Geophys. Res. Lett. 41, 5861–5867.

Booth, A.L., et al., 2004. U–Pb zircon constraints on the tectonic evolution of southeastern Tibet, Namche Barwa Area. Am. J. Sci. 304, 889–929.

Booth, A.L., Chamberlain, C.P., Kidd, W.S.F., Zeitler, P.K., 2009. Constraints on the metamorphic evolution of the eastern Himalayan syntaxis from geochronologic and petrologic studies of Namche Barwa. Geol. Soc. Am. Bull. 121, 385–407.

Bracciali, L., Marroni, M., Pandolfi, L., Rocchi, S., 2007. Geochemistry and petrography of Western Tethys Cretaceous sedimentary covers (Corsica and Northern Apennines): from source area to configuration of margins. In: Arribas, J., Critelli, S., Johnsson, M.J. (Eds.), Sedimentary Provenance and Petrogenesis: Perspectives From Petrography and Geochemistry. Geological Society of America, Special Paper 420, pp. 73–93.

Bracciali, L., Parrish, R.R., Horstwood, M.S.A., Condon, D.J., Najman, Y., 2013. U–Pb LA-(MC)-ICP-MS dating of rutile: new reference materials and applications to sedimentary provenance. Chem. Geol. 347, 82–101.

Bracciali, L., Pandolfi, L., Rocchi, S., 2014. A snapshot of the Late Jurassic Western Tethys seafloor composition and morphology provided by the geochemistry of pelitic sediments (Corsica, Central Alps and Northern Apennines). Basin Res. 26, 461–485.

Bracciali, L., Najman, Y., Parrish, R.R., Akhter, S.H., Millar, I., 2015. The Brahmaputra tale of tectonics and erosion: Early Miocene river capture in the Eastern Himalaya. Earth Planet. Sci. Lett. 415, 25–37.

Brookfield, M.E., 1998. The evolution of the great river systems of southern Asia during the Cenozoic India–Asia collision: rivers draining southwards. Geomorphology 22, 285–312.

Brozović, N., Burbank, D.W., Meigs, A.J., 1997. Climatic limits on landscape development in the Northwestern Himalaya. Science 276, 571–574.

Burbank, D.W., Leland, J., Fielding, E., Anderson, R.S., Brozovic, N., Reid, M.R., Duncan, C., 1996. Bedrock incision, rock uplift and threshold hillslopes in the northwestern Himalayas. Nature 379, 505–510.

Burbank, D.W., et al., 2003. Decoupling of erosion and precipitation in the Himalayas. Nature 426, 652–655.

Burbank, D.W., Bookhagen, B., Gabet, E.J., Putkonen, J., 2012. Modern climate and erosion in the Himalaya. Compt. Rendus Geosci. 344, 610–626.

Burbank, D.W., Bookhagen, B., Gabet, E.J., Putkonen, J., 2013. Modern climate and erosion in the Himalaya. Compt. Rendus Geosci. 344, 610–626.

Burg, J.-P., Podladchikov, Y., 1999. Lithospheric scale folding: numerical modelling and application to the Himalayan syntaxes. Int. J. Earth Sci. 88, 190–200.

Burg, J.-P., Podladchikov, Y., 2000. From buckling to asymmetric folding of the continental lithosphere: numerical modelling and application to the Himalayan syntaxes. Geol. Soc. Lond., Spec. Publ. 170, 219–236.

Burg, J.-P., Schmalholz, S., 2008. Viscous heating allows thrusting to overcome crustal-scale buckling: numerical investigation with application to the Himalayan syntaxes. Earth Planet. Sci. Lett. 274, 189–203.

Burg, J.-P., Davy, P., Nievergelt, P., Oberli, F., Seward, D., Diao, Z., Meier, M., 1997. Exhumation during crustal folding in the Namche–Barwa syntaxis. Terra Nova 9, 53–56.

Burg, J.-P., et al., 1998. The Namche Barwa syntaxis: evidence for exhumation related to compressional crustal folding. J. Asian Earth Sci. 16, 239–252.

Carslaw, H.S., Jaeger, J.C., 1959. Conduction of Heat in Solids. second ed. Clarendon Press, Oxford.

Cawood, P.A., Johnson, M.R.W., Nemchin, A.A., 2007. Early Palaeozoic orogenesis along the Indian margin of Gondwana: tectonic response to Gondwana assembly. Earth Planet. Sci. Lett. 255, 70–84.

Cherniak, D., 1993. Lead diffusion in titanite and preliminary results on the effects of radiation damage on Pb transport. Chem. Geol. 110, 177–194.

Cherniak, D.J., 2000. Pb diffusion in rutile. Contrib. Mineral. Petrol. 139, 198–207.

Cherniak, D., 2006. Pb and rare earth element diffusion in xenotime. Lithos 88, 1–14.

Cherniak, D.J., 2010. Diffusion in accessory minerals: zircon, titanite, apatite, monazite and xenotime. Rev. Mineral. Geochem. 72, 827–869.

Cherniak, D., Watson, E., 2000. Pb diffusion in zircon. Chem. Geol. 172, 5–24.

Chirouze, F., Dupont-Nivet, G., Huyghe, P., Beek, P.v.d., Chakraborti, T., Bernet, M., Erens, V., 2012. Magnetostratigraphy of the Neogene Siwalik Group in the far eastern Himalaya: Kameng section, Arunachal Pradesh, India. J. Asian Earth Sci. 44, 117–135.

Chirouze, F., Huyghe, P., van der Beek, P., Chauvel, C., Chakraborty, T., Dupont-Nivet, G., Bernet, M., 2013. Tectonics, exhumation, and drainage evolution of the eastern Himalaya since 13 Ma from detrital geochemistry and thermochronology, Kameng River Section, Arunachal Pradesh. Geol. Soc. Am. Bull. 125, 523–538.

Chu, M.-F., et al., 2006. Zircon U–Pb and Hf isotope constraints on the Mesozoic tectonics and crustal evolution of southern Tibet. Geology 34, 745–748.

Chung, S.-L., et al., 2003. Adakites from continental collision zones: melting of thickened lower crust beneath southern Tibet. Geology 31, 1021–1024.

Chung, S.-L., et al., 2009. The nature and timing of crustal thickening in Southern Tibet: geochemical and zircon Hf isotopic constraints from postcollisional adakites. Tectonophysics 477, 36–48.

Cina, S.E., et al., 2009. Gangdese arc detritus within the eastern Himalayan Neogene foreland basin: implications for the Neogene evolution of the Yalu–Brahmaputra River system. Earth Planet. Sci. Lett. 285, 150–162.

Clark, M.K., et al., 2004. Surface uplift, tectonics, and erosion of eastern Tibet from large-scale drainage patterns. Tectonics 23, TC1006.

Copley, A., Avouac, J.-P., Wernicke, B.P., 2011. Evidence for mechanical coupling and strong Indian lower crust beneath southern Tibet. Nature 472, 79–81.

Craw, D., Koons, P.O., Zeitler, P.K., Kidd, W.S.F., 2005. Fluid evolution and thermal structure in the rapidly exhuming gneiss complex of Namche Barwa–Gyala Peri, eastern Himalayan syntaxis. J. Metamorph. Geol. 23, 829–845.

Dahl, P.S., 1997. A crystal–chemical basis for Pb retention and fission-track annealing systematics in U-bearing minerals, with implications for geochronology. Earth Planet. Sci. Lett. 150, 277–290.

de Sigoyer, J., et al., 2000. Dating the Indian continental subduction and collisional thickening in the northwest Himalaya: multichronology of the Tso Morari eclogites. Geology 28, 487–490.

Deb, P.K., Howladar, M.F., Miah, M.I., Faruque, M.O., Islam, M.S., Mia, M.B., Quamruzzaman, C., 2014. Structural Interpretation of Fenchuganj Gas Field. J. Eng. Geol. Hydrogeol. 2, 29–36.

DeCelles, P., Gehrels, G., Quade, J., LaReau, B., Spurlin, M., 2000. Tectonic implications of U–Pb zircon ages of the Himalayan orogenic belt in Nepal. Science 288, 497–499.

Ding, L., Zhong, D., 1999. Metamorphic characteristics and geotectonic implications of the high-pressure granulites from Namjagbarwa, eastern Tibet. Sci. China Ser. D Earth Sci. 42, 491–505.

Ding, L., Zhong, D., Yin, A., Kapp, P., Harrison, T.M., 2001. Cenozoic structural and metamorphic evolution of the eastern Himalayan syntaxis (Namche Barwa). Earth Planet. Sci. Lett. 192, 423–438.

Egholm, D., Nielsen, S., Pedersen, V.K., Lesemann, J.-E., 2009. Glacial effects limiting mountain height. Nature 460, 884–887.

Enkelmann, E., Ehlers, T.A., Zeitler, P.K., Hallet, B., 2011. Denudation of the Namche Barwa antiform, eastern Himalaya. Earth Planet. Sci. Lett. 307, 323–333.

Evans, P., 1932. The Tertiary succession in Assam. Trans. Miner. Geol. Metall. Inst. India 30, 174–233.

Finlayson, D.P., Montgomery, D.R., Hallet, B., 2002. Spatial coincidence of rapid inferred erosion with young metamorphic massifs in the Himalayas. Geology 30, 219–222.

Finnegan, N.J., Hallet, B., Montgomery, D.R., Zeitler, P.K., Stone, J.O., Anders, A.M., Yuping, L., 2008. Coupling of rock uplift and river incision in the Namche Barwa–Gyala Peri massif, Tibet. Geol. Soc. Am. Bull. 120, 142–155.

France-Lanord, C., Spiess, V., Klaus, A., the Expedition 354 Scientists, 2015. Bengal Fan: Neogene and late Paleogene record of Himalayan orogeny and climate: a transect across the Middle Bengal Fan. International Ocean Discovery Program Preliminary Report 353.

Galbraith, R., Green, P., 1990. Estimating the component ages in a finite mixture. Int. J. Radiat. Appl. Instrum Part D Nucl. Tracks Radiat. Meas. 17, 197–206.

Galbraith, R., Laslett, G., 1993. Statistical models for mixed fission track ages. Nucl. Tracks Radiat. Meas. 21, 459–470.

Galy, A., France-Lanord, C., 2001. Higher erosion rates in the Himalaya: geochemical constraints on riverine fluxes. Geology 29, 23–26.

Galy, V., France-Lanord, C., Peucker-Ehrenbrink, B., Huyghe, P., 2010. Sr–Nd–Os evidence for a stable erosion regime in the Himalaya during the past 12 Myr. Earth Planet. Sci. Lett. 290, 474–480.

Gansser, A., 1966. The Indian Ocean and the Himalayas: a geological interpretation. Eclogae Geol. Helv. 59.

Garzanti, E., Baud, A., Mascle, G., 1987. Sedimentary record of the northward flight of India and its collision with Eurasia (Ladakh Himalaya, India). Geodin. Acta 1, 297–312.

Garzanti, E., Vezzoli, G., Andò, S., France-Lanord, C., Singh, S.K., Foster, G., 2004. Sand petrology and focused erosion in collision orogens: the Brahmaputra case. Earth Planet. Sci. Lett. 220, 157–174.

Garzanti, E., Andò, S., Vezzoli, G., 2009. Grain-size dependence of sediment composition and environmental bias in provenance studies. Earth Planet. Sci. Lett. 277, 422–432.

Gehrels, G., et al., 2011. Detrital zircon geochronology of pre-Tertiary strata in the Tibetan–Himalayan orogen. Tectonics 30, TC5016.

Gemignani, L., Wijbrans, J.R., Najman, Y., van der Beek, P., Bernet, M., 2016. Downstream Evolution of the Eastern Himalayan Detrital Signal as Recorded by Thermochronology in the Tsangpo–Siang–Brahmaputra River Sediments. Himalayan–Karakorum–Tibet Workshop, Aussois, France.

Godard, V., et al., 2014. Dominance of tectonics over climate in Himalayan denudation. Geology 42, 243–246.

Guilmette, C., Indares, A., Hébert, R., 2011. High-pressure anatectic paragneisses from the Namche Barwa, Eastern Himalayan Syntaxis: textural evidence for partial melting, phase equilibria modeling and tectonic implications. Lithos 124, 66–81.

Guo, L., Zhang, H.-F., Harris, N., Pan, F.-B., Xu, W.-C., 2011. Origin and evolution of multi-stage felsic melts in eastern Gangdese belt: constraints from U–Pb zircon dating and Hf isotopic composition. Lithos 127, 54–67.

Guo, L., Zhang, H.-F., Harris, N., Parrish, R., Xu, W.-C., Shi, Z.-L., 2012. Paleogene crustal anatexis and metamorphism in Lhasa terrane, eastern Himalayan syntaxis: evidence from U–Pb zircon ages and Hf isotopic compositions of the Nyingchi Complex. Gondwana Res. 21, 100–111.

Guo, L., Zhang, H.-F., Harris, N., Xu, W.-C., Pan, F.-B., 2016. Detrital zircon U–Pb geochronology, trace-element and Hf isotope geochemistry of the metasedimentary rocks in the Eastern Himalayan syntaxis: tectonic and paleogeographic implications. Gondwana Res. (in press).

Hallet, B., Molnar, P., 2001. Distorted drainage basins as markers of crustal strain east of the Himalaya. J. Geophys. Res. Solid Earth 106, 13697–13709.

Hames, W.E., Bowring, S.A., 1994. An empirical evaluation of the Argon diffusion geometry in muscovite. Earth Planet. Sci. Lett. 124, 161–169.

Harris, N., 2006. The elevation history of the Tibetan Plateau and its implications for the Asian monsoon. Palaeogeogr. Palaeoclimatol. Palaeoecol. 241, 4–15.

Harris, N., 2007. Channel flow and the Himalayan–Tibetan orogen: a critical review. J. Geol. Soc. 164, 511–523.

Harrison, T.M., Copeland, P., Kidd, W.S.F., Yin, A., 1992. Raising Tibet. Science 255, 1663–1670.

Harrison, T.M., Célérier, J., Aikman, A.B., Hermann, J., Heizler, M.T., 2009. Diffusion of ^{40}Ar in muscovite. Geochim. Cosmochim. Acta 73, 1039–1051.

Henderson, A.L., Najman, Y., Parrish, R., BouDagher-Fadel, M., Barford, D., Garzanti, E., Andò, S., 2010. Geology of the Cenozoic Indus Basin sedimentary rocks: paleoenvironmental interpretation of sedimentation from the western Himalaya during the early phases of India–Eurasia collision. Tectonics 29, TC6015.

Henderson, A.L., Najman, Y., Parrish, R., Mark, D.F., Foster, G.L., 2011. Constraints to the timing of India–Eurasia collision; a re-evaluation of evidence from the Indus Basin sedimentary rocks of the Indus–Tsangpo Suture Zone, Ladakh, India. Earth Sci. Rev. 106, 265–292.

Hodges, K.V., 2000. Tectonics of the Himalaya and southern Tibet from two perspectives. Geol. Soc. Am. Bull. 112, 324–350.

Hodges, K.V., Wobus, C., Ruhl, K., Schildgen, T., Whipple, K., 2004. Quaternary deformation, river steepening, and heavy precipitation at the front of the Higher Himalayan ranges. Earth Planet. Sci. Lett. 220, 379–389.

Houseman, G., England, P., 1993. Crustal thickening versus lateral expulsion in the Indian–Asian continental collision. J. Geophys. Res. Solid Earth 98, 12233–12249.

Hurford, A.J., 1990. Standardization of fission track dating calibration: recommendation by the Fission Track Working Group of the I.U.G.S. Subcommission on Geochronology. Chem. Geol. Isot. Geosci. Sect. 80, 171–178.

Iaffaldano, G., Husson, L., Bunge, H.-P., 2011. Monsoon speeds up Indian plate motion. Earth Planet. Sci. Lett. 304, 503–510.

Johnson, S.Y., Alam, A.M.N., 1991. Sedimentation and tectonics of the Sylhet Trough, Bangladesh. Geol. Soc. Am. Bull. 103, 1513–1527.

Johnsson, M.J., Basu, A., 1993. Processes controlling the composition of clastic sediments. GSA Special Paper 284. Geological Society of America, Boulder, CO.

Ketcham, R.A., Carter, A., Donelick, R.A., Barbarand, J., Hurford, A.J., 2007. Improved modeling of fission-track annealing in apatite. Am. Mineral. 92, 799–810.

Kidd, W.F., et al., 2006. Structural and tectonic geology of the Namche Barwa–Gyala Peri Antiform, Southeastern Tibet. AGU Fall Meeting. EOS Trans. Amer. Geophys. Union (Abstract T23B-0480).

Koons, P., Zeitler, P., Chamberlain, C., Craw, D., Meltzer, A., 2002. Mechanical links between erosion and metamorphism in Nanga Parbat, Pakistan Himalaya. Am. J. Sci. 302, 749–773.

Koons, P.O., Zeitler, P., Hallet, B., 2013. Tectonic aneurysm and mountain building. In: Shroder, J.E.i.C., Owen, L.A.E. (Eds.), Treatise on Geomorphology. Academic Press, San Diego, CA, pp. 318–349.

Koppers, A.A., 2002. ArArCALC— software for $^{40}Ar/^{39}$ Ar age calculations. Comput. Geosci. 28, 605–619.

Korup, O., Montgomery, D.R., 2008. Tibetan plateau river incision inhibited by glacial stabilization of the Tsangpo gorge. Nature 455, 786–789.

Korup, O., Montgomery, D.R., Hewitt, K., 2010. Glacier and landslide feedbacks to topographic relief in the Himalayan syntaxes. Proc. Natl. Acad. Sci. 107, 5317–5322.

Krishnaswami, S., Trivedi, J.R., Sarin, M.M., Ramesh, R., Sharma, K.K., 1992. Strontium isotopes and rubidium in the Ganga–Brahmaputra river system: weathering in the Himalaya, fluxes to the Bay of Bengal and contributions to the evolution of oceanic $^{87}Sr/^{86}Sr$. Earth Planet. Sci. Lett. 109, 243–253.

Lang, K.A., Huntington, K.W., 2014. Antecedence of the Yarlung–Siang–Brahmaputra River, eastern Himalaya. Earth Planet. Sci. Lett. 397, 145–158.

Lang, K.A., Huntington, K.W., Montgomery, D.R., 2013. Erosion of the Tsangpo Gorge by Megafloods. Eastern Himalaya, Geology.

Lang, K.A., Huntington, K.W., Burmester, R., Housen, B., 2016. Rapid exhumation of the eastern Himalayan syntaxis since the late Miocene. Geol. Soc. Am. Bull. (B31419.1).

Langille, J., Jessup, M., Cottle, J., Lederer, G., Ahmad, T., 2012. Timing of metamorphism, melting and exhumation of the Leo Pargil dome, northwest India. J. Metamorph. Geol. 30, 769–791.

Larsen, I.J., Montgomery, D.R., 2012. Landslide erosion coupled to tectonics and river incision. Nat. Geosci. 5, 468–473.

Laslett, G.M., Green, P.F., Duddy, I.R., Gleadow, A.J.W., 1987. Thermal annealing of fission tracks in apatite 2. A quantitative analysis. Chem. Geol. Isot. Geosci. Sect. 65, 1–13.

Lee, J., et al., 2000. Evolution of the Kangmar Dome, southern Tibet: structural, petrologic, and thermochronologic constraints. Tectonics 19, 872–895.

Lee, H.-Y., et al., 2003. Miocene Jiali faulting and its implications for Tibetan tectonic evolution. Earth Planet. Sci. Lett. 205, 185–194.

Liang, Y.-H., et al., 2008. Detrital zircon evidence from Burma for reorganization of the eastern Himalayan river system. Am. J. Sci. 308, 618–638.

Lietz, J.K., Kabir, J., 1982. Prospects and Constraints of Oil Exploration in Bangladesh, Fourth Offshore South East Asia Show. Society of Petroleum Engineers, Singapore, pp. 1–6.

Liu, Y., Zhong, D., 1997. Petrology of high-pressure granulites from the eastern Himalayan syntaxis. J. Metamorph. Geol. 15, 451–466.

Liu, Y., Berner, Z., Massonne, H.-J., Zhong, D., 2006. Carbonatite-like dykes from the eastern Himalayan syntaxis: geochemical, isotopic, and petrogenetic evidence for melting of metasedimentary carbonate rocks within the orogenic crust. J. Asian Earth Sci. 26, 105–120.

Liu, Y., Siebel, W., Theye, T., Massonne, H.-J., 2011. Isotopic and structural constraints on the late Miocene to Pliocene evolution of the Namche Barwa area, eastern Himalayan syntaxis, SE Tibet. Gondwana Res. 19, 894–909.

Malusà, M.G., Carter, A., Limoncelli, M., Villa, I.M., Garzanti, E., 2013. Bias in detrital zircon geochronology and thermochronometry. Chem. Geol. 359, 90–107.

Malusà, M.G., Resentini, A., Garzanti, E., 2015. Hydraulic sorting and mineral fertility bias in detrital geochronology. Gondwana Res. 31, 1–19.

Maurin, T., Rangin, C., 2009. Structure and kinematics of the Indo-Burmese Wedge: recent and fast growth of the outer wedge. Tectonics 28, TC2010.

McDougall, I., Harrison, T.M., 1999. Geochronology and Thermochronology by the $^{40}Ar/^{39}Ar$ Method. Oxford University Press, New York (269 pp.).

Meng, J., Wang, C., Zhao, X., Coe, R., Li, Y., Finn, D., 2012. India–Asia collision was at 24°N and 50 Ma: palaeomagnetic proof from southernmost Asia. Sci. Rep. 2.

Mezger, K., Hanson, G.N., Bohlen, S.R., 1989. High-precision U–Pb ages of metamorphic rutile: application to the cooling history of high-grade terranes. Earth Planet. Sci. Lett. 96, 106–118.

Mitchell, S.G., Montgomery, D.R., 2006. Influence of a glacial buzzsaw on the height and morphology of the Cascade Range in central Washington State, USA. Quat. Res. 65, 96–107.

Moecher, D.P., Samson, S.D., 2006. Differential zircon fertility of source terranes and natural bias in the detrital zircon record: implications for sedimentary provenance analysis. Earth Planet. Sci. Lett. 247, 252–266.

Molnar, P., England, P., 1990. Late Cenozoic uplift of mountain ranges and global climate change: chicken or egg? Nature 346, 29–34.

Molnar, P., England, P., Martinod, J., 1993. Mantle dynamics, uplift of the Tibetan Plateau, and the Indian Monsoon. Rev. Geophys. 31, 357–396.

Montgomery, D.R., Balco, G., Willett, S.D., 2001. Climate, tectonics, and the morphology of the Andes. Geology 29, 579–582.

Montgomery, D.R., Hallet, B., Yuping, L., Finnegan, N., Anders, A., Gillespie, A., Greenberg, H.M., 2004. Evidence for Holocene megafloods down the Tsangpo River gorge, southeastern Tibet. Quat. Res. 62, 201–207.

Morton, A.C., Hallsworth, C.R., 1999. Processes controlling the composition of heavy mineral assemblages in sandstones. Sediment. Geol. 124, 3–29.

Mottram, C.M., Parrish, R.R., Regis, D., Warren, C.J., Argles, T.W., Harris, N.B., Roberts, N.M., 2015. Using U–Th–Pb petrochronology to determine rates of ductile thrusting: time windows into the Main Central Thrust, Sikkim Himalaya. Tectonics.

Najman, Y., et al., 2008. The Paleogene record of Himalayan erosion: Bengal Basin, Bangladesh. Earth Planet. Sci. Lett. 273, 1–14.

Najman, Y., et al., 2010. Timing of India–Asia collision: geological, biostratigraphic, and palaeomagnetic constraints. J. Geophys. Res. 115, B12416.

Najman, Y., et al., 2012. The record of Himalayan erosion preserved in the sedimentary rocks of the Hatia Trough of the Bengal Basin and the Chittagong Hill Tracts, Bangladesh. Basin Res. 24, 499–519.

Najman, Y., Bracciali, L., Parrish, R.R., Chisty, E., Copley, A., 2016. Evolving strain partitioning in the Eastern Himalaya: the growth of the Shillong Plateau. Earth Planet. Sci. Lett. 433, 1–9.

Ouimet, W., Whipple, K., Royden, L., Reiners, P., Hodges, K., Pringle, M., 2010. Regional incision of the eastern margin of the Tibetan Plateau. Lithosphere 2, 50–63.

Owen, L.A., 2008. Geomorphology: how Tibet might keep its edge. Nature 455, 748–749.

Palin, R., et al., 2014. Monazite geochronology and petrology of kyanite- and sillimanite-grade migmatites from the northwestern flank of the eastern Himalayan syntaxis. Gondwana Res. 26, 323–347.

Palin, R.M., et al., 2015. Two-stage cooling history of pelitic and semi-pelitic mylonite (sensu lato) from the Dongjiu–Milin shear zone, northwest flank of the eastern Himalayan syntaxis. Gondwana Res. 28, 509–530.

Pan, F.-B., Zhang, H.-F., Harris, N., Xu, W.-C., Guo, L., 2012. Oligocene magmatism in the eastern margin of the east Himalayan syntaxis and its implication for the India–Asia post-collisional process. Lithos 154, 181–192.

Prell, W.L., Kutzbach, J.E., 1992. Sensitivity of the Indian monsoon to forcing parameters and implications for its evolution. Nature 360, 647–652.

Quanru, G., et al., 2006. The Eastern Himalayan syntaxis: major tectonic domains, ophiolitic mélanges and geologic evolution. J. Asian Earth Sci. 27, 265–285.

Raymo, M.E., Ruddiman, W.F., 1992. Tectonic forcing of late Cenozoic climate. Nature 359, 117–122.

Reimann, K.-U., 1993. Geology of Bangladesh. Borntraeger, Berlin (154 pp.).

Reiners, P.W., Spell, T.L., Nicolescu, S., Zanetti, K.A., 2004. Zircon (U–Th)/He thermochronometry: He diffusion and comparisons with $^{40}Ar/^{39}Ar$ dating. Geochim. Cosmochim. Acta 68, 1857–1887.

Renne, P., Swisher, C.C., Deino, A.L., Karner, D.B., Owens, T.L., DePaolo, D.J., 1998. Intercalibrations of standards, absolute ages and uncertainties in $^{40}Ar–^{39}Ar$ dating. Chem. Geol. 145, 117–152.

Robinson, R.A.J., et al., 2014. Large rivers and orogens: the evolution of the Yarlung Tsangpo–Irrawaddy system and the eastern Himalayan syntaxis. Gondwana Res. 26, 112–121.

Robl, J., Stüwe, K., Hergarten, S., 2008. Channel profiles around Himalayan river anticlines: constraints on their formation from digital elevation model analysis. Tectonics 27, TC3010.

Royden, L.H., Burchfiel, B.C., King, R.W., Wang, E., Chen, Z., Shen, F., Liu, Y., 1997. Surface deformation and lower crustal flow in eastern Tibet. Science 276, 788–790.

Schneider, D., Edwards, M., Kidd, W., Khan, M.A., Seeber, L.t., Zeitler, P., 1999. Tectonics of Nanga Parbat, western Himalaya: synkinematic plutonism within the doubly vergent shear zones of a crustal-scale pop-up structure. Geology 27, 999–1002.

Scott, D.J., St-Onge, M.R., 1995. Constraints on Pb closure temperature in titanite based on rocks from the Ungava orogen, Canada: implications for U–Pb geochronology and P–T–t path determinations. Geology 23, 1123–1126.

Searle, M., et al., 1987. The closing of Tethys and the tectonics of the Himalaya. Geol. Soc. Am. Bull. 98, 678–701.

Seeber, L., Gornitz, V., 1983. River profiles along the Himalayan arc as indicators of active tectonics. Tectonophysics 92, 335–367.

Seward, D., Burg, J.-P., 2008. Growth of the Namche Barwa Syntaxis and associated evolution of the Tsangpo Gorge: constraints from structural and thermochronological data. Tectonophysics 451, 282–289.

Singh, S.K., 2006. Spatial variability in erosion in the Brahmaputra basin: causes and impacts. Curr. Sci. 90, 1272–1275.

Singh, S.K., France-Lanord, C., 2002. Tracing the distribution of erosion in the Brahmaputra watershed from isotopic compositions of stream sediments. Earth Planet. Sci. Lett. 202, 645–662.

Smye, A.J., Stockli, D.F., 2014. Rutile U–Pb age depth profiling: a continuous record of lithospheric thermal evolution. Earth Planet. Sci. Lett. 408, 171–182.

Sol, S., et al., 2007. Geodynamics of the southeastern Tibetan Plateau from seismic anisotropy and geodesy. Geology 35, 563–566.

Spotila, J.A., Buscher, J.T., Meigs, A.J., Reiners, P.W., 2004. Long-term glacial erosion of active mountain belts: example of the Chugach–St. Elias Range, Alaska. Geology 32, 501–504.

Stewart, R.J., Hallet, B., Zeitler, P.K., Malloy, M.A., Allen, C.M., Trippett, D., 2008. Brahmaputra sediment flux dominated by highly localized rapid erosion from the easternmost Himalaya. Geology 36, 711–714.

Stüwe, K., White, L., Brown, R., 1994. The influence of eroding topography on steady-state isotherms. Application to fission track analysis. Earth Planet. Sci. Lett. 124, 63–74.

Stüwe, K., Robl, J., Hergarten, S., Evans, L., 2008. Modeling the influence of horizontal advection, deformation, and late uplift on the drainage development in the India–Asia collision zone. Tectonics 27, TC6011.

Tagami, T., Carter, A., Hurford, A.J., 1996. Natural long-term annealing of the zircon fission-track system in Vienna Basin deep borehole samples: constraints upon the partial annealing zone and closure temperature. Chem. Geol. 130, 147–157.

Tapponnier, P., Zhiqin, X., Roger, F., Meyer, B., Arnaud, N., Wittlinger, G., Jingsui, Y., 2001. Oblique stepwise rise and growth of the Tibet Plateau. Science 294, 1671–1677.

Thiede, R.C., Bookhagen, B., Arrowsmith, J.R., Sobel, E.R., Strecker, M.R., 2004. Climatic control on rapid exhumation along the Southern Himalayan Front. Earth Planet. Sci. Lett. 222, 791–806.

Thiede, R.C., Arrowsmith, J.R., Bookhagen, B., McWilliams, M.O., Sobel, E.R., Strecker, M.R., 2005. From tectonically to erosionally controlled development of the Himalayan orogen. Geology 33, 689–692.

Uddin, A., Lundberg, N., 1998. Cenozoic history of the Himalayan–Bengal system: sand composition in the Bengal basin, Bangladesh. Geol. Soc. Am. Bull. 110, 497–511.

Uddin, A., Lundberg, N., 1999. A paleo-Brahmaputra? Subsurface lithofacies analysis of Miocene deltaic sediments in the Himalayan–Bengal system, Bangladesh. Sediment. Geol. 123, 239–254.
Uddin, A., Hames, W.E., Zahid, K.M., 2010. Laser $^{40}Ar/^{39}Ar$ age constraints on Miocene sequences from the Bengal basin: implications for middle Miocene denudation of the eastern Himalayas. J. Geophys. Res. Solid Earth 115, B07416.
Vermeesch, P., 2007. Quantitative geomorphology of the White Mountains (California) using detrital apatite fission track thermochronology. J. Geophys. Res. Earth Surf. 112.
Vermeesch, P., 2009. RadialPlotter: a Java application for fission track, luminescence and other radial plots. Radiat. Meas. 44, 409–410.
von Eynatten, H., Dunkl, I., 2012. Assessing the sediment factory: the role of single grain analysis. Earth Sci. Rev. 115, 97–120.
Wadia, D.N., 1931. The syntaxis of the northwest Himalaya: its rocks, tectonics and orogen. Rec. Geol. Surv. India 65, 189–220.
Wagner, G.A., Reimer, G.M., 1972. Fission track tectonics: the tectonic interpretation of fission track apatite ages. Earth Planet. Sci. Lett. 14, 263–268.
Wang, P., Scherler, D., Liu-Zeng, J., Mey, J.r., Avouac, J.-P., Zhang, Y., Shi, D., 2014. Tectonic control of Yarlung Tsangpo Gorge revealed by a buried canyon in Southern Tibet. Science 346, 978–981.
Wang, P., Scherler, D., Liu-Zeng, J., Mey, J., Avouac, J.-P., Zhang, Y., Shi, D., 2015. Response to Comment on "Tectonic control of Yarlung Tsangpo Gorge revealed by a buried canyon in Southern Tibet". Science 349, 799.
Weltje, G.J., von Eynatten, H., 2004. Quantitative provenance analysis of sediments: review and outlook. Sediment. Geol. 171, 1–11.
Whipple, K.X., 2009. The influence of climate on the tectonic evolution of mountain belts. Nat. Geosci. 2, 97–104.
Whitney, D.L., Teyssier, C., Fayon, A.K., 2004. Isothermal decompression, partial melting and exhumation of deep continental crust. Geol. Soc. Lond., Spec. Publ. 227, 313–326.
Willett, S., Beaumont, C., Fullsack, P., 1993. Mechanical model for the tectonics of doubly vergent compressional orogens. Geology 21, 371–374.
Wobus, C.W., Hodges, K.V., Whipple, K.X., 2003. Has focused denudation sustained active thrusting at the Himalayan topographic front? Geology 31, 861–864.
Worm, H.-U., Ahmed, A.M.M., Ahmed, N.U., Islam, H.O., Huq, M.M., Hambach, U., Lietz, J., 1998. Large sedimentation rate in the Bengal delta: magnetostratigraphic dating of Cenozoic sediments from northeastern Bangladesh. Geology 26, 487–490.
Xu, W.-C., Zhang, H.-F., Parrish, R., Harris, N., Guo, L., Yuan, H.-L., 2010. Timing of granulite-facies metamorphism in the eastern Himalayan syntaxis and its tectonic implications. Tectonophysics 485, 231–244.
Xu, Z., Ji, S., Cai, Z., Zeng, L., Geng, Q., Cao, H., 2012. Kinematics and dynamics of the Namche Barwa Syntaxis, eastern Himalaya: constraints from deformation, fabrics and geochronology. Gondwana Res. 21, 19–36.
Xu, W.-C., Zhang, H.-F., Harris, N., Guo, L., Pan, F.-B., 2013. Rapid Eocene erosion, sedimentation and burial in the eastern Himalayan syntaxis and its geodynamic significance. Gondwana Res. 23, 715–725.
Yin, A., Dubey, C.S., Kelty, T.K., Webb, A.A.G., Harrison, T.M., Chou, C.Y., Célérier, J., 2010a. Geologic correlation of the Himalayan orogen and Indian craton: part 2. Structural geology, geochronology, and tectonic evolution of the Eastern Himalaya. Geol. Soc. Am. Bull. 122, 360–395.
Yin, A., Dubey, C.S., Webb, A.A.G., Kelty, T.K., Grove, M., Gehrels, G.E., Burgess, W.P., 2010b. Geologic correlation of the Himalayan orogen and Indian craton: part 1. Structural geology, U–Pb zircon geochronology, and tectonic evolution of the Shillong Plateau and its neighboring regions in NE India. Geol. Soc. Am. Bull. 122, 336–359.
Zeitler, P.K., Chamberlain, C.P., Smith, H.A., 1993. Synchronous anatexis, metamorphism, and rapid denudation at Nanga Parbat (Pakistan Himalaya). Geology 21, 347–350.
Zeitler, P.K., et al., 2001a. Crustal reworking at Nanga Parbat, Pakistan: metamorphic consequences of thermal–mechanical coupling facilitated by erosion. Tectonics 20, 712–728.
Zeitler, P.K., et al., 2001b. Erosion, Himalayan geodynamics, and the geomorphology of metamorphism. GSA Today 11, 4–8.
Zeitler, P.K., Meltzer, A.S., Brown, L., Kidd, W.S.F., Lim, C., Enkelmann, E., 2014. Tectonics and topographic evolution of Namche Barwa and the easternmost Lhasa Block. In: Nie, J., Hoke, G.D., Horton, B. (Eds.), Towards an Improved Understanding of Uplift Mechanisms and the Elevation History of the Tibetan Plateau. Geological Society of America Special Paper, pp. 23–58.
Zeitler, P.K., Koons, P.O., Hallet, B., Meltzer, A.S., 2015. Comment on "Tectonic control of Yarlung Tsangpo Gorge revealed by a buried canyon in Southern Tibet". Science 349, 799.
Zeng, L., Gao, L.-E., Dong, C., Tang, S., 2012. High-pressure melting of metapelite and the formation of Ca-rich granitic melts in the Namche Barwa Massif, southern Tibet. Gondwana Res. 21, 138–151.
Zhang, Y., Dai, T., Hong, A., 1981. Isotopic geochronology of granitoid rocks in southern Xizang plateau. Proc. Symp. Qinghai Xizang (Tibet) Plateau. Science Press, Beijing, pp. 483–495.
Zhang, Z.M., Zhao, G.C., Santosh, M., Wang, J.L., Dong, X., Liou, J.G., 2010a. Two stages of granulite facies metamorphism in the eastern Himalayan syntaxis, south Tibet: petrology, zircon geochronology and implications for the subduction of Neo-Tethys and the Indian continent beneath Asia. J. Metamorph. Geol. 28, 719–733.
Zhang, H., Harris, N., Guo, L., Xu, W., 2010b. The significance of Cenozoic magmatism from the western margin of the eastern syntaxis, southeast Tibet. Contrib. Mineral. Petrol. 160, 83–98.
Zhang, Z., Zhao, G., Santosh, M., Wang, J., Dong, X., Shen, K., 2010c. Late Cretaceous charnockite with adakitic affinities from the Gangdese batholith, southeastern Tibet: evidence for Neo-Tethyan mid-ocean ridge subduction? Gondwana Res. 17, 615–631.
Zhang, Z., et al., 2012a. Petrology and geochronology of the Namche Barwa Complex in the eastern Himalayan syntaxis, Tibet: constraints on the origin and evolution of the north-eastern margin of the Indian Craton. Gondwana Res. 21, 123–137.
Zhang, J., Yin, A., Liu, W., Wu, F., Lin, D., Grove, M., 2012b. Coupled U–Pb dating and Hf isotopic analysis of detrital zircon of modern river sand from the Yalu River (Yarlung Tsangpo) drainage system in southern Tibet: constraints on the transport processes and evolution of Himalayan rivers. Geol. Soc. Am. Bull. 124, 1449–1473.
Zhu, D.-C., et al., 2011. The Lhasa Terrane: record of a microcontinent and its histories of drift and growth. Earth Planet. Sci. Lett. 301, 241–255.